INVESTIGATION AND OPTIMIZATION OF THERMAL CHARACTERISTICS OF A VERTICAL SHELL-AND-TUBE PHASE CHANGE ENERGY STORAGE SYSTEM

By

Gang Shen

B. Eng. (Hons) (Mechanical Engineering)

Xi'an Jiaotong University

M. Eng. (Mechanical Engineering)

Huazhong University of Science & Technology

School of Engineering, University of Tasmania

Submitted in fulfilment of the requirements for the degree of

Doctor of Philosophy

June 2020

UNIVERSITY*of* TASMANIA

SUMMARY

Latent heat thermal energy storage is a promising technology to solve the mismatch problem between demand and supply in renewable energy utilization due to its high energy density and a nearly constant temperature heat storage or release. In this thesis, the research aims to investigate and optimize the thermal characteristics of a vertical shell-and-tube latent heat thermal energy storage (LHTES) system which receives the most intensive research in the last decades. A comprehensive literature review was first conducted to evaluate the current research status and gaps. It was found that optimization in heat exchanger design and configurations is very important to improve the thermal energy storage performance. It can eliminate the reliance on expensive highly conductive material embedded in the phase change material (PCM) without reducing the energy storage capacity and density. This motivate this study to focus on investigating and optimizing the designs and configurations in a vertical shell-and-tube LHTES system.

A comprehensive numerical model was then established by integrating the heat transfer fluid (HTF) flow model, HTF tube conduction model and heat transfer model in the PCM. The model eliminates the limitations in previous numerical studies that the PCM heat transfer model is subject to constant temperature boundary conditions during melting and solidification cycles. The model also enables evaluating both natural convection in PCM, and turbulent and lamina flows in HTF. It allows to study the effect of the HTF flow on the thermal performance of the LHTES system under a wide range of working conditions.

The validation work showed that the predicted results agreed well with the experimental data. It demonstrated that the numerical model can reliably and accurately predict the thermal and heat transfer characteristics in the LHTES system during the phase transition cycles. The proposed model was then used to investigate energy storage and release performances in a

vertical cylindrical LHTES system with different lateral tilting angles. The optimal tilting angle was examined for both energy storage and release processes. The results revealed that the total melting time was substantially shortened by up to 43% along with the tilting lateral surface angle varying from 0° to 7°; however, the increase in the tilting angle adversely affected the total solidification time. The optimal tilting angle selection must trade off between the heat storage and release performances. The tilting shell design stores heat energy much faster and can be applied for areas with short sunshine duration to enhance the storage of solar energy.

The results regarding the tilting lateral surface demonstrated that the performance of the LHTES system is highly determined by the heat exchanger design. It further motivates research to investigate effects of the shell-to-tube radius ratio and unit height on the thermal characteristics of the cylindrical LHTES system. For this purpose, two series of LHTES system configurations were evaluated and studied. The first series varies the PCM shell radius (R) under a fixed HTF-tube radius (r_f) and the second series changes the HTF-tube radius with the PCM shell radius fixed. Based on the developed PCM-HTF conjugate analytic model, the numerical investigation assessed the vertical LHTES system using the energy storage/release ratio (E), total and average stored/release energy rate ($\bar{q}_{ch}/\bar{q}_{dis}$), and energy storage/release density ($Q_{ch}^{tot}/Q_{dis}^{tot}$) as performance indicator during the charging and discharging processes. The investigation on the first series of configuration indicated that the optimal R/r_f is close to 5 under long charging/discharging time and close to 4 under short charging/discharging time. The results from the second series revealed that the R_f/r range of 4 to 5 can substantially accelerate both energy storage and retrieval processes without significant effect on the energy storage capacity. Furthermore, the optimal radius ratio is found to be nearly independent on the unit height.

The optimal radius ratio obtained from the numerical investigation was applied to build a vertical multitube LHTES rig to demonstrate the efficacy of the theoretical study. The study

then proceeds to an experimental investigation of the multiple tube heat exchanger. This experimental study first validated a well-known numerical solution to simplify the multiple-tube physical model into a single-tube one. This was done by comparing the experimental results between the multiple-tube heat exchanger (MTHX) and a single-tube heat exchanger (STHX). The STHX's geometrical parameters are the same as those of the virtual cylindrical domain in the MTHX, being similar to the single-tube model formulated by the simplifying numerical solution. The comparison concludes only an experimental study or a three-dimensional numerical modelling can reliably address the thermal characteristics of the multitube heat exchanger. The different inner tube numbers in the MTHXs were also experimentally compared. The results showed the added tubes in vertical MTHX boosted both charging and discharging cycles without hindering the PCM natural convection flow.

Finally, the experimental results of five-tube MTHX were compared and analysed subject to different HTF operating conditions. The result confirms the numerical finding which indicates the PCM melting is dominated by natural convection while the solidification is mainly influenced by thermal conduction.

The shell tilting angle, the shell-to-tube radius ratio and inner-tube arrangement are prominent design parameters to be considered when designing a shell-and-tube LHTES heat exchanger. The analysis of these parameters and operating conditions will provide the useful guidelines and implications for future research and practical designs.

DECLARATION OF ORIGINALITY

This thesis contains no material which has been accepted for a degree or diploma by the University or any other institution, except by way of background information and duly acknowledged in the thesis, and to the best of my knowledge and belief no material previously published or written by another person except where due acknowledgement is made in the text of the thesis, nor does the thesis contain any material that infringes copyright.

AUTHORITY OF ACCESS

This thesis may be made available for loan and limited copying and communication in accordance with the Copyright Act 1968.

Gang Shen

11/06/2020

ACKNOWLEDGEMENTS

I wish to express sincere appreciation to my primary supervisor, Professor Xiaolin Wang, whose support, insights and guidance have been invaluable throughout my study. I would also like to thank my co-supervisor, Professor Andrew Chan who made valuable advices and thoughtful comments to the project. Thanks are extended to the team at the workshop of School of Engineering for their technical support and Mr Zane Smith who proofread the thesis. Special thanks are given to Dr Xiang Yin, the visiting scholar to School of Engineering, from Xi'an Jiaotong University, China, for his kindly support on the project.

The thesis is dedicated to my parents, my wife and my son, for their endless inspiration and support in the pursuit of this project.

STATEMENT REGARDING PUBLISHED WORK CONTAINED IN THESIS

The publishers of the papers comprising Chapter 3 and part of Chapter 6 hold the copyright for that content and access to the material should be sought from the respective journals. The remaining non published content of the thesis may be made available for loan and limited copying and communication in accordance with the Copyright Act 1968.

STATEMENT OF CO-AUTHORSHIP

The following people and institutions contributed to the publication of work undertaken as part of this thesis:

Candidate: Gang Shen, School of Engineering, University of Tasmania, Hobart, Tasmania, Australia.

Author 1: Associate Professor Xiaolin Wang, Primary Supervisor, School of Engineering, University of Tasmania, Hobart, Tasmania, Australia.

Author 2: Professor Andrew Chan, Co-Supervisor, School of Engineering, University of Tasmania, Hobart, Tasmania, Australia.

Author 3: Professor Feng Cao, School of Energy and Power Engineering, Xi'an Jiaotong University, Xi'an, China.

Author 4: Dr Xiang Yin, School of Energy and Power Engineering, Xi'an Jiaotong University, Xi'an, China.

PAPER 1: Located in Chapter 3

Gang Shen, Xiaolin Wang, Andrew Chan, Feng Cao, Xiang Yin. 'Study of the effect of tilting lateral surface angle and operating parameters on the performance of a vertical shell-and-tube latent heat energy storage system'. Solar Energy, 194 (2019) pp.103-113.

PAPER 2: Located in Chapters 4 and 5

Gang Shen, Xiaolin Wang, Andrew Chan, Feng Cao, Xiang Yin. 'Investigation on optimal shell-to-tube radius ratio of a vertical shell-and-tube latent heat energy storage system'. Submitted to the Journal of Solar Energy for reviewing.

Author contributions for papers 1 and 2:

The Candidate designed the physical model, developed the numerical model, performed the simulations, analysed the results, and drafted the manuscript. Author 1 was the corresponding author who evaluated the physical model, analysed the results and finalized the manuscript. Author 3 provided valuable comments on the manuscript, edited and enhanced the writings. Authors 4 and 5 advised on and assisted with the numerical modelling and the validation work.

PAPER 3: Located in Chapter 2

Gang Shen, Xiaolin Wang, Andrew Chan. 'A review on the numerical studies to predict the transient thermal behaviours of the latent heat thermal energy storage systems'. Proceedings of the 5th International Conference on Polygeneration (ICP2019), Fukuoka, Japan.

Author contributions for paper 3:

The candidate decided the review topics, searched and collected the relevant literature, summarized previous works and drafted the manuscript. Author 1 analysed the findings and improved the contents and was the corresponding author. Author 2 contributed to improving the writing.

PAPER 4: Located in Chapter 6

Gang Shen, Xiaolin Wang, Andrew Chan. 'Experimental investigation of heat transfer characteristics in a vertical multi-tube latent heat thermal energy storage system', Energy Procedia. 160 (2019) 332-339.

PAPER 5: Located in Chapter 6

Gang Shen, Xiaolin Wang, Andrew Chan. 'Experimental investigation of the multitube design and operating parameters on complete charging and discharging cycles in vertical cylindrical latent heat storage systems'. Submitted to the Journal of Heat and Mass Transfer for reviewing.

Author contributions for papers 4 and 5:

As the primary author, the candidate assessed the research gap, formulated the conceptual design, set up the experimental facilities, run tests, analysed the experimental results, and drafted the manuscript. Author 1 was the corresponding author, advised on the experimental setup, analysed the experimental results and finalized the manuscript. Author 2 provided vital feedbacks on the related research work and edited the manuscript.

We, the undersigned, endorse the above stated contribution of work undertaken for each of the published (or submitted) peer-reviewed manuscripts contributing to this thesis:

Signed:

	Gang Shen Candidate School of Engineering University of Tasmania	Xiaolin Wang Associate Professor Primary Supervisor School of Engineering University of Tasmania	Damien Holloway Associate Professor On behalf of Head of School School of Engineering University of Tasmania
Date:	11/06/2020	11/06/2020	11/06/2020

NOMENCLATURE

A_{cons}	Mushy zone constant	(kg/(m^3·s))
C_p	PCM specific heat	(J/(kg·K))
$C_{p,var}$	PCM variable specific heat	(J/(kg·K))
E	Energy storage/release ratio	(-)
g	Acceleration of gravity	(m/s^2)
h	Enthalpy	(J/kg)
H	PCM total volumetric enthalpy (J/kg) or Unit height (m)	
h_{var}	PCM variable enthalpy	(J/kg)
k	Thermal conductivity(W/(m·K)) or turbulence kinetic energy(J)	
L	Latent heat	(J/kg)
m	Mass of PCM	(kg)
p	Pressure	(Pa)
Q	Energy	(J)
Q_m	Average heat storage/release density	(J/kg)
r	Tube radius	(mm)
R	Shell inner radius	(mm)
Re	Reynolds number	(-)
$\vec{S}$	Momentum sink term	(kg/(m^2·s^2))
t	Time	(s)
T	Temperature	(°C)
T_o	Reference temperature	(°C)

u, v	Radial, axial velocity component	(m/s)
U	Heat transfer coefficient	(W/(m^2·K))
V	Volume (m^3) or volume flow rate (L/min)	
$\vec{v}$	Velocity vector	(m/s)
x	Radial coordinate	(m)
z	Axial coordinate	(m)

Greek letters

β	Volumetric thermal expansion coefficient	(1/K)
γ	Constant small number (0.001)	(-)
Γ	Total discharging-to-charging time ratio	(-)
ε	Turbulence kinetic energy dissipation rate (m^2/s^3) or eccentricity (-)	
θ	Tilting angle	(°)
μ	Dynamic viscosity	(kg/(m·s))
μ_t	Turbulent viscosity	(kg/(m·s))
ρ	Density	(kg/m^3)
ρ_o	PCM density at T_o	(kg/m^3)
ϕ_l	Liquid fraction	(-)
ω	Weighting factor	(-)

Subscripts

ch	Charging
dis	Discharging

f	Heat transfer fluid or fixed
i	Element
in	Inlet
ini	Initial time
liquidus	Liquid phase
max	Maximum
P	Phase change material
ref	Reference
solidus	Solid phase
w	Water
wall	Wall between PCM and HTF

Superscripts

opt	Optimal
tot	Total

LIST OF FIGURES

LIST OF TABLES

Contents

Chapter 1: Introduction

1.1. Background

Renewable energy is abundant and environmentally friendly. Its share in the total energy supply has increased steadily in the last decades. As one of main types of renewable energy, solar energy has become more competitive in energy market owing to vast policy support and cost decrease resulted from technology improvement [1]. In addition to household users, solar heating applications have extended to large-scale customers such as hotels, schools, and agriculture greenhouses, and even commercial and industry sections. The share of solar water heating is expected to continually grow around the globe. For example, in order to improve energy efficiency and reduce emissions of greenhouse gases China has targeted to reach a total solar heat collecting area of 300 million square metres by 2020. This represents a more than 100% increase, compared to 145 million square metres it installed in 2009 [2]. Fig. 1.1 shows that the cumulative global capacity of solar water heating has increased steadily over the last decade, reaching 480 GW_{th} in 2018 [3].

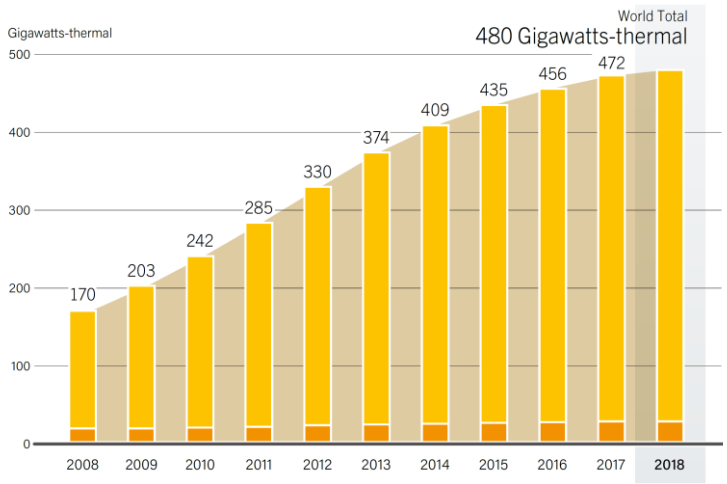

Fig. 1.1. Annual global capacities of solar water heating, from 2008 to 2018 [3].

However, solar energy is intermittent and naturally unsteady which causes mismatch between energy supply to demand. Solar thermal energy storage is essential for providing stable energy supply to the users. The major thermal energy storage methods include sensible heat storage, latent heat storage and chemical heat storage. Latent heat storage using phase change material (PCM) becomes more and more attractive due to its high energy storage density, and energy stored or released at a nearly constant temperature. Fig. 1.2 illustrates a proposed scheme to integrate a PCM storage system to a solar hot water system [4]. Many research works have been performed on solar energy storage using PCM in the last few decades. Some researchers had devoted to thermal, physical, chemical and economic properties of PCMs while others focused more on system configurations and interactions between the thermal energy storage systems and the solar heat collecting systems [5]. Sharma et al. [6] evaluated thermal characteristics of various types of PCMs and reviewed various applications of LHTES systems, including hot water supply, solar greenhouse, space conditioning and so on.

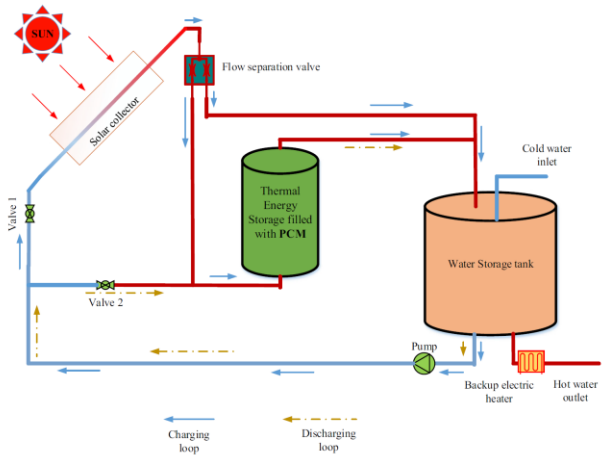

Fig. 1.2. A proposed loop for the LHTES to assist a solar hot water system [4].

One of the barriers to the commercial and large-scale applications of the LHTES system is the unsatisfactory charging and discharging rates mainly due to the low thermal conductivity of most PCMs. Researchers have put numerous efforts to improve thermal behaviour from different research directions. Finned tube [7-10] and highly conductive additives embedded in

PCM [11-15] are the main enhancement techniques to improve the thermal conductivity of bulk-packed PCM in LHTES system. Highly conductive additives include metal particles, metal foam, metal sheet, exfoliated graphite, carbon fibre, or carbon brush. While encapsulations of PCM (most with size above 1 mm for thermal energy storage), a technology of holding PCM separately to increase overall system heat transfer rates, have also attracted increasingly researching interests. Salunkhe and Shembekar [16] reviewed research efforts of examining effects of PCM encapsulation on phase change and thermal behaviour of the energy storage system. Thermal performances of LHTES system are generally determined by system design parameters, properties of PCM, heat transfer fluid (HTF) operating parameters, and environmental conditions. Liu et al. [17] summarized mathematical and numerical approaches to analyse phase change process and heat transfer mechanisms of various geometrical capsules and packages of PCMs. Their study sought to assist researchers to select the appropriate methodology for investigating the LHTES system. Li [18] conduct a detailed survey of the enhancement techniques of LHTES systems. He highlighted the significance of taking the entropy generation into account when investigating the shell-and-tube type LHTES system.

The shell-and-tube LHTES system is the most intensely-studied solar energy storage system [19], due to its compact structure with minimal heat loss, high efficiency and low manufacturing cost. Typically, the shell-and-tube system consists of an outer cylindrical shell and an inner tube parallel to the shell central axis. Either PCM is loaded in shell side and heat transfer fluid (HTF) flows in tube side, or vice versa. The fluid flowing through the unit serves as the working medium to transfer thermal energy to the PCM or carry energy away from the PCM. Lacroix [20] developed a two-dimensional numerical model considering effects of PCM natural convection and theoretically examined the thermal performance of a system with PCM in shell side and HTF in tube side. His research identified the sensitivity of system thermal performance to geometrical parameters and HTF working conditions. The reverse packing

model, i.e., PCM in tube side and HTF in shell side was examined by Esen and Ayhan [21]. Furthermore, Esen et al. [22] compared the thermal performance of the above two typical shell-and-tube packing configurations by means of numerical analysis. They examined the optimal radii of shell and tube to reduce melting time and it was concluded that the packing mode of PCM in shell side and HTF in tube side had higher heat transfer rate in melting process. Vyshak and Jilani [23] conducted a numerical investigation to compare the total PCM melting times of three geometrical configurations, rectangular slab, cylindrical container (i.e., PCM in tube side and HTF in shell side) and cylindrical shell container (i.e., PCM in shell side and HTF in tube side). They confirmed that the cylindrical shell container spent less melting time, compared with the rectangular slab and cylindrical tube container. But the last two publications drew conclusions based on numerical studies of the charging process and did not validate the numerical result with physical experiment and conduct discharging process studies.

Based on the research work on a shell and single-tube system, researchers studied the single-shell and multi-tube system, a configuration of multiple HTF tubes going through the PCM in shell to acquire extended heat transfer surface area. Agyenim et al. [19] compared thermal performance of a horizontal multi-tube system with the single tube system and found that the multi-tube configuration increased heat transfer rate in charging section and displayed different solid-liquid interface shape compared with the single tube. They also emphasized the needs of further studies of complicated properties of multi-tube arrangement. More recently Esapour et al. [24] numerically examined effects of tube numbers on melting times. They compared melting processes of one, two, three and four tube(s) and concluded that reductions of melting time were nonlinear when increasing heat transfer surface area. However, more research efforts need to be devoted to multi-tube systems, especially the vertically mounted system.

The above literature review showed that the heat transfer mechanism in the LHTES system was clear. The natural convection played an important role in the melting and solidification processes. However, there are still the following key research questions to be addressed: (1) How do the specific geometric parameters like the shell tilting angle affect natural convection, heat transfer and thermal performance in the vertical LHTES system? (2) Does an optimal shell-to-tube radius ratio exist in the shell-and-tube type LHTES system, which can best balance the charging and discharging performances? and (3) How does the tube arrangement influences natural convection and thermal performance in a multi-tube vertical LHTES system when the LHTES is scaled for practical use? These research questions form the basis of the research objectives in this study.

1.2. Research objectives

This research aims to study effects of geometric parameters and multiple-tube on heat transfer and thermal performance in the LHTES systems. It comprises the key components detailed as follows:

(1) Review the methodologies of studying the LHTES system, its configurations and arrangement and the state-of-the-art techniques for enhancing the energy storage based on PCM.

(2) Develop a comprehensive conjugate analytic model to integrate the HTF flow model, HTF tube model as well as PCM heat transfer and phase transition model to eliminate the constant HTF temperature boundary assumption used by the previous numerical investigations and investigate the thermal behaviour of LHTES systems.

(3) Investigate the effects of titling shell lateral surface and HTF operating parameters in a vertical shell-and-tube latent heat storage system on natural convection, heat transfer and thermal performance; And investigate the optimal shell-to-tube radius ratio in a vertical

cylindrical LHTES system under different correlated categories: varying the shell size with a fixed tube diameter and changing the tube size while holding the shell size.

(4) Experimentally investigate and visualize the heat transfer mechanism in PCMs in single tube and multi-tube LHTES systems.

(5) Experimentally study the efficacy of the developed heat transfer model by investigating the effects of the tube arrangement and operating parameters in the single and multiple-tube LHTES systems.

1.3. Thesis outline

Latent heat storage has the potential to play a critical role in the storage of solar thermal energy thanks to its promising energy-storage density and capacity. Among different techniques, the shell-and-tube type LHTES system is the most intensely investigated in literature due to its simplicity in design, structural compactness and low heat loss to the environment [25, 26]. To assess the current research status and identify research gaps, Chapter 2 carried out a comprehensive review on the shell-and-tube LHTES systems in respect of system configuration, design parameters and HTF operating conditions.

The literature review of Chapter 2 draws two main conclusions that (1) the configuration and design of an LHTES unit are critical to improve heat transfer inside the unit and (2) PCM natural convection not only exhibits a positive effect on enhancing thermal performance in an LHTES system, but also plays a vital role on understanding the heat transfer mechanism in PCM melting and solidification. *The part work of chapter 2 was published in Proceedings of the 5th International Conference on Polygeneration (ICP 2019), PP. 61-62, Fukuoka, Japan, 2019.*

The role of natural convection in the PCM prompted researchers to make use of natural convection to improve the heat transfer in the LHTES system. This chapter aims to investigate

the effect of tilting the lateral surface on the performance of a vertical LHTES system. The experimental results [27-29] demonstrated that the conical design contributes to a better melting performance. **Chapter 3** of this thesis was committed to the theoretical analysis of optimal tilting lateral surface angle in vertical cylindrical LHTES systems. This chapter developed a numerical model to solve the HTF, HTF tube and PCM storage zones in a whole domain. The validation work showed that the conjugate model could reliably reflect thermal characteristics of melting and solidification processes in a vertical shell-and-tube LHTES system. The numerical results revealed that the total melting time was decreased substantially with the tilting lateral surface angle increasing from 0° to 7°. On the other hand, the tilting lateral surface design was found to lower the solidification rate. An optimal tilting angle needs to balance the melting and solidification performance in an LHTES unit based on the practical conditions. The tilting lateral surface design is promising for areas with less sunshine hours to capture solar energy. *The findings of chapter 3 were published in the journal of Solar Energy 194, PP. 103-113, ELSEVIER, 2019.*

Significant research has been carried out to investigate the correlations between the thermal performance of an LHTES unit and its configuration and design. However, very limited studies obtained optimal design parameters based on investigating both energy storage and energy release processes. Chapters 4 and 5 focused on numerically investigating the effect of a critical parameter, the shell-to-tube radius ratio in vertical cylindrical LHTES systems, expecting to find an optimal radius ratio which could enhance both energy storage and release performance.

Chapter 4 investigated the effect of the shell-to-tube radius ratio through varying the shell radius while fixing the HTF-tube radius. It was found that the radius ratio range of 5-6 shows the best charging performance. However, a radius ratio greater than 5 significantly lowers the discharging performance. In the case of varying the shell radius, a radius ratio of 5 can best

balance the charging and discharging performance over a total charging-and-discharging duration of 24 h.

Following the work presented in chapter 4**, chapter 5** continued to investigate the effect of radius ratio, varied in a way that the HTF-tube radius is changed with the outer shell radius fixed. It was shown that a decrease in the radius ratio from 5 to 4 significantly enhances the charging and discharging rates while with minor influence on the energy storage capacity. Moreover, two sets of results in Chapters 4 and 5 demonstrate that the unit height exhibits a negligible influence on the optimal radius ratio selection. Combining data in Chapters 4 and 5, the radius ratio between 4 to 5 is proposed to be applied in a vertical shell-and-tube LHTES system to obtain the optimal charging and discharging performance. *The findings of chapters 4 and 5 were combined to be submitted for review to the journal of Solar Energy.*

Chapter 6 presents an experimental test of an in-house built multiple tube heat exchanger (MTHX), in which the tube spacing was set up according to the optimal radius ratio result deduced from Chapters 4 and 5.

The first aim of the experimental study is to verify a well-known numerical solution used in literature, which simplifies a three-dimensional multitube problem to a two-dimensional model by formulating a virtual single-tube domain. The verification was done by experimentally comparing thermal characteristics between the MTHX and the STHX (single-tube heat exchanger) which geometry agrees exactly with the virtual simplified domain formulated in the MTHX. It was found that the STHX and MTHX showed significant differences in the overall thermal behaviour. The study of the vertical multitube problem may need to rely on the experimental approach or three-dimensional numerical modelling to achieve precise and reliable results. The second aim is to examine the impacts of inner tube number and HTF operating parameters in the MTHX. The results show that more tubes in the vertical MTHX substantially improved both charging and discharging performance without inhibiting

the natural convection flow. *The part work of chapter 6 was published in Energy Procedia 160, PP. 332-339 2018. The main findings of chapter 6 will be submitted for review to the Journal of International Journal of Energy Research.*

Chapter 7 summarizes the major conclusions of this research and bring forward the possible future research directions on the PCM-based heat energy storage systems.

1.4. References

[1] Timilsina, G. R. , Kurdgelashvili, L. ,Narbel, P. A., Solar energy: Markets, economics and policies, Renew. Sust. Energ. Rev. 16 (2012) 449-465.

[2] Urban, F. ,Geall, S., Pathways Towards Renewable Energy in China: Prospects, Politics and Practices, STEPS Centre, (2014) 20-21.

[3] Ren21, Renewables 2019 Global Status Report, REN21 Secretariat, (2019) 110.

[4] Mahfuz, M. H. , Anisur, M. R. , Kibria, M. A. , Saidur, R. ,Metselaar, I. H. S. C., Performance investigation of thermal energy storage system with Phase Change Material (PCM) for solar water heating application, Int. Commun. Heat Mass. 57 (2014) 132-139.

[5] Zalba, B. , MaríN, J. M. , Cabeza, L. F. ,Mehling, H., Review on thermal energy storage with phase change: materials, heat transfer analysis and applications, Appl. Therm. Eng. 23 (2003) 251-283.

[6] Sharma, A. , Tyagi, V. V. , Chen, C. R. ,Buddhi, D., Review on thermal energy storage with phase change materials and applications, Renew. Sust. Energ. Rev. 13 (2009) 318-345.

[7] Ismail, K. , Alves, C. ,Modesto, M., Numerical and experimental study on the solidification of PCM around a vertical axially finned isothermal cylinder, Appl. Therm. Eng. 21 (2001) 53-77.

[8] Erek, A. , Ilken, Z. ,Acar, M. A., Experimental and numerical investigation of thermal energy storage with a finned tube, Int. J. Energy Res. 29 (2005) 283-301.

[9] Agyenim, F. , Eames, P. ,Smyth, M., A comparison of heat transfer enhancement in a medium temperature thermal energy storage heat exchanger using fins, Sol. Energy. 83 (2009) 1509-1520.

[10] Hosseini, M. , Rahimi, M. ,Bahrampoury, R., Thermal analysis of PCM containing heat exchanger enhanced with normal annular fines, MECHANICAL SCIENCES. 6 (2015) 221-234.

[11] Hamada, Y. , Ohtsu, W. ,Fukai, J., Thermal response in thermal energy storage material around heat transfer tubes: effect of additives on heat transfer rates, Sol. Energy. 75 (2003) 317-328.

[12] Zeng, J. , Sun, L. , Xu, F. , Tan, Z. , Zhang, Z. , Zhang, J. ,Zhang, T., Study of a PCM based energy storage system containing Ag nanoparticles, J. Therm. Anal. Calorim. 87 (2006) 371-375.

[13] Mettawee, E.-B. S. ,Assassa, G. M. R., Thermal conductivity enhancement in a latent heat storage system, Sol. Energy. 81 (2007) 839-845.

[14] Jegadheeswaran, S. , Pohekar, S. D. ,Kousksou, T., Performance enhancement of solar latent heat thermal storage system with particle dispersion—an exergy approach, CLEAN–Soil, Air, Water. 39 (2011) 964-971.
[15] Yang, J. , Yang, L. , Xu, C. ,Du, X., Experimental study on enhancement of thermal energy storage with phase-change material, Appl. Energy. 169 (2016) 164-176.
[16] Salunkhe, P. B. ,Shembekar, P. S., A review on effect of phase change material encapsulation on the thermal performance of a system, Renew. Sust. Energ. Rev. 16 (2012) 5603-5616.
[17] Liu, S. , Li, Y. ,Zhang, Y., Mathematical solutions and numerical models employed for the investigations of PCMs′ phase transformations, Renew. Sust. Energ. Rev. 33 (2014) 659-674.
[18] Li, G., Energy and exergy performance assessments for latent heat thermal energy storage systems, Renew. Sust. Energ. Rev. 51 (2015) 926-954.
[19] Agyenim, F. , Eames, P. ,Smyth, M., Heat transfer enhancement in medium temperature thermal energy storage system using a multitube heat transfer array, Renew. Energy. 35 (2010) 198-207.
[20] Lacroix, M., Numerical simulation of a shell-and-tube latent heat thermal energy storage unit, Sol. Energy. 50 (1993) 357-367.
[21] Esen, M. ,Ayhan, T., Development of a model compatible with solar assisted cylindrical energy storage tank and variation of stored energy with time for different phase change materials, Energy Conv. Manag. 37 (1996) 1775-1785.
[22] Esen, M. , Durmuş, A. ,Durmuş, A., Geometric design of solar-aided latent heat store depending on various parameters and phase change materials, Sol. Energy. 62 (1998) 19-28.
[23] Vyshak, N. ,Jilani, G., Numerical analysis of latent heat thermal energy storage system, Energy Conv. Manag. 48 (2007) 2161-2168.
[24] Esapour, M. , Hosseini, M. J. , Ranjbar, A. A. , Pahamli, Y. ,Bahrampoury, R., Phase change in multi-tube heat exchangers, Renew. Energy. 85 (2016) 1017-1025.
[25] Khan, Z. , Khan, Z. ,Ghafoor, A., A review of performance enhancement of PCM based latent heat storage system within the context of materials, thermal stability and compatibility, Energy Conv. Manag. 115 (2016) 132-158.
[26] Seddegh, S. , Wang, X. , Henderson, A. D. ,Xing, Z., Solar domestic hot water systems using latent heat energy storage medium: A review, Renew. Sust. Energ. Rev. 49 (2015) 517-533.
[27] Akgün, M. , Aydın, O. ,Kaygusuz, K., Thermal energy storage performance of paraffin in a novel tube-in-shell system, Appl. Therm. Eng. 28 (2008) 405-413.
[28] Aydın, O. , Akgün, M. ,Kaygusuz, K., An experimental optimization study on a tube‐in‐shell latent heat storage, Int. J. Energy Res. 31 (2007) 274-287.
[29] Seddegh, S. , Tehrani, S. S. M. , Wang, X. , Cao, F. ,Taylor, R. A., Comparison of heat transfer between cylindrical and conical vertical shell-and-tube latent heat thermal energy storage systems, Appl. Therm. Eng. 130 (2018) 1349-1362.

Chapter 2: A review of system configuration, design and operating conditions to enhance the performance of cylindrical latent heat thermal energy storage systems

2.1. Chapter summary

This chapter reviews the current research status and gaps, starting with briefing on the important thermal energy storage and latent heat storage methods. Then the chapter summarizes the research efforts and progresses on investigating system configurations, geometrical designs and HTF operating conditions in the shell-and-tube type heat exchanger. Finally, the current research status and gaps are outlined in the conclusion section.

2.2. Introduction

The thermal energy storage arises from a critical need to overcome the mismatch between energy demand and supply from renewable energy sources. Fig. 2.1 shows the three main energy storage techniques: thermochemical heat, sensible heat, and latent heat energy storage [1]. Thermochemical storage is achieved through a reversible chemical reaction to break and reunite molecular bonds of the working medium. Sensible heat storage relies on an increase in

temperature of the storage medium to store the thermal energy. The critical properties to evaluate a storage medium for sensible heat storage include the specific heat, density and temperature change range. Latent heat storage stores and releases thermal energy when its working medium undergoes phase transitions between solid and liquid, or liquid and gas. Compared to sensible heat storage, latent heat storage is more attractive due to its high storage density and relatively small working temperature range. Depending on the material property, phase transition can take place in the form of solid-liquid, liquid-gas, solid-gas, or solid-solid. In the perspective of latent heat storage application, the solid-liquid phase transition is more desirable due to the following factors, (1) a much smaller change in volume compared to liquid-gas or solid-gas phase transition, and (2) plenty of storage materials available, potentially meeting the diverse demands for heat storage [1, 2].

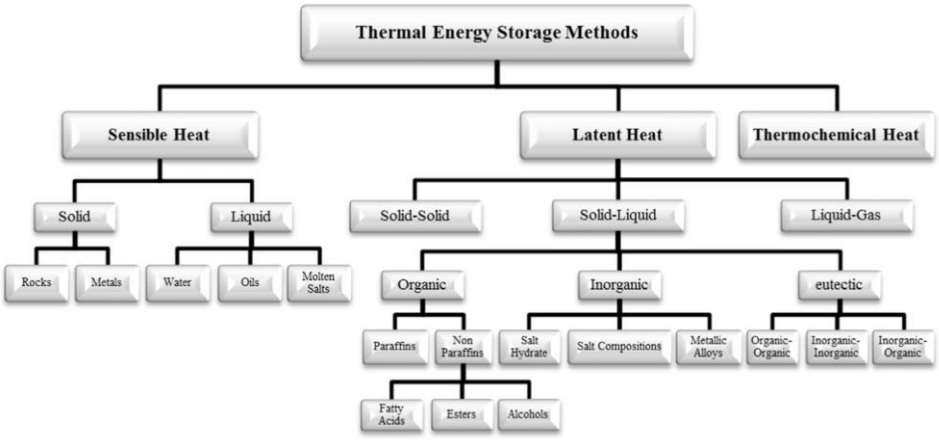

Fig. 2.1 Thermal energy storage techniques [1].

The low-temperature solar energy applications include solar air heaters, solar stills, solar domestic hot water, and etc. [3]. The studies [4-6] stated that the PCM with a phase transition temperature in the range of 50-70 °C are the promising selection to assist the solar energy storage, especially the solar domestic water heating. The commercial paraffin product RT60 [7], which perfectly matches the solar energy storage, is chosen as the storage medium in this study.

The recent methods for improving thermal performance in a PCM heat exchanger include the enhancement on thermal conductivity of the heat exchanger and optimizations in system configuration and design. The thermal conductivity enhancements comprise the addition of fins and the embedding of highly conductive materials like metal foam, graphite composite, or nanomaterials into PCM. Comparatively, the optimizations in system configuration, design parameters and HTF operating conditions will not lead to the use of expensive highly conductive material and in turn a reduction in the energy storage capacity and density [8, 9]. These advantages motivate this study to focus on investigating the effects of geometrical designs and HTF operating conditions and optimizing the design parameters in the shell-and-tube LHTES system. This chapter presents a detailed survey of research efforts committed to investigating system configuration, geometrical designs, and the effects of HTF operating conditions.

The system configuration, geometrical design parameters and HTF operating conditions are key aspects which significantly affect the heat transfer rate in the LHTES system. In this study, the system configuration involves the PCM packing modes and unit orientation. The geometrical design parameters are comprised primarily of the shell lateral surface tilting angle, the shell-to-tube radius ratio and the eccentricity of the inner-tube. The HTF operating conditions include the HTF injection side, the HTF mass flow rate and inlet temperature. The following sections survey the studies in respect of these categories.

2.3. Configuration of a cylindrical LHTES system

2.3.1 The PCM packing modes

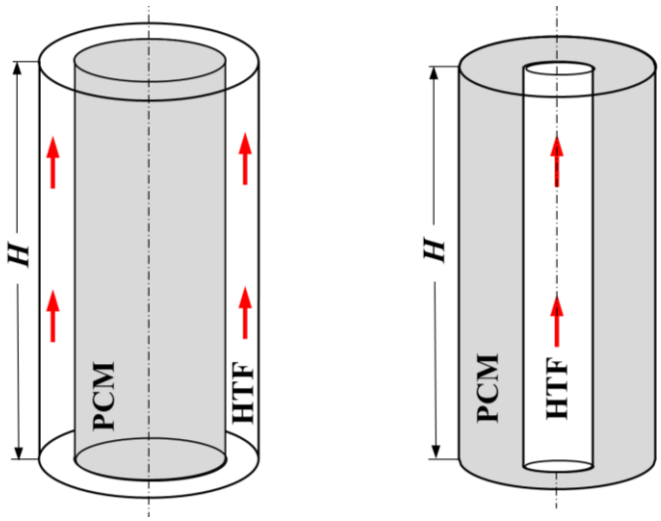

Fig. 2.2. Schematic of PCM packing modes, left: the cylinder mode (PCM in tube side) and right: the pipe mode (PCM in shell side) [10].

Fig. 2.2 shows the schematic drawing of two PCM packing modes, the cylinder and pipe modes, which were introduced by Esen et al. [10] in a numerical analysis to compare the performance of PCM packing arrangements. Their results showed the pipe mode, i.e., PCM packed in the shell side can store much more energy under a given melting duration. Tao et al. [11] investigated the two PCM packing modes in horizontal LHTES systems with overall dimensions, the PCM amount and the operating conditions kept the same. The numerical data demonstrated the cylinder mode melts PCM faster, resulting in a higher heat storage rate.

Han et al. [12] compared the two PCM packing modes in both horizontally and vertically mounted LHTES systems. All the studied cases were configured with the constant PCM amount and heat transfer surface area. The horizontal cylinder mode was found to be superior with the melting time reduced by 23.5%.

It is evident that there is still limited research endeavour on the two PCM packing arrangements. In the meantime, the available studies present no results on the solidification process and the effect of HTF flow. The Reynolds number and HTF flow state vary substantially between the two arrangements and the needs to explore these key effects on thermal performance still exist.

2.3.2 The system orientation

PCM thermal behaviour in a cylindrical LHTES system is sensitive to the system orientation (horizontal, vertical, or inclined) as the liquid PCM flowing pattern and path are remarkably affected by system orientations. These flowing patterns and paths affect the convection heat transfer which plays significant roles in PCM heat transfer. A pioneering effort investigating the system orientation was conducted by Hasan [5, 6] in experimental studies, in which a cylindrical storage system contained the PCM in the inner tube and heat transfer fluid, water flowed along the annulus. It was shown that the horizontal placement of the system showed higher melting and solidification rates over the vertical placement. Sari and Kaygusuz [13] presented a similar result through an experimental study, demonstrating that the horizontal shell-and-tube rig was more desirable due to faster charging and discharging cycles. However, the earlier literature [5, 6, 13] provided very limited discussions on this topic.

Seddegh et al. [14] numerically compared the horizontal and vertical configurations in the shell-and-tube LHTES systems. The results showed that the horizontally mounted unit presented a superior thermal performance when undergoing a part-load charging. Comparatively, the vertical configuration featured less fluctuation in charging and discharging rates.

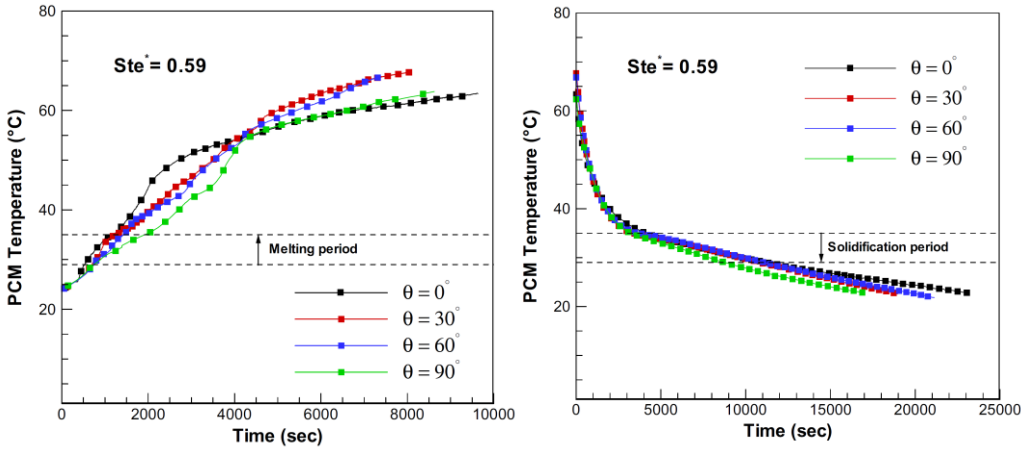

Fig. 2.3. Experimental results of PCM average temperature during melting (left) and solidification (right) [15].

Kousha et al. [15] experimentally and numerically studied melting and solidification processes in a shell-and-tube heat exchanger with various inclination angles 0°, 30°, 60° and 90°. Fig. 2.3 shows the measured PCM temperatures during melting and solidification cycles under different inclination angles. It is noted that the orientation angle influences the melting cycle more significantly than the solidification, due to the different dominate mode of heat transfer between the cycles. On the other hand, the numerical data indicate the horizontal configuration delivers the highest heat transfer rate during melting while the vertical one does the same during solidification.

The effect of system orientation may be influenced by the thermal conductivity enhancement applied in PCM side, as revealed by an experimental study [16], which embedded the copper foam into the PCM. The horizontal rig was observed to have longer charging and discharging durations compared to the vertical one. This phenomenon was attributed to the presence of metal foam and its influence on PCM natural convection.

The above literature indicates that the effect of the PCM storage orientation deviates between charging and discharging and also correlates with the conductive enhancement technique applied in the PCM side. More investigations are expected to reveal the potential influence of the system orientation.

2.4. Geometrical designs

The thermal characteristic of an LHTES unit is affected by various design and operating parameters. A primary goal of this work is to evaluate the potential of the designs without using highly conductive materials on influencing the strength of PCM natural convection. Such designing aspects identified through literature review include the shell tilting angle, the shell-to-tube radius ratio, and the eccentric tube placement.

2.4.1 Tilting shell/tube lateral surface in a vertical LHTES system

Except for the system configuration, the LHTES enclosure and HTF-tube shapes can also critically affect the thermal response of LHTES systems by facilitating natural convection flow in the PCM. Particularly in the vertical LHTES system, natural convection flow transports hot melted PCM upwards and thus substantially accelerates the heat transfer rate in the unit upper section. This prompted researchers to tilt the shell or tube lateral surface such that more PCM is packed to the upper section in the PCM unit. Fig. 2.4 shows schematics of the conventional straight design, the conical shell and the conical tube.

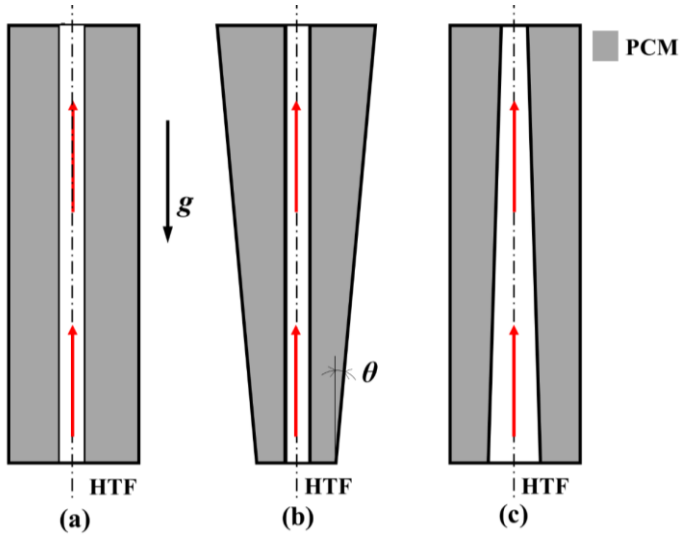

Fig. 2.4. (a) vertically straight design, (b) conical shell, and (c) conical tube.

Akgün et al. [9] built two different cylindrical LHTES rigs to investigate the melting and solidification processes. One unit was vertically straight and another was inclined by an angle of 5° in the lateral surface. The conical design shortened the total melting time by 30% compared with the vertically straight design with the same HTF flow conditions operated.

In another experimental study by Aydın et al. [17], the effects of lateral surface tilt angles on the melting cycle were examined. Five units with different tilt angles 0°, 5°, 10°, 15° and 20° while containing the same amount of PCM were constructed. The results indicated that an increase in the tilt angle from 0° to 5° led to a 40% decrease in melting time.

Recently, Seddegh et al. [18] experimentally compared the thermal performances between the straight shell-and-tube unit and the conical one with a tilting angle of 15°. The energy storage process in the conical unit was found to be 15% quicker than in the straight unit, while the solidification processes showed no significant difference in terms of the discharged energy and total solidification time.

Hu et al. [19] developed a two-dimensional numerical model to study the PCM melting characteristics in rectangle latent heat storage units with various tilt vertical side angles. Their work revealed appropriate length ratios (corresponding to different tilting angles) could accelerate the melting progress and the optimal length ratio was obtained based on the evaluations of full melting time and heat transfer intensity.

Apart from the conical shell design, tilting the HTF-tube lateral surface also received a few research attentions. Korawan et al. [20] reported the numerical comparison of the melting performances between the straight and conical tubes (shown in Fig. 2.4 a and c respectively). The conical tube spent 6130 s for the liquid fraction to increase to 1, melting 25.3% faster than the straight tube. Similar findings were reported in a subsequent study by Korawan et al. [21], in which the conical tube design spent 40% less charging time compared to the conventional straight tube design. However, the studies [20, 21] on the conical HTF-tube design lack analysing the influence of the conical tube on the HTF flow conditions.

The studies reviewed indicate that tilting the outer shell or the inner tube is a very promising technique to accelerate the melting process and enhance the energy storage rate. This is important for solar energy storage. As sunlight varies substantially during the daytime, accelerating the storage rate during the melting process would offer faster capture of solar thermal energy, which is especially beneficial to areas with low sunshine hours. However, the research works available mostly relied on experimental studies to deal with particular designs.

There is lack of research that addresses the comprehensive theoretical analysis of the effect of tilting lateral surface angle in the vertical LHTES system.

2.4.2 Effect of radius ratio in an LHTES system

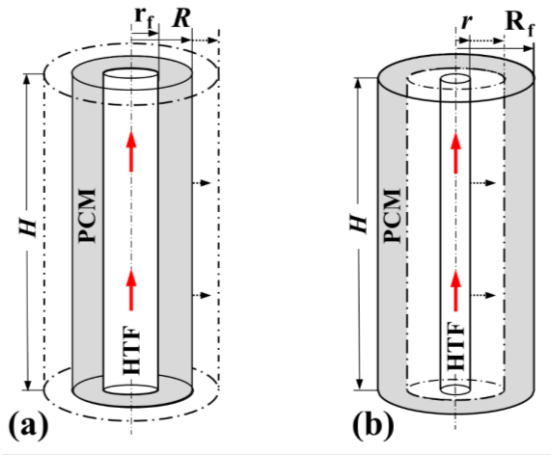

Fig. 2.5. Schematic of the *R*/r definition in cylindrical LHTES system, (a) varying the shell radius or (b) varying the tube radius.

Fig. 2.5 shows the schematic of the *R*/r definition in cylindrical LHTES system. Along with varying the *R*/*r*, a variation in the unit height (*H*) or length (*L*) is always considered. The potentials in the *R*/r designs to improve the thermal response have been examined in a horizontal or vertical LHTES system.

Cao and Faghri [22] conducted a pioneering study to numerically investigate the influences of radius ratio (r_o/D) and length-to-diameter ratio (L/D) in a horizontal cylindrical LHTES system. The results indicated a larger value of r_o/D considerably decreased the energy storage density, while a larger value of L/D effectively boosted the latent heat stored. Cao et al. [23] further numerically compared two types of cylindrical horizontal LHTES systems, one with HTF flowing through the annular channel and another with HTF flowing through both central and annular channels. It was stated a greater L/D in both types of storage units increased the total stored heat but dramatically decreased the heat storage density. Lacroix [24]'s numerical

study signalled the significance of the shell radii and working conditions on enhancing the thermal performance in a horizontal cylindrical PCM storage unit.

Conti et al. [25] conducted a numerical analysis to investigate the factors which affected the Second-Law efficiency in a horizontal PCM storage system. They found a higher L/D ($\geqslant$ 45) under a constant radius ratio of 2.6 enabled a minimal entropy generation number. Tao et al. [26] claimed that in a series of horizontal storage units with the same PCM amount packed, a larger HTF-tube radius led to a lower HTF flow velocity and in turn a longer melting time. Wang et al. [27] found that an increase in R/r contributed to a reduction in both the energy efficiency ratio and the heat storage rate in a horizontal cylindrical LHTES module, but the reducing effect turned less significant when R/r surpassed a certain value. A subsequent study by the same authors [28] indicated that an increase in the shell length L accelerated the heat storage rate but lowered the energy efficiency ratio in a horizontal finned-tube module, whereas the shell radius showed a more pronounced effect on the thermal responses than the shell length.

Ezan et al. [29] experimentally compared the charging and discharging capabilities of horizontal shell-and-tube units with different inner-tube and shell radii. The results revealed the shell diameter greatly influenced the total stored energy. Erek and Dincer [30] numerically studied the thermal characteristics of a horizontal cylindrical PCM storage and stated that a larger shell radius improved the exergy efficiency.

The geometrical designs in vertical LHTES systems also received a lot of research efforts. Ismail and Melo [31] examined the roles of geometrical parameters including H/r_0 and R_0/r_0 in vertical cylindrical LHTES units. The correlation between the mean heat transfer rate and R_0/r_0 was formulated and it was noted that a rise in H/r_0 or R_0/r_0 resulted in a longer melting time. Ismail and Abugderah [32] reported that the stored sensible and latent heat energy was nearly linearly in proportion with the height variation in a vertical LHTES system and the PCM layer

thickness (shell radius) substantially influenced the complete melting time. Trp et al. [33] experimentally studied effects of L/D and r_o/D on charging and discharging processes. They concluded that the selection of geometrical parameters was highly determined by the required heat transfer rate and the energy storage/release time. Seddegh et al. [34] experimentally compared the thermal performances of vertical LHTES units with different R/r. The R/r of 5.4 was recommended as the optimal selection.

Ismail and Goncalves [35] numerically studied the solidification cycle in a cylindrical LHTES unit. The optimal outer-to-inner radius ratio of 4 was obtained based upon an enthalpy and pure conduction numerical model. Guo and Zhang [36] stated that the complete discharging duration in a high-temperature PCM application turned to be less sensitive to the HTF-tube dimension when it increased to a certain value. Fang et al. [37] conducted a series of parametric studies of a cylindrical LHTES unit without taking account of the effect of PCM natural convection. It was reported that the volume ratio of PCM to the whole unit played a key role in obtaining the maximum effective energy storage ratio.

Through surveying the available research works investigating the R/r in the shell-and-tube LHTES system, the following limitations and gaps can be identified, (1) Evaluating the effect of geometrical designs was made based only on investigating a sole energy storage process, energy charging or discharging; (2) PCM natural convection was not taken into account; and (3) Most studies presented general trends in thermal performance from the impacts of R/r without obtaining the optimal design.

2.4.3 Eccentric tube placement in a horizontal cylindrical LHTES

Similar as the tilting shell lateral surface in a vertical LHTES system, the eccentric tube placement in a horizontal cylindrical LHTES system seeks to increase the PCM region exposed to convection flow and in turn improving the heat transfer to PCM. Fig. 2.6 shows the

schematic of eccentric HTF-tube placement in a horizontal cylindrical system. The eccentricity of inner HTF-tube, ε is defined as,

$$\varepsilon = \frac{l}{R} \tag{2.1}$$

Where l stands for the vertical distance between the HTF-tube and shell centres and R is the shell inner radius.

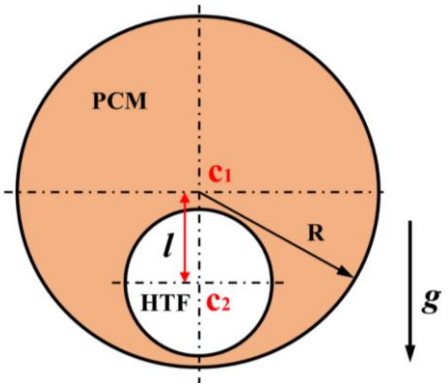

Fig. 2.6. Eccentric HTF-tube placement in a horizontal cylindrical LHTES system.

Zhang and Faghri [38] in 1997 used the analytical solution to investigate the effect of the eccentric placement in the inner tube. More recently, some studies were committed to investigating impacts of the eccentricity of inner tube combined with factors such as inclination angle, tube size or multitube. Dutta et al. [39] experimentally and numerically studied the heat transfer in a horizontal annulus, in which the inner tube was placed both eccentrically and inclined. The numerical results revealed the maximum heat flux through the inner tube surface was achieved when the eccentricity of inner tube increased to 0.5.

Pahamli et al. [40] claimed that moving the inner pipe downward in a horizontal shell-and-tube heat exchanger led to a significant acceleration in the melting rate. The authors used a similar physical model to carry out a subsequent numerical study [41], which observed 33%, 57% and 64% decreases in RT 50 melting time as the eccentricity of the inner tube (ε) reached 0.25, 0.5 and 0.75 respectively.

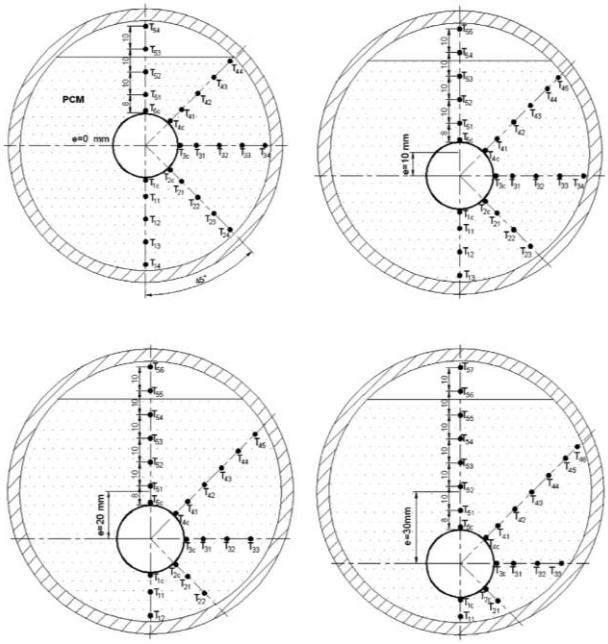

Fig. 2.7. Thermocouple positions in different eccentricities [42].

Yusuf Yazıcı et al. [42, 43] employed paraffin wax as the storage medium in a horizontal shell-and-tube rig and experimentally investigated the charging and discharging performances under different inner tube eccentricities. The different positions of inner tube and thermocouples are shown in Fig. 2.7. It was found that a vertically downward move in the inner-tube placement resulted in faster melting rate, while an eccentric position either upward or downward resulted in an undesirable longer solidification time. The finding confirmed the negative effect on the freezing rate by an eccentric annulus structure, reported in an earlier study [38]. The numerical analysis by Darzi et al. [44] also agreed that a downward placed inner tube contributed to a shorter PCM melting duration.

Dhaidan et al. [45] performed the experimental and numerical investigations of the melting process within a horizontal annular cavity. They applied the high conductivity nanoparticle into the storage medium n-octadecane to enhance the melting rate. A concentric shell and tube arrangement in the experiment recorded higher temperatures in the upper region of the cavity, whereas a lower tube placement with $\varepsilon = 0.5$ in the numerical examination was found to save the melting time by 18.7%, compared to the concentric arrangement.

With the assistance of the Lattice Boltzmann numerical scheme, Jourabian et al. [46] concluded that the inner tube moved to the bottom of a horizontal annulus could maximize the PCM melted fraction. Li et al. [47] claimed that eccentricity and size of the inner tube influenced the strength of natural convection, the solid-liquid interface evolution, and the total melting rate.

The effect of eccentric placement of multiple inner tubes was analysed by Esapour et al. [48]. The numerical result revealed that when the inner tube number stays the same, the lower placement of tubes leads to the increased melted PCM volume and thus accelerates the melting process.

Zheng et al. [8] proposed a numerical model combing the fixed-grid and enthalpy double-porosities approaches to investigate the melting and solidifying performances in horizontal LHTES units with the different eccentricities of inner tube. The authors stated that when the charging process was evaluated alone, the optimal eccentricity, which had the shortest melting duration, was found to correlate linearly with the Rayleigh number. On the other hand, with both the charging and discharging processes evaluated, the optimal eccentricity could only be obtained provided that the ratio of the solidifying Rayleigh number to the melting Rayleigh number was greater than 2.0.

The summarised works in this section agree that the lower eccentricity in inner tube contributes significantly to accelerating the melting cycle due to the increased convection heat transfer. Meanwhile, the eccentricity either upward or downward brings negative impact to the PCM solidification. Based on the practical application, the optimal eccentricity should balance the charging and discharging performances. Zheng et al. [8]' work reveals the optimal eccentricity selection also depends on the HTF working conditions operated during charging and discharging.

2.5. Effect of operating conditions

The temperature and mass flow rate of the HTF delivered to the PCM storage component fluctuate at various levels over time depending on the practical working scenario and solar energy applications. It is evident that the studies of HTF operating conditions will provide valuable information on performance optimization in an LHTES system.

2.5.1 Effect of the HTF inlet side in an LHTES system

Fig. 2.8 presents the schematic of top and bottom HTF injections in a vertical LHTES system [49]. The studies [12, 50] show the HTF flow direction affects the magnitude of the effect of PCM natural flow, particularly in the charging process dominated by convection heat transfer. In addition, as discussed earlier in this chapter, the cylinder and pipe modes substantially affect the HTF flow state and Reynolds number, therefore, the effect of HTF injection side may be significantly different between the two PCM packing modes.

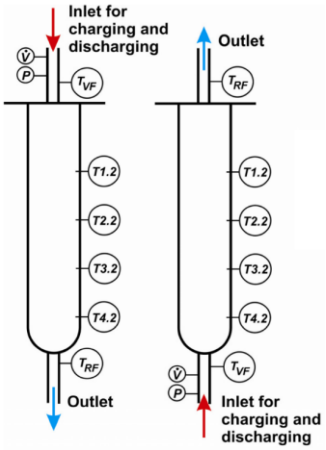

Fig. 2.8. Top and bottom HTF injections in a vertical PCM storage rig [49].

Gong and Mujumdar [51] reported a pioneering study on the HTF flow direction in a shell-and-tube type LHTES unit. Based on a conduction-controlled numerical model, they concluded that a consecutive charging and discharging process with the HTFs circulating from the same end exhibited faster heat storage and release rates than the process in which the HTFs were

introduced from the different ends. Ettouney et al. [52] investigated the effects of HTF flow directions through an experimental study in a vertical shell-and-tube LHTES system. The results and analysis showed the upward HTF flow led to more effective natural convection during melting than the downward HTF flow.

Through both experimental and numerical trials, Longeon et al. [50] claimed that a top HTF injection during charging was favourable for the thermocline form in PCM and then resulted in a stronger natural convection flow. The HTF injection side played a less important role on heat transfer during discharging, but the bottom HTF injection could facilitate the liquid PCM to refill the voids resulted from the PCM volume change during phase transition. Therefore, the study recommended that the charging process employed a top HTF injection while the discharging did the opposite.

Marin et al. [53] tested the thermal response of a vertical LHTES unit with two inner-HTF-tube installed to facilitate a simultaneously charging and discharging operation. It was found that the heat transfer was enhanced when the hot and cold HTFs flowed at the same direction, i.e., circulated into the LHTES unit from the same end, either top or bottom side.

Urschitz et al. [49] tested a vertical finned-tube LHTES system and found that the PCM melted faster with the hot HTF flowing downward. Martinelli et al. [16]'s experimental study showed that a top HTF injection in a vertical LHTES could achieve 1.6 times faster melting and solidification sections compared to a bottom injection.

Han et al. [12] employed solar salt as the PCM and air as the HTF to numerically investigate the effect of different HTF inlets in LHTES systems. They concluded that the bottom HTF inlet showed superior performance in the PCM melting rate and energy storage rate in the vertical pipe model. In contrast, the bottom HTF inlet showed no difference in the total melting duration between the horizontal and vertical cylinder models.

The survey within this section indicates most of the works were committed to the melting process in vertical LHTES systems. The available studies present contradictory concluding remarks and there is a need to further clarify the effect of HTF inlet side.

2.5.2 Effect of HTF flow rate in a cylindrical LHTES

The HTF mass flow rate determines the HTF flow regime, i.e., lamina flow, turbulent flow or the transition flow. It is one of the most important parameters affecting the overall heat transfer coefficient between HTF and PCM thus significantly influences the heat transfer rate. A higher HTF mass flow rate enhances the charging and discharging rates, as shown in the works [14, 54, 55]. But it also leads to increased mechanical energy consumed for circulating the HTF and a decreased temperature difference between HTF inlet and outlet. This indicates a trade-off in setting HTF mass flow rate is essential for an LHTES system to achieve optimal performance. An experimental study [56] found that a variation in the Reynolds number during the charging process showed a more pronounced effect on the average heat transfer coefficient than the same variation during the discharging process

With a transient two-dimensional mathematical model developed, Wang et al. [57] carried out a numerical study on the working conditions in a PCM thermal energy storage system. The total charging and discharging times were found to decrease nonlinearly versus increases in the HTF mass flow rate.

It can be deduced from Wang et al.'s work [27] that an LHTES may have an optimal flow rate in relation to the energy efficiency ratio, defined as the heat stored by PCM for per unit of mechanical energy consumed by HTF during phase change. The results showed that the energy efficiency ratio achieves the maximum value once Reynolds number amounts to 2100 and then decreases along with Reynolds number continually increasing. The numerical work by Wang et al. [28] revealed that once the Reynolds number exceeds a specific threshold, its effects start

to conflict between on the energy efficiency ratio and on heat storage rate. It was suggested to maintain the HTF flow in laminar region to achieve the balanced performance.

Seddegh et al. [34] stated that increase in HTF mass flow rate affects the heat transfer coefficient between the HTF and the tube and its enhancement effect on the heat transfer to PCM will be limited by heat transfer coefficient between the PCM and the tube. This finding is supported by a recent study [58], which claimed that the promotion effect in HTF flow velocity was more effective when PCM side thermal transfer was enhanced by fins or metal foam. Mahfuz et al. [59] reported an increase in HTF flow rate from 0.033 to 0.167 kg/min boosted the energy efficiency (η) from 63.88% to 77.41% whereas resulted in an undesirable reduction from 9.58% to 6.02% in the exergy efficiency (ε). Trp et al. [33] reported that Reynolds number less than 2000 showed small influence on the total thermal energy stored or released in an LHTES system.

The survey in this section suggests the following research gaps regarding the HTF flow rate to be filled by future work: (1) the different influences on charging and discharging resulted from varying the HTF flow rate, and (2) how the effect of HTF flow rate correlates with the thermal conductivity of PCM region.

2.5.3 Effect of HTF inlet temperature in a cylindrical LHTES

As the difference between the initial temperature of PCM and inlet temperature of HTF increases, the heat transfer rate in the LHTES significantly enhances. A considerable number of studies have been dedicated to examining the effect of HTF inlet temperatures on the thermal characteristics of the LHTES.

Rathod and Banerjee [55] reported an experimental study in which the total time for PCM liquid fraction to reach 1 increased by 78.5% when HTF inlet temperature changed from 85°C to 75°C in a vertical shell-and-tube LHTES system. A subsequent experimental work by the

same team [60] found that even an increase of 5°C in the HTF inlet temperature (from 80°C to 85°C) led to a significant reduction in the charging time regardless of whether fin was present.

An experimental study by Seddegh et al. [34] indicated that an increase of 10 °C in the HTF charging temperature (from 70 to 80 °C) significantly decreased the total charging time by between 54% to 68% among cylinders with different radius ratios. However, the subsequent discharging processes presented a minor difference in durations following being charging with different temperatures. This means the complete charging and discharging time was determined mostly by the charging temperature.

Avci and Yazici [61] carried out charging and discharging tests in a horizontal storage component to study phase transition characteristics of paraffin (P56-58) subject to different HTF temperatures. The charging tests were run with the water inlet temperatures of 75 °C, 80 °C and 85 °C while the discharging with temperatures of 20 °C, 25 °C and 30 °C. Both melting and solidification processes were seen to speed up with a higher difference in temperature between PCM and HTF. Following more tests on different eccentricities of the inner tube in the same experimental rig, Yusuf Yazıcı et al. [42] confirmed the enhanced effects of higher inlet temperature on the melting rate.

Establishing a two-dimensional numerical model based on enthalpy theory, Tao and He [62] analysed the non-steady inlet conditions of HTF on melting performance in water/n-octadecane LHTES system. An increase from 30 °C to 90 °C in the initial HTF inlet temperature resulted in a significant 51.9% decline in the melting time but decreased the total TES capacity evaluated during one hour of charging. Moreover, the variation in the initial inlet mass flow rate from 2.0 E-4 to 8.0 E-4 kg/s shorten the melting time by ~36.5% while showed a marginal effect on the TES capacity of PCM.

In summary, all reviewed studies confirm an increase in the temperature difference between the PCM and HTF brings a significant boost to the heat transfer rate in the LHTES.

However, most studies evaluate the effect of inlet temperatures on a separate charging or discharging process rather than a consecutive charging and discharging process. Besides, the results in literature [62] demonstrate that future research efforts are expected to access the non-steady HTF working condition on the phase transition characteristics.

2.6. Conclusions

This chapter summarises the studies of the system configuration, geometrical parameters and HTF operating conditions in the shell-and-tube type LHTES system. The research gaps and limitations are highlighted for each factor reviewed and the concluding remarks are drawn as follows,

(1) The system configuration, geometrical design and operating conditions effectively influence heat transfer within an LHTES unit. The optimization on these factors is preferable because it will not incur any cost on expensive highly conductive materials. This reviewing outcome further validates the necessity to address the research question (RQ) 1 and partially fulfills the research objectives (ROs) 1 and 3.

(2) Natural convection exhibits a positive effect to heat transfer and plays a dominated role in PCM melting. An improvement in the heat exchanger configuration and design can strengthen the effect of natural convection (RQ 1 and RO 3).(3) The PCM storage orientation shows different (positive or negative) effects between the charging and discharging performances and its influence also correlates with the thermal conductivity enhancement technique applied in the PCM side (RQ 1 and RO 2).

(4) It is expected for the future study to compare the pipe and cylinder modes with the effects of the Reynolds number and HTF flow state to be considered (RO 2).

(5) It is essential to evaluate both charging and discharging performances to determine an optimal design in system orientation and geometry. Moreover, it is important to simultaneously

assess the HTF working conditions when evaluating the design parameters (RQs 1 and 2, as well as RO 3).

2.7. References

[1] Seddegh, S., Wang, X., Henderson, A. D. ,Xing, Z., Solar domestic hot water systems using latent heat energy storage medium: A review, Renew. Sust. Energ. Rev. 49 (2015) 517-533.

[2] Regin, A. F., Solanki, S. C. ,Saini, J. S., Heat transfer characteristics of thermal energy storage system using PCM capsules: A review, Renew. Sust. Energ. Rev. 12 (2008) 2438-2451.

[3] Du, K., Calautit, J., Wang, Z., Wu, Y. ,Liu, H., A review of the applications of phase change materials in cooling, heating and power generation in different temperature ranges, Appl. Energy. 220 (2018) 242-273.

[4] Shukla, A., Buddhi, D. ,Sawhney, R. L., Solar water heaters with phase change material thermal energy storage medium: A review, Renew. Sust. Energ. Rev. 13 (2009) 2119-2125.

[5] Hasan, A., Phase change material energy storage system employing palmitic acid, Sol. Energy. 52 (1994) 143-154.

[6] Hasan, A., Thermal energy storage system with stearic acid as phase change material, Energy Conv. Manag. 35 (1994) 843-856.

[7] RT60 Data Sheet. Rubitherm Technologies GmbH, (2019).

[8] Zheng, Z.-J., Xu, Y. ,Li, M.-J., Eccentricity optimization of a horizontal shell-and-tube latent-heat thermal energy storage unit based on melting and melting-solidifying performance, Appl. Energy. 220 (2018) 447-454.

[9] Akgün, M., Aydın, O. ,Kaygusuz, K., Thermal energy storage performance of paraffin in a novel tube-in-shell system, Appl. Therm. Eng. 28 (2008) 405-413.

[10] Esen, M., Durmuş, A. ,Durmuş, A., Geometric design of solar-aided latent heat store depending on various parameters and phase change materials, Sol. Energy. 62 (1998) 19-28.

[11] Tao, Y. B., Liu, Y. K. ,He, Y.-L., Effects of PCM arrangement and natural convection on charging and discharging performance of shell-and-tube LHS unit, Int. J. Heat Mass Transf. 115 (2017) 99-107.

[12] Han, G.-S., Ding, H.-S., Huang, Y., Tong, L.-G. ,Ding, Y.-L., A comparative study on the performances of different shell-and-tube type latent heat thermal energy storage units including the effects of natural convection, Int. Commun. Heat Mass. 88 (2017) 228-235.

[13] Sari, A. ,Kaygusuz, K., Thermal energy storage system using stearic acid as a phase change material, Sol. Energy. 71 (2001) 365-376.

[14] Seddegh, S., Wang, X. ,Henderson, A. D., A comparative study of thermal behaviour of a horizontal and vertical shell-and-tube energy storage using phase change materials, Appl. Therm. Eng. 93 (2016) 348-358.

[15] Kousha, N., Hosseini, M. J., Aligoodarz, M. R., Pakrouh, R. ,Bahrampoury, R., Effect of inclination angle on the performance of a shell and tube heat storage unit – An experimental study, Appl. Therm. Eng. 112 (2017) 1497-1509.

[16] Martinelli, M., Bentivoglio, F., Caron-Soupart, A., Couturier, R., Fourmigue, J.-F. ,Marty, P., Experimental study of a phase change thermal energy storage with copper foam, Appl. Therm. Eng. (2016).
[17] Aydın, O., Akgün, M. ,Kaygusuz, K., An experimental optimization study on a tube‐in‐shell latent heat storage, Int. J. Energy Res. 31 (2007) 274-287.
[18] Seddegh, S., Tehrani, S. S. M., Wang, X., Cao, F. ,Taylor, R. A., Comparison of heat transfer between cylindrical and conical vertical shell-and-tube latent heat thermal energy storage systems, Appl. Therm. Eng. 130 (2018) 1349-1362.
[19] Hu, Z., Li, A., Gao, R. ,Yin, H., Effect of the length ratio on thermal energy storage in wedge-shaped enclosures, J. Therm. Anal. Calorim. 117 (2014) 807-816.
[20] Korawan, A. D., Soeparman, S., Wijayanti, W. ,Widhiyanuriyawan, D., 3D numerical and experimental study on paraffin wax melting in thermal storage for the nozzle-and-shell, tube-and-shell, and reducer-and-shell models, Modelling and Simulation in Engineering. 2017 (2017).
[21] Korawan, A. D., Soeparman, S., Wijayanti, W. ,Widhiyanuriyawan, D., Increased Melting Heat Transfer in the Latent Heat Energy Storage from the Tube-and-Shell Model to the Combine-and-Shell Model, Modelling and Simulation in Engineering. 2017 (2017).
[22] Cao, Y. ,Faghri, A., Performance characteristics of a thermal energy storage module: a transient PCM/forced convection conjugate analysis, Int. J. Heat Mass Transf. 34 (1991) 93-101.
[23] Cao, Y., Faghri, A. ,Juhasz, A., A PCM/forced convection conjugate transient analysis of energy storage systems with annular and countercurrent flows, J Heat Transf. 113 (1991) 37-42.
[24] Lacroix, M., Numerical simulation of a shell-and-tube latent heat thermal energy storage unit, Sol. Energy. 50 (1993) 357-367.
[25] Conti, M., Bellecci, C. ,Charach, C., Thermodynamic design of a phase change thermal storage module, Journal of solar energy engineering. 118 (1996) 89-96.
[26] Tao, Y.-B., Li, M.-J., He, Y.-L. ,Tao, W.-Q., Effects of parameters on performance of high temperature molten salt latent heat storage unit, Appl. Therm. Eng. 72 (2014) 48-55.
[27] Wang, W.-W., Wang, L.-B. ,He, Y.-L., The energy efficiency ratio of heat storage in one shell-and-one tube phase change thermal energy storage unit, Appl. Energy. 138 (2015) 169-182.
[28] Wang, W.-W., Wang, L.-B. ,He, Y.-L., Parameter effect of a phase change thermal energy storage unit with one shell and one finned tube on its energy efficiency ratio and heat storage rate, Appl. Therm. Eng. 93 (2016) 50-60.
[29] Ezan, M. A., Ozdogan, M. ,Erek, A., Experimental study on charging and discharging periods of water in a latent heat storage unit, Int. J. Therm. Sci. 50 (2011) 2205-2219.
[30] Erek, A. ,Dincer, I., An approach to entropy analysis of a latent heat storage module, Int. J. Therm. Sci. 47 (2008) 1077-1085.
[31] Ismail, K. ,Melo, C., Convection‐based model for a PCM vertical storage unit, Int. J. Energy Res. 22 (1998) 1249-1265.
[32] Ismail, K. a. R. ,Abugderah, M. M., Performance of a thermal storage system of the vertical tube type, Energy Conv. Manag. 41 (2000) 1165-1190.
[33] Trp, A., Lenic, K. ,Frankovic, B., Analysis of the influence of operating conditions and geometric parameters on heat transfer in water-paraffin shell-and-tube latent thermal energy storage unit, Appl. Therm. Eng. 26 (2006) 1830-1839.

[34] Seddegh, S., Wang, X., Joybari, M. M. ,Haghighat, F., Investigation of the effect of geometric and operating parameters on thermal behavior of vertical shell-and-tube latent heat energy storage systems, Energy. 137 (2017) 69-82.
[35] Ismail, K. ,Goncalves, M., Thermal performance of a PCM storage unit, Energy Conv. Manag. 40 (1999) 115-138.
[36] Guo, C. ,Zhang, W., Numerical simulation and parametric study on new type of high temperature latent heat thermal energy storage system, Energy Conv. Manag. 49 (2008) 919-927.
[37] Fang, Y., Niu, J. ,Deng, S., Numerical analysis for maximizing effective energy storage capacity of thermal energy storage systems by enhancing heat transfer in PCM, Energy Build. 160 (2018) 10-18.
[38] Zhang, Y. ,Faghri, A., Analysis of Freezing in an Eccentric Annulus, Journal of Solar Energy Engineering. 119 (1997) 237-241.
[39] Dutta, R., Atta, A. ,Dutta, T. K., Experimental and numerical study of heat transfer in horizontal concentric annulus containing phase change material, The Canadian Journal of Chemical Engineering. 86 (2008) 700-710.
[40] Pahamli, Y., Hosseini, M. J., Ranjbar, A. A. ,Bahrampoury, R., Analysis of the effect of eccentricity and operational parameters in PCM-filled single-pass shell and tube heat exchangers, Renew. Energy. 97 (2016) 344-357.
[41] Pahamli, Y., Hosseini, M. J., Ranjbar, A. A. ,Bahrampoury, R., Inner pipe downward movement effect on melting of PCM in a double pipe heat exchanger, Applied Mathematics and Computation. 316 (2018) 30-42.
[42] Yusuf Yazıcı, M., Avcı, M., Aydın, O. ,Akgun, M., Effect of eccentricity on melting behavior of paraffin in a horizontal tube-in-shell storage unit: An experimental study, Sol. Energy. 101 (2014) 291-298.
[43] Yazici, M. Y., Avci, M., Aydin, O. ,Akgun, M., On the effect of eccentricity of a horizontal tube-in-shell storage unit on solidification of a PCM, Appl. Therm. Eng. 64 (2014) 1-9.
[44] Darzi, A. R., Farhadi, M. ,Sedighi, K., Numerical study of melting inside concentric and eccentric horizontal annulus, Appl. Math. Model. 36 (2012) 4080-4086.
[45] Dhaidan, N. S., Khodadadi, J., Al-Hattab, T. A. ,Al-Mashat, S. M., Experimental and numerical investigation of melting of NePCM inside an annular container under a constant heat flux including the effect of eccentricity, Int. J. Heat Mass Transf. 67 (2013) 455-468.
[46] Jourabian, M., Farhadi, M., Rabienataj, D. a. A. ,Abouei, A., Lattice Boltzmann simulation of melting phenomenon with natural convection from an eccentric annulus, Therm. Sci. 17 (2013) 877-890.
[47] Li, S., Chen, Y. ,Sun, Z., Numerical simulation and optimization of the melting process of phase change material inside horizontal annulus, Energies. 10 (2017) 1249.
[48] Esapour, M., Hosseini, M. J., Ranjbar, A. A. ,Bahrampoury, R., Numerical study on geometrical specifications and operational parameters of multi-tube heat storage systems, Appl. Therm. Eng. 109 (2016) 351-363.
[49] Urschitz, G., Walter, H. ,Hameter, M., Laboratory test rig of a LHTES (Latent Heat Thermal Energy Storage): Construction and first experimental results, Journal of Energy and Power Engineering. 8 (2014).
[50] Longeon, M., Soupart, A., Fourmigué, J.-F., Bruch, A. ,Marty, P., Experimental and numerical study of annular PCM storage in the presence of natural convection, Appl. Energy. 112 (2013) 175-184.

[51] Gong, Z.-X. ,Mujumdar, A. S., Finite-element analysis of cyclic heat transfer in a shell-and-tube latent heat energy storage exchanger, Appl. Therm. Eng. 17 (1997) 583-591.
[52] Ettouney, H., El-Dessouky, H. ,Al-Kandari, E., Heat transfer characteristics during melting and solidification of phase change energy storage process, Industrial & engineering chemistry research. 43 (2004) 5350-5357.
[53] Marin, G., Murray, R. E. ,Groulx, D. The effect of inlet orientation on the phase change heat transfer in a vertical cylindrical latent heat energy storage system. Canadian Congress of Applied Mechanics (CANCAM) 2013, Saskatoon, Canada, 2013. 5.
[54] Kibria, M. A., Anisur, M. R., Mahfuz, M. H., Saidur, R. ,Metselaar, I. H. S. C., Numerical and experimental investigation of heat transfer in a shell and tube thermal energy storage system, Int. Commun. Heat Mass. 53 (2014) 71-78.
[55] Rathod, M. ,Banerjee, J., Experimental investigations on latent heat storage unit using paraffin wax as phase change material, Exp. Heat Transf. 27 (2014) 40-55.
[56] Sarı, A. ,Kaygusuz, K., Thermal and heat transfer characteristics in a latent heat storage system using lauric acid, Energy Conv. Manag. 43 (2002) 2493-2507.
[57] Wang, W.-W., Zhang, K., Wang, L.-B. ,He, Y.-L., Numerical study of the heat charging and discharging characteristics of a shell-and-tube phase change heat storage unit, Appl. Therm. Eng. 58 (2013) 542-553.
[58] Yang, X., Yu, J., Xiao, T., Hu, Z. ,He, Y.-L., Design and operating evaluation of a finned shell-and-tube thermal energy storage unit filled with metal foam, Appl. Energy. 261 (2020) 114385.
[59] Mahfuz, M. H., Anisur, M. R., Kibria, M. A., Saidur, R. ,Metselaar, I. H. S. C., Performance investigation of thermal energy storage system with Phase Change Material (PCM) for solar water heating application, Int. Commun. Heat Mass. 57 (2014) 132-139.
[60] Rathod, M. K. ,Banerjee, J., Thermal performance enhancement of shell and tube Latent Heat Storage Unit using longitudinal fins, Appl. Therm. Eng. 75 (2015) 1084-1092.
[61] Avci, M. ,Yazici, M. Y., Experimental study of thermal energy storage characteristics of a paraffin in a horizontal tube-in-shell storage unit, Energy Conv. Manag. 73 (2013) 271-277.
[62] Tao, Y. ,He, Y., Numerical study on thermal energy storage performance of phase change material under non-steady-state inlet boundary, Appl. Energy. 88 (2011) 4172-4179.

Chapter 3: Study of the effect of tilting lateral surface angle and operating parameters on performance of a vertical shell-and-tube latent heat energy storage system

3.1 Chapter summary

In this chapter, a comprehensive numerical model is developed to study the thermal energy storage performance in a vertical shell-and-tube latent heat thermal energy storage (LHTES) system with different tilting lateral surface angles under different operating conditions (Tables 3.1 and 3.2). This model integrates heat transfer in heat transfer fluid (HTF), HTF tube and phase change materials (PCM). It is first validated using experimental data and then applied to investigate the effect of tilting lateral surface angles on enhancement of natural convection in a vertical shell-and-tube LHTES system. The results show that increasing tilting lateral surface angle can significantly enhance heat transfer in the melting process whilst it has a negative effect on the solidification process. The total melting time reduces by 43% when the tilting angle increases from 0° to 7°. An optimal tilting angle is identified based on the trade-off between melting and solidification processes. Furthermore, the effect of HTF operating parameters on the performance of the LHTES system is evaluated. The analysis shows that for an HTF flow in laminar or transition flow regions increasing Reynolds number from 630 to 2500 for the tilting angle 4° results in 22% less meting time and 8.5% less solidification time. While increasing the HTF flow Reynolds number does not show significant effect under

turbulent flow regions. The variation of the HTF outlet temperature is also investigated. It is found that the temperature difference between HTF inlet and outlet is small at all studied HTF flow rates, which indicates that assumption of constant HTF surface temperature boundary in simulation models in the literature is reasonable for studying the heat transfer mechanism in PCMs of the vertical LHTES system.

The study within this chapter has been published as: Gang Shen, Wang Xiaolin, Andrew Chan, Feng Cao, Xiang Yin, "Study of the effect of tilting lateral surface angle and operating parameters on the performance of a vertical shell-and-tube latent heat energy storage system" Solar Energy Vol. 194 PP. 103-113, ELSEVIER, 2019. The remainder of the chapter is a direct transfer from the paper.

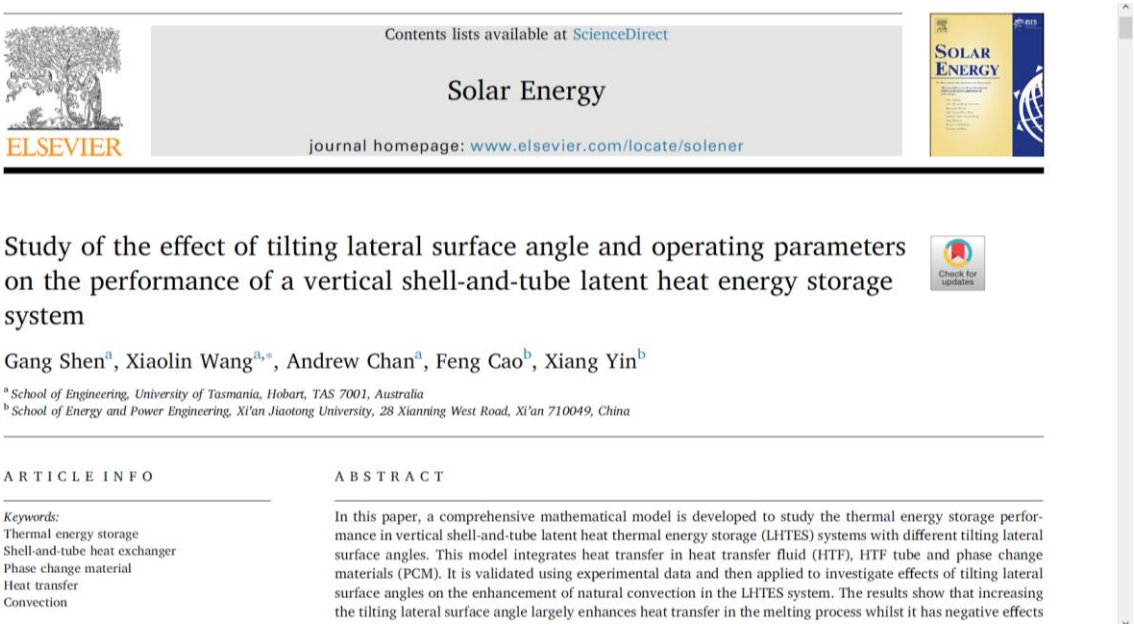

Contents lists available at ScienceDirect

Solar Energy

journal homepage: www.elsevier.com/locate/solener

Study of the effect of tilting lateral surface angle and operating parameters on the performance of a vertical shell-and-tube latent heat energy storage system

Gang Shen[a], Xiaolin Wang[a,*], Andrew Chan[a], Feng Cao[b], Xiang Yin[b]

[a] School of Engineering, University of Tasmania, Hobart, TAS 7001, Australia
[b] School of Energy and Power Engineering, Xi'an Jiaotong University, 28 Xianning West Road, Xi'an 710049, China

ARTICLE INFO

Keywords:
Thermal energy storage
Shell-and-tube heat exchanger
Phase change material
Heat transfer
Convection

ABSTRACT

In this paper, a comprehensive mathematical model is developed to study the thermal energy storage performance in vertical shell-and-tube latent heat thermal energy storage (LHTES) systems with different tilting lateral surface angles. This model integrates heat transfer in heat transfer fluid (HTF), HTF tube and phase change materials (PCM). It is validated using experimental data and then applied to investigate effects of tilting lateral surface angles on the enhancement of natural convection in the LHTES system. The results show that increasing the tilting lateral surface angle largely enhances heat transfer in the melting process whilst it has negative effects

3.2 Introduction

Latent heat thermal energy storage (LHTES) is an effective means to store solar thermal energy due to its high storage density, compactness and low energy loss (Seddegh et al., 2015). Among different LHTES techniques, the shell-and-tube LHTES system is the most intensely studied due to its design simplicity and minimal heat loss from the system (Khan et al., 2016).

Much research has investigated the effect of HTF flow configuration, operating and geometric parameters, and shell and tube configuration on the shell-and-tube LHTES system performance. Following the chronological development, Bellecci and Conti (1993a, 1993b)

investigated the size optimization of a horizontal solar receiver unit considering different shell radii. It was reported that the shell must be smaller than a certain size beyond which that part of PCM did not contribute to energy storage. Esen et al. (1998) established a two-dimensional enthalpy-method and investigated effects of PCM properties, cylinder and pipe radii, PCM volume and HTF working conditions on the performance of an LHTES system. Results showed that the configuration of HTF flowing through pipes embedded in the PCM required much less melting time than that for HTF flowing outside the PCM. Ismail and Melo (1998) investigated the relationship between thermal characteristics and geometrical parameters in a vertical cylindrical LHTES unit. Based on numerical results, a formula was proposed to correlate the mean heat transfer rate with the modified Rayleigh number, Stefan number and radius ratio. Ismail and Goncalves (1999) studied the effect of the shell-to-tube radius ratio on the thermal performance in a vertical LHTES system. The results showed that increasing the radius ratio slowed down the complete fusion and solidification. Trp et al. (2006) analysed the influence of operating conditions and geometric parameters on heat transfer in water-paraffin shell-and-tube LHTES systems. The analysis showed that the selection of operating conditions and geometrical parameters depended on the desired heat transfer rate and the time duration of energy stored or delivered. Aydın et al. (2007) experimentally examined the melting process in a series of vertical shell-and-tube LHTES units. Each unit was constructed with a specific lateral surface tilt angle. The results showed that the unit with a 5° tilt angle required 40% less melting time than the straight unit. Akgün et al. (2008) conducted experimental studies to investigate the melting and solidification processes in two vertical cylindrical LHTES units, one with a vertically straight lateral surface and the other with a lateral surface inclined by an angle of 5°. The total melting time for this conical unit reduced by 20%, compared with the vertically straight unit under the same conditions.

Recently, Rathod and Banerjee (2014, 2015) experimentally investigated the effect of HTF mass flow rate and temperature on the thermal performance of a shell-and-tube LHTES unit. The results showed that increasing the HTF mass flow rate and temperature decreased the melting time. Seddegh et al. (2018) experimentally compared the thermal performance of conical and straight vertical shell-and-tube units. The study showed that energy storage in the

conical unit was around 15% faster than that in the straight cylindrical unit. No significant difference was observed in the solidification process. Seddegh et al. (2017) further studied the effect of geometric parameters on the performance of an LHTES system. The experimental results revealed that the shell-to-tube radius ratio significantly influenced the PCM melting and solidification processes. An optimal shell-to-tube radius ratio, around 5.4 was observed in terms of melting and solidification times. Sciacovelli et al. (2013) reported that amid HTF turbulent flows, a variation in Reynolds number showed little impact on the heat transfer process in a vertical PCM storage unit. Seddegh et al. (2016) compared the performance of the horizontal and vertical shell-and-tube LHTES systems. The results indicated that the horizontal orientation has superior thermal performance during part-load energy charging. However, the vertical system can provide a more uniform charging or discharging rate.

The above literature review showed that the enclosure shape, system orientation, shell and tube arrangement, and HTF flow conditions all significantly affect the thermal performance of shell-and-tube LHTES systems. All these studies aimed to utilize the natural convection in the PCM to improve thermal performance by optimizing operating and geometric parameters of the LHTES system. In particular, in the vertical LHTES system, natural convection moves hot liquid PCM upwards and substantially increases the heat transfer rate in the upper section of the PCM unit. This motivated researchers to add more PCM in the upper section by tilting the lateral surface to form a conical vertical LHTES system. The studies (Aydm et al., 2007; Akgün et al., 2008; Seddegh et al., 2018) showed that this technique looks very promising to improve the LHTES thermal performance. However, these works were based on experimental studies for particular cases. There is no literature that provides comprehensive theoretical analysis on the effect of tilting lateral surface angle on the vertical LHTES system performance. In this chapter, a comprehensive thermal model is developed by integrating the HTF flow model, HTF tube conduction model and heat transfer model in the PCM. This model eliminates the constant HTF temperature boundary assumption for the PCM heat transfer model used in the previous simulation studies (Seddegh et al., 2016, 2017). It allows evaluation of the HTF flow behaviour and its effect on heat transfer in PCM, which has never been conducted in other literature. This proposed model is first validated using experimental data and then applied to investigate the

effect of tilting lateral surface angle and HTF operating parameters on thermal storage performance of the vertical LHTES system. The optimal tilting lateral surface angle is studied for both melting and solidification processes. Thereafter, the effect of the temperature difference between the HTF and PCM on the LHTES performance is evaluated. Furthermore, the effect of the HTF flow rate on the melting and solidification processes in the LHTES system is investigated when the HTF flow is in both laminar and turbulent flow regions. Finally, the HTF temperature difference between the HTF flow inlet and outlet is examined to investigate if the assumption of a constant HTF temperature bourndary in the literature (Seddegh et al., 2016, 2017) is reasonable. This study provides useful information for engineers and researchers in the design and optimization of a vertical LHTES system.

3.3 Mathematical model

3.3.1 Physical model

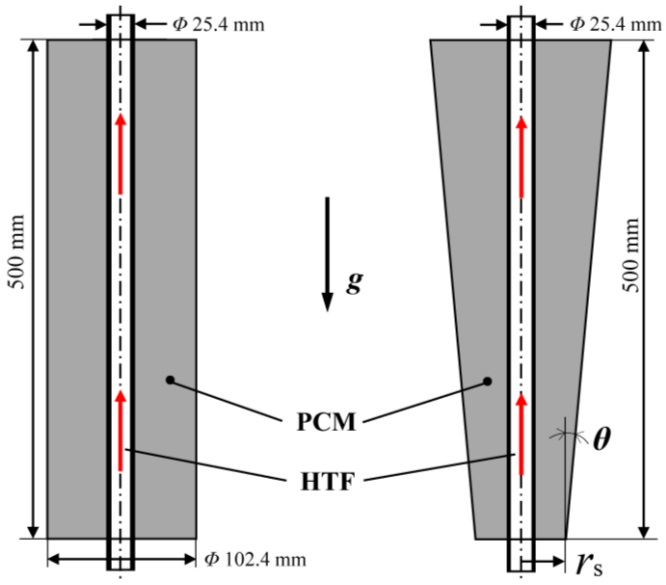

Fig. 3.1. Schematic drawing of the physical model. Left, the vertical straight LHTES system ($\theta=0$). Right, the conical LHTES system with a tilting lateral surface angle, θ.

Figure 3.1 shows the physical model of a vertical shell-and-tube LHTES system. A copper tube with an outer radius of 12.7 mm and a wall thickness of 1.2 mm is used as the HTF tube which size is kept constant for all studied cases. The lateral surface of the LHTES system can

be tilted with an angle θ. When θ is 0 degree, the unit is the conventional straight vertical cylindrical LHTES system which has a height of 500 mm and inside shell radius of 51.2 mm. When the angle θ varies to a specific value the height of the unit keeps the same as the straight vertical unit. The radius of the top surface increases and the radius of the bottom surface reduces. The LHTES system becomes a conical vertical system. The volume of the conical system at the upper part increases and at the lower part decreases. The actual volume of the conical vertical LHTES system is always maintained the same as that of the straight vertical system. The tilting angle can only vary from 0° to 7° according to the actual bottom and top surface to maintain the same annual volume in which 3.0 kg RT60 from the Rubitherm Technologies Gmbh is packed. Water is used as the HTF circulating from the bottom to the top of the LHTES heat exchanger. Table 3.1 shows the studied tilting angles and radii of the bottom surface. Table 3.2 lists the studied working conditions.

TABLE 3.1 Geometrical configurations of studied LHTES system

Case description	Tilting angle, θ (degree)	Container inner radius at the bottom end, r_s (mm)
Case 1	0	51.2
Case 2	2	42.2
Case 3	4	32.7
Case 4	5	27.7
Case 5	6	22.6
Case 6	6.5	20.3
Case 7	7	17.3

TABLE 3.2 Studied working conditions.

Working conditions	HTF inlet temperature (°C)	HTF average inlet velocity (m/s)
Melting	80	0.01, 0.04, 0.1, 0.4
	75	0.01

	70	0.01
Solidification	36	0.01, 0.04, 0.1, 0.4
	26	0.01
	16	0.01
	11	0.01

3.3.2. PCM properties

The PCMs with melting temperature between 50-70 °C is a promising selection for low-temperature heat applications (Seddegh et al., 2015a; Shukla et al., 2009; Hasan, 1994a, 1994b). Along with other factors considered including cost, reliability and availability, this study selects paraffin wax RT60 as the storage medium, which is manufactured by Rubitherm Technologies Gmbh (2019). As reported in the literature (Iten et al., 2017), the latent heat of the PCM is not distributed evenly across the broad phase temperature range during the heating and cooling processes. To accurately predict PCM melting and solidification behaviours, a variable specific heat is used in the present study to represent the PCM latent heat as suggested in the literature (Longeon et al., 2013; Xiao and Zhang, 2015). Figure 3.2 shows the variable specific heat of paraffin RT60. Table 3.3 lists the other properties.

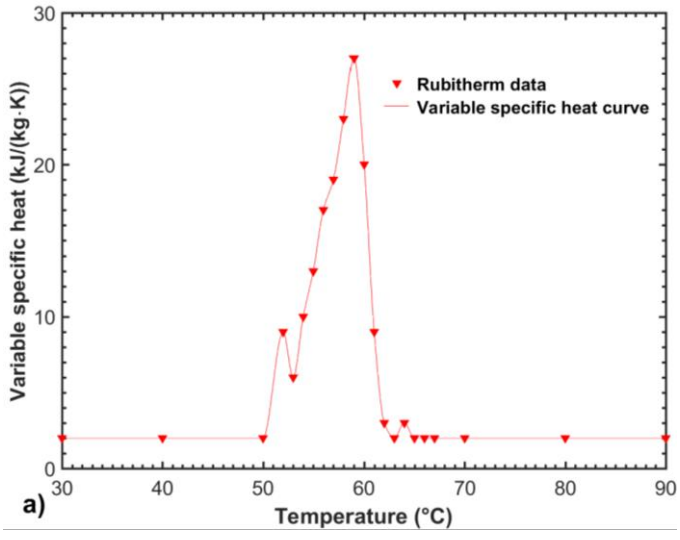

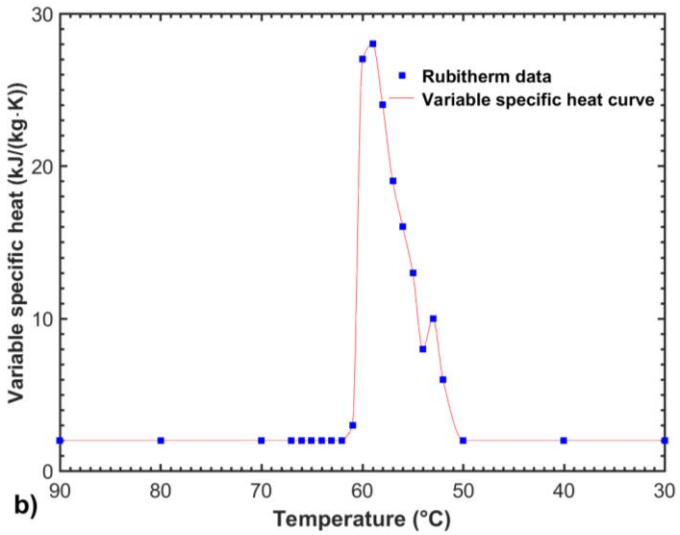

Fig. 3.2. Variable specific heat of RT60 at charging (a) and discharging (b) processes.

TABLE 3.3 Thermophysical properties of RT60 (Rubitherm Technologies Gmbh, 2019).

RT60 Properties	Value
Melting temperature range	55-61 °C
Solidification temperature range	61-55 °C
Average melting temperature	58 °C
Density, liquid (80 °C)	770 kg/m^3
Density, solid (15 °C)	880 kg/m^3
Thermal conductivity	0.2 W/(m·K)
Thermal expansion coefficient of liquid	0.76E-3 /K
Dynamic viscosity	3.08E-3 kg/(m·s)

3.3.3 Numerical model

A quasi-three-dimensional axisymmetric model is developed to simulate heat transfer and melting/solidification characteristics in vertical LHTES systems. The model incorporates three regions, the HTF zone, HTF tube wall and PCM in the annulus to allow examination of the HTF flow behaviour in both lamina and turbulent regions and its effect on PCM thermal characteristics. It can also help verify the validity of the constant HTF temperature boundary assumption used in previous numerical studies. A standard k-ε model is employed to calculate

the turbulent kinetic energy, the dissipation rate and turbulent viscosity in the HTF flow. The enthalpy method is applied for the numerical model. The assumptions of the numerical model are: i) PCM is incompressible and homogeneous. PCM volume change during phase transition is not considered; ii) viscous dissipation in liquid PCM motion is negligible; and iii) thermal properties of PCM are constant with temperature.

3.3.3.1 HTF model

For the HTF fluid flow, the model can be expressed by the following equations (Zheng et al., 2017).

Continuity equation:

$$\nabla\cdot\left(\rho_{\mathrm{w}}\vec{v}_{\mathrm{w}}\right)=0 \tag{3.1}$$

Momentum equation:

$$\rho_{\mathrm{w}}\left(\frac{\partial}{\partial t}\left(\vec{v}_{\mathrm{w}}\right)+\nabla\cdot\left(\vec{v}_{\mathrm{w}}\vec{v}_{\mathrm{w}}\right)\right)=\nabla\cdot\left(\left(\mu_{\mathrm{t}}+\mu_{\mathrm{w}}\right)\nabla\vec{v}_{\mathrm{w}}\right)-\nabla p_{\mathrm{w}}+\rho_{\mathrm{w}}g \tag{3.2}$$

Energy equation:

$$\frac{\partial\left(\rho_{\mathrm{w}}C_{p,\mathrm{w}}T_{\mathrm{w}}\right)}{\partial t}+\nabla\cdot\left(\vec{v}_{\mathrm{w}}\left(\rho_{\mathrm{w}}C_{p,\mathrm{w}}T_{\mathrm{w}}+p_{\mathrm{w}}\right)\right)=\nabla\cdot\left(\left(\frac{\mu_{\mathrm{t}}C_{p,\mathrm{w}}}{0.85}+k_{\mathrm{w}}\right)\nabla T_{\mathrm{w}}\right) \tag{3.3}$$

In Equations (2) and (3) $C_{p,\mathrm{w}}$, k_{w}, and μ_{w} are the HTF specific heat, thermal conductivity and dynamic viscosity, respectively. The HTF viscosity μ_{t} is computed by

$$\mu_{\mathrm{t}}=0.09\rho_{\mathrm{w}}\frac{k^2}{\varepsilon} \tag{3.4}$$

where k and ε are kinetic energy and the dissipation rate of turbulence kinetic energy, respectively. Equations. (1)-(4) are combined with the standard k-ε modelto solve the HTF flow.

3.3.3.2 HTF tube wall model

The energy equation for the tube wall is expressed by,

$$\rho_{\mathrm{wall}}\frac{\partial}{\partial t}\left(h_{\mathrm{wall}}\right)=k_{\mathrm{wall}}\nabla\cdot\left(\nabla T_{\mathrm{wall}}\right) \tag{3.5}$$

where the enthalpy of the tube wall h_{wall} is defined as

$$h_{\text{wall}} = \int_{T_{\text{ref}}}^{T_{\text{wall}}} C_{p,\text{wall}} dT \tag{3.6}$$

3.3.3.3 PCM model

The governing equations for PCM zoneare detailed below:

Mass conservation equation:

$$\frac{\partial \rho_{\text{P}}}{\partial t} + \nabla \cdot \left(\rho_{\text{P}} \vec{v}_{\text{P}} \right) = 0 \tag{3.7}$$

Momentum equation:

$$\rho_{\text{P}} \left(\frac{\partial}{\partial t} \left(\vec{v}_{\text{P}} \right) + \nabla \cdot \left(\vec{v}_{\text{P}} \vec{v}_{\text{P}} \right) \right) = \nabla \cdot \left(\mu_{\text{P}} \nabla \left(\vec{v}_{\text{P}} \right) \right) - \nabla p_{\text{P}} + \rho_{\text{P}} g + \vec{S} \tag{3.8}$$

Energy equation:

$$\frac{\partial \left(\rho_{\text{P}} H \right)}{\partial t} + \nabla \cdot \left(\rho_{\text{P}} \vec{v}_{\text{P}} H \right) = \nabla \cdot \left(k_{\text{P}} \nabla (T_{\text{P}}) \right) \tag{3.9}$$

In Equations (7)-(9), ρ_{P} and k_{P} are PCM density and thermal conductivity, respectively, $\vec{v}_{\text{P}}$ is the liquid PCM velocity, μ_{P} is PCM dynamic viscosity, p_{P} is the static pressure, $\vec{S}$ is the momentum sink term, and H is the total volumetric enthalpy given by,

$$H = h_{\text{var}} + \phi_{\text{l}} L \tag{3.10}$$

where L is the latent heat of PCM. The PCM latent heat is set to zero as the pure solvent melting heat is taken into account by the variable specific heat. h_{var} is the enthalpy given by Equation (11), and ϕ_{l} is liquid volume fraction defined by Equation (12).

$$h_{\text{var}} = h_{\text{ref}} + \int_{T_{\text{ref}}}^{T} C_{p,\text{var}} dT \tag{3.11}$$

$$\phi_{\text{l}} = \begin{cases} 0, & T \le T_{\text{P,solidus}} \\ \dfrac{T - T_{\text{P,solidus}}}{T_{\text{P,liquidus}} - T_{\text{P,solidus}}}, & T_{\text{P,solidus}} < T < T_{\text{P,liquidus}} \\ 1, & T \ge T_{\text{P,liquidus}} \end{cases} \tag{3.12}$$

where h_{ref} is the reference enthalpy evaluated at the reference temperature T_{ref} (298.15 K), and $C_{p,var}$ is variable specific heat and its value is shown in Figure 3.2. ϕ_l is between zero and one indicating the existence of a mushy zone, which is treated as a porous medium where porosity is equal to the liquid fraction. The momentum sink term $\vec{S}$ is expressed as follows (Fornarelli et al., 2016),

$$\vec{S} = \frac{(1-\phi_l)^2}{\phi_l^3 + \gamma} A_{cons} \vec{v}_P \tag{3.13}$$

where A_{cons} is the mushy zone constant, reflecting the steepness of the velocity decreasing to zero as the cell solidifies and γ is a small number (0.001) to avoid division by zero when the liquid fraction decreases to zero. In the present study A_{cons} is set as 10^5 according to the literature (Seddegh et al. 2016; Al-Abidi et al., 2013).

The Boussinesq approximation is used in the model. It assumes that PCM density is constant except for the body force term $\rho_P g$ in the Eqution (8), which is formulated as,

$$\rho_P g = \rho_o (1 - \beta(T - T_o)) g \tag{3.14}$$

where β is the volumetric thermal expansion coefficient, ρ_o is the liquid PCM density at the reference temperature T_o (80 °C).

The geometrical model and mesh are generated using ANSYS DesignModeler and Meshing applications, respectively, and the computational study is performed using Fluent 17.2 of ANSYS. The energy equations of the three zones are combined to solve in a whole domain. The SIMPLE algorithm is selected to accomplish the coupling relationship between cell pressure correction and velocity to solve the mass continuity equation. The Least Squares Cell-Based method and Second Order Upwind scheme are employed to calculate the variable gradients and face values, respectively. The PRESTO! procedure is chosen for pressure correction equations. The convergence levels for continuity, momentum and energy equations are 10^{-5}, 10^{-6} and 10^{-9}, respectively.

3.3.3.4 Boundary and initial conditions

For the HTF domain, the constant inlet velocities and temperatures are set as the inlet conditions. For the tube wall, the surfaces adjacent to HTF and PCM zones are defined as shear

no-slip and coupled energy transfer conditions. The two ends of the tube wall are set as an adiabatic boundary condition, along with PCM boundaries except for the surface adjacent to the HTF tube.

The initial temperature in the HTF zone is equal to the inlet temperature, whereas the initial temperatures in PCM and the tube wall are 54.8 °C for the melting process and 80.0 °C for the solidification process.

3.4 Model verifications and validation

The grid and time step sizes were first verified on the geometry with the tilting angle of 4°. The HTF inlet temperatures were set at 80 °C for the melting cycle and 36 °C for the solidification cycle and a constant HTF flow velocity 0.01 m/s was operated in both cycles. Four grid arrangements of 300 × 20, 300 × 40, 500 × 40, 1000 × 40 (axial grid number × radial grid number) in the PCM domain were evaluated with time steps of 0.05, 0.1 and 0.15 s during melting and 0.15, 0.25 and 0.35 s for solidification. The results showed that the grid arrangement of 500 × 40 with the time step of 0.1 s for melting and 0.25 s for solidification were appropriate to both maintain the accuracy in results and save the computing time.

The numerical model was validated using experimental results available in the literature (Longeon et al., 2013). The validation adopts the same geometric configuration, operating condition and PCM (RT35) as the experimental study in the literature. Water is used as the HTF which has an inlet temperature of 52 °C for charging and 19 °C for discharging, and has a flow velocity of 0.01 m/s. The geometric configuration is shown in Figure 3.3 (section view of the system). Figure 3.3 shows temperature comparisons between the experimental data and numerical predictions at three radial positions a1, a2, a3 in the shell-and-tube vertical LHTES system. The relative root-mean-square deviation (RRMSD) is used to measure the difference between the predicted and experimental temperatures. The maximum values of RRMSD for charging and discharging are 3% and 4.5%, respectively, indicating the numerical predictions agree well with the experimental data. The deviations in the solidification cycle can be

attributed to differences in the initial conditions between the simulation and the experiments. The numerical model set the uniform temperature across the domain, which was difficult to achieve in the experiment at the beginning of the solidification process (Longeon et al., 2013). However, this good agreement demonstrates that the established numerical model can reliably predict transient characteristics of heat transfer and liquid flow during the melting and solidification processes in the vertical LHTES system.

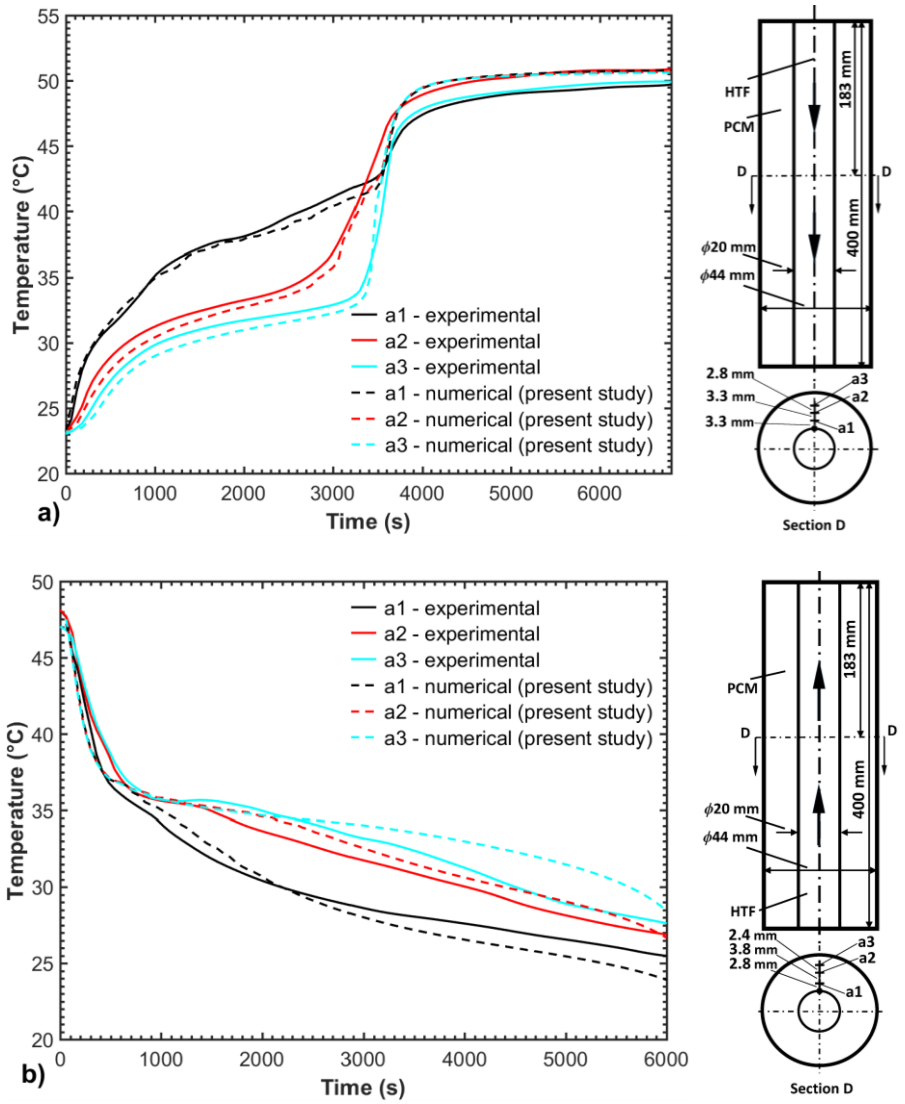

Fig. 3.3. Comparisons of the experimental and numerical results during (a) melting and (b) solidification cycles. The right-hand side drawings show the thermocouple positions in the experiments.

3.5 Results and discussion

3.5.1 Charging process

The thermal behaviour of the vertical LHTES system was first studied under different tilting lateral surface angles during the charging process, in which the HTF temperature and velocity at the system inlet are set at 80 °C and 0.01 m/s, respectively.

Figure 3.4 compares the liquid fraction and temperature contours of the PCM in the LHTES system with different tilting lateral surface angles at different melting times. The general trends for the four different cases are the same. As heat is transferred from the HTF to the PCM, the PCM adjacent to the HTF tube outer surface absorbs thermal energy and melts. The melted PCM around the HTF tube outer surface forms a liquid convection channel in which the liquid PCM moves upward. Liquid PCM gradually accumulates in the upper part of the system and the PCM melts downwards in the system. As the tilting lateral surface angle increases from 0° to 6°, the liquid channel size around the HTF outer surface increases indicating stronger natural convection. This implies that the system with a larger tilting angle has the potential to store energy faster. Furthermore, in comparison to the small tilting angle units, the temperature of the upper part PCM in the large tilting angle unit is lower while the temperature of the lower part PCM in the large tilting angle system is higher. This is mainly due to the amount of PCM packed in the system. As the tilting angle increases, the amount of PCM packed in the upper part increases and in the lower part decreases in the unit.

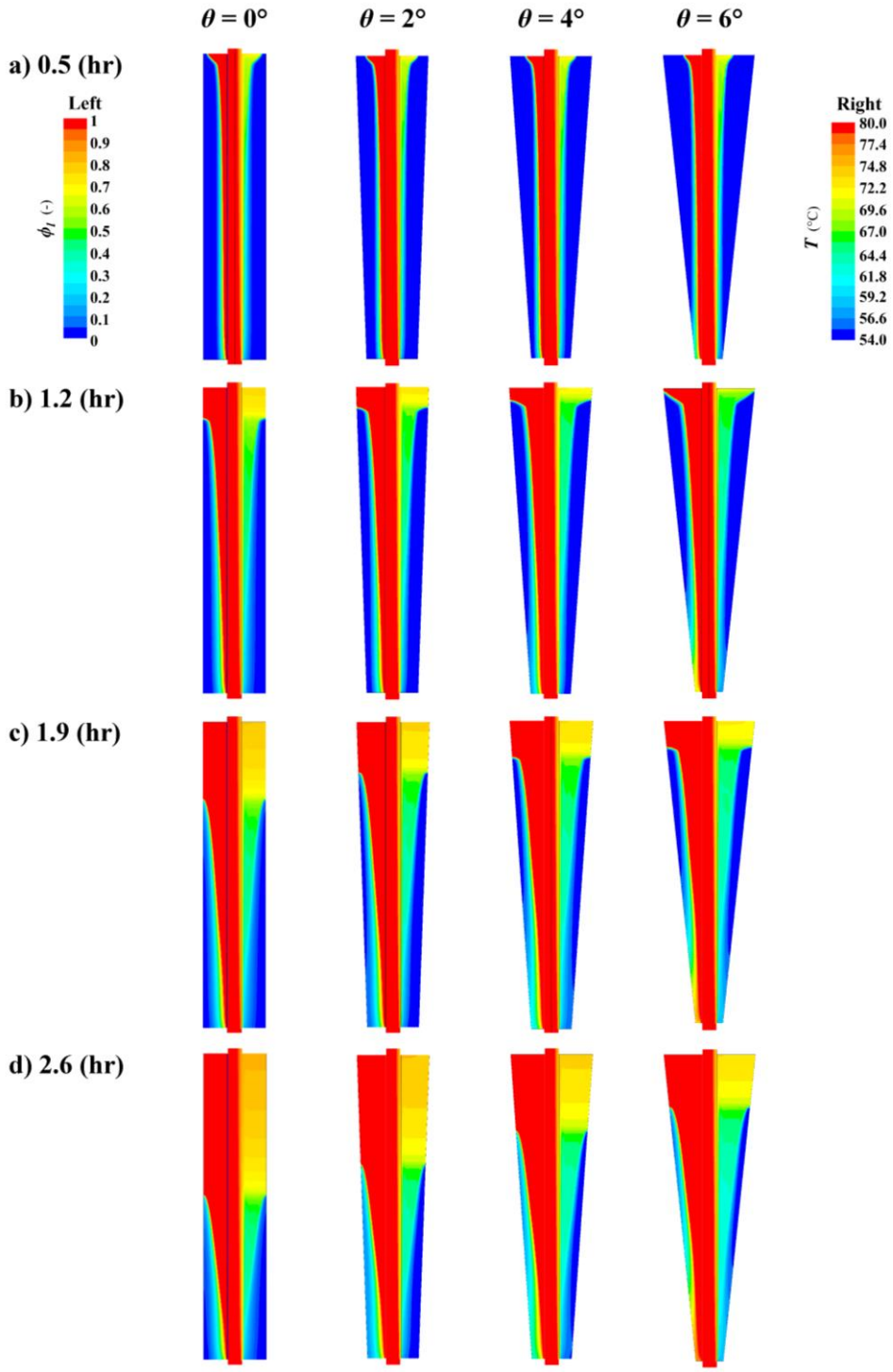

Fig. 3.4. PCM liquid fraction field (the left side of the symmetry axis) and temperature field (the right side of the symmetry axis) during the melting process.

Figure 3.5 shows the average PCM temperature in the LHTES system with different tilting angles. As the tilting angle increases from 0° to 7°, the average temperature of the PCM in the system initially decreases slightly. This is due to natural convection which causes more PCM

in the upper part to melt. Therefore, the average PCM temperature is lower for the large tilting angle unit with more PCM packed in the upper part. As more PCM melts (t >3 hrs), natural convection becomes stronger in the large tilting angle unit and more energy is transferred from the HTF to the liquid PCM. Therefore, the average PCM temperature increases quickly in the large tilting angle unit and becomes higher than that in the small tilting angle units. This further indicates that the natural convection in the large tilting angle system is more effective. These results are consistent with the finding obtained from the experimental study in the literature (Seddegh et al., 2018).

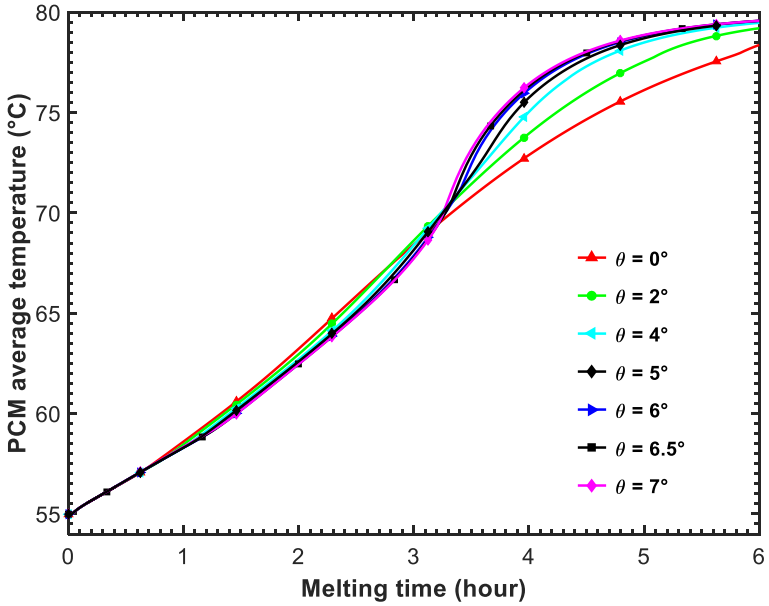

Fig. 3.5. PCM average temperature during the melting process.

Figure 3.6a shows the variation of liquid fraction under different tilting angles during the melting process. As the tilting angle increases from 0° to 7°, the total melting time (from the beginning of charging to the instant when all PCM melts) decreases from 5.8 to 3.2 hrs. This clearly demonstrates that tilting the lateral surface enhances natural convection and accelerates the PCM melting rate as more PCM is packed at the upper part of the system. However, the effect of the tilting angle on the melting process varies. As the tilting angle increases from 0° to 4°, the total melting time decreases by 28%. But the decreases in total melting time become less noticeable as the tilting angle increases from 4° to 7°. This finding is further evidenced by the energy storage fraction in Figure 3.6b.

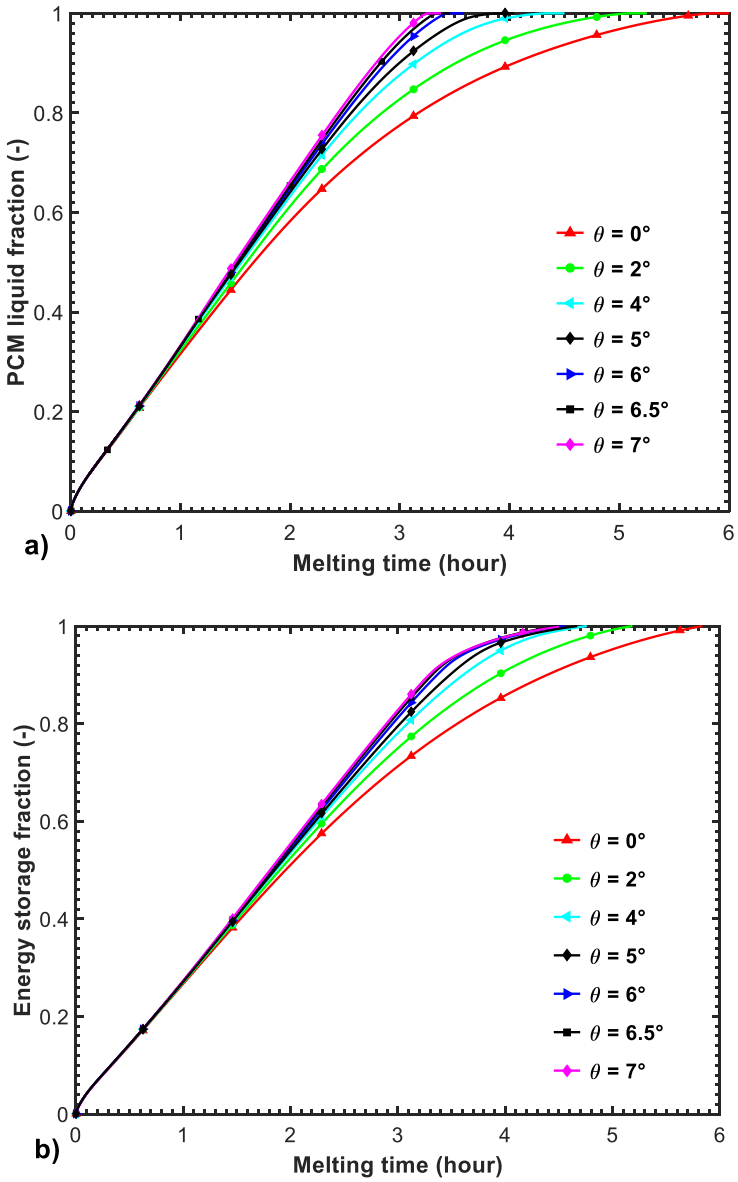

Fig. 3.6. The effect of the tilting angle on the performance of an LHTES system during the melting process, (a) PCM liquid fraction and (b) energy storage fraction. Note: The markers on curves which evolve against time only differentiate between the different curves and not stand for specific time points. This applies to the whole thesis unless otherwise specified.

Figure 3.6b shows the variation of energy storage fraction under different tilting angles. The energy storage fraction is defined as the ratio of the cumulatively stored energy at a time instant in a specific storage unit to the total stored energy at the end of melting in the LHTES system with a 0° tilting angle. Initially, the energy storage fraction in all units with different tilting angles is almost the same. This means that the same amount of energy is stored in all units. During this period, the PCM around the HTF outer surface absorbs energy from the HTF

and melts. The liquid PCM forms a vertical liquid circulation channel around the HTF tube. The PCM melting rate is almost the same. Once this vertical liquid circulation channel is formed, more and more liquid PCM moves upward and accumulates at the upper part of the unit. Natural convection becomes more effective in the upper part and hence more PCM melts in the storage units with large tilting angles. As the melting process continues, the energy storage fraction increases faster in the large tilting angle unit. Further analysis shows that this increasing rate is more significant in the small tilting angles (less than 4°) and is insignificant as the tilting angle is beyond 4° as shown in the Figure. The energy storage fraction increases to 1 at almost the same melting time of 4.6 hrs for the LHTES units with tilting angles between 4 and 7°. Compared to the analysis of the liquid fraction in Figure 3.6a, the results indicate that a tilting angle of 4° for the LHTES system can almost achieve the best energy storage performance. Further increase in the tilting angle will not substantially increase the energy storage performance of the LHTES system.

3.5.2 Solidification process

Figure 3.7a shows variation of the PCM liquid fraction in the studied LHTES systems during the solidification process, in which the HTF inlet temperature is set at 36 °C and HTF inlet velocity is 0.01 m/s. During the early solidification stage (t < 1 hour) the PCM liquid fraction plots show that no significant difference in the solidifying rate is observed across all the units. The energy transfer rate is almost the same for all the studied units during the early stage. As the solidification process continues beyond 2 hours, the liquid fraction in the large tilting angle unit decreases slower than that in the small tilting angle unit. This is due to the heat transfer mechanism. As the solidification process continues, the liquid PCM gradually solidifies and forms a solid PCM layer around the HTF tube outer surface. The solid PCM layer around the HTF tube surface gets thicker and thicker, increasing the thermal resistance between the HTF and the liquid PCM. Therefore, the thermal conduction dominates the heat transfer between the HTF and PCM. The energy transfer from the PCM to the HTF is then dominated by two factors, the thickness of the solid PCM around the HTF tube and the solid-liquid front length. Once the bottom PCM solidifies in the system, for the conical unit which packs less PCM at the bottom section, the solid-liquid front shrinks and the interface length decreases. As

the tilting angle increases, the solid-liquid front length shrinks fast and heat transfer slows. As a result, the liquid PCM in the large tilting angle unit solidifies slower than that in the small tilting angle unit. As shown in Figure 3.7a, the total solidification time increases from 10.0 to 18.8 hrs as the tilting angle increases from 0° to 4°. The total solidification time is calculated from the beginning of solidification to the time instant when PCM liquid fraction drops to 0.01.

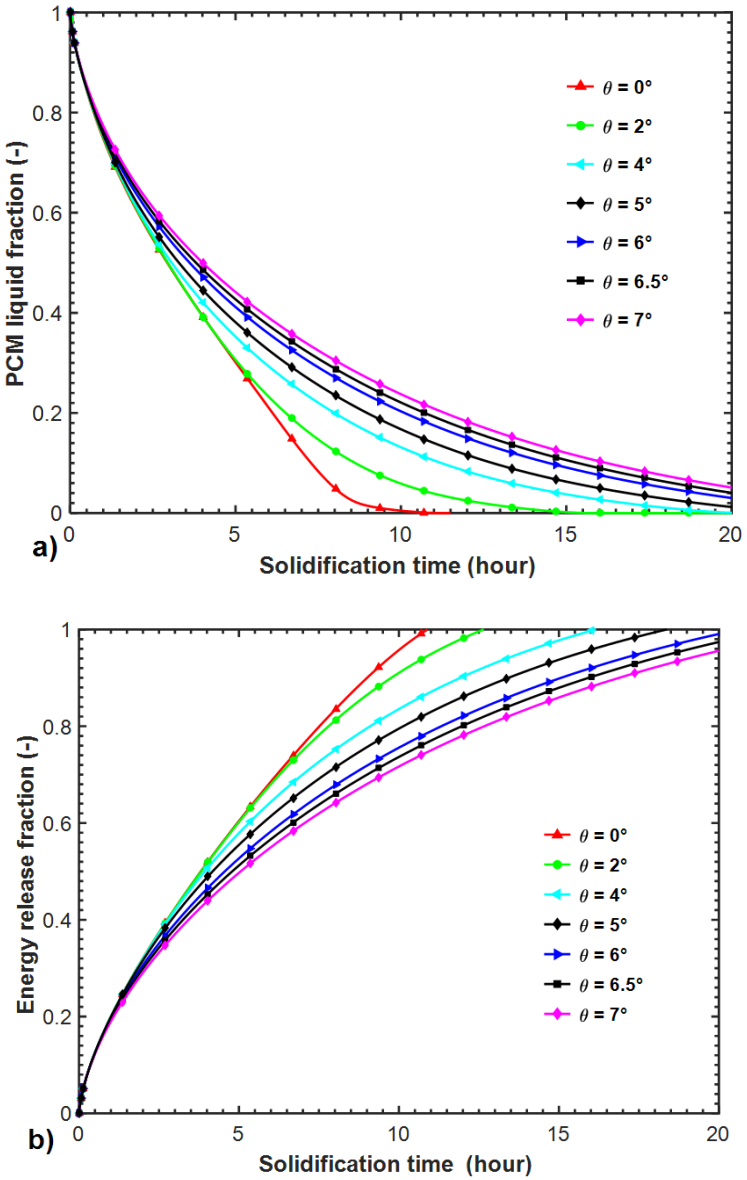

Fig. 3.7. The effect of shell tilting angles on (a) PCM liquid fraction and (b) energy release fraction during the solidification process.

This heat transfer mechanism is further evidenced by the energy release fraction curves in Figure 3.7b. The energy release fraction is defined as the ratio of the cumulatively released energy at a time instant for a specific LHTES unit to the total released energy at the end of

solidification ($\phi_1 = 0$) from PCM in the straight LHTES system. As shown in Figure 3.7b, the energy release rate in the large tilting angle unit is slower than that in the small tilting angle unit during the solidification process. This is mainly caused by the shrinking of the solid-liquid front length as discussed above.

3.5.3 Optimization of tilting angle

Table 3.4 summarizes the charging, discharging and total cycle times for the LHTES system with different tilting angles. It shows that increasing the tilting angle reduces the charging time, increases the discharging time, and increases the total cycle time. This indicates that the large tilting angle unit should be selected in the application that needs to fast store thermal energy. However, in the application of fast releasing thermal energy, the conventional straight LHTES is preferred. From the analysis in section 4.1, if the tilting angle is larger than a certain value (4° in the studied cases), further increase in tilting angle will not significantly enhance the charging process. This is also applicable for the discharging process. The effect of the tilting angle on the discharging time is more significant at the small tilting angle and is less significant at the large tilting angle. These analyses demonstrate that the selection of the optimal tilting angle is determined by the real applications. It needs to consider trade-off between the charging and discharging processes. Given that solar radiation level varies significantly across locations, the PCM storage unit with tilting lateral surface is advantageous to areas with lower sunshine duration for exploiting solar energy. This provides a guideline for the design of vertical LHTES systems.

TABLE 3.4 Charging, discharging and total cycle times (HTF inlet velocity = 0.01 m/s).

Tilting angle	Charging time (hr)	Discharging time (hr, T_{in} = 80 °C)	Total cycle time (hr, T_{in} = 36 °C)
0 °	5.83	10.01	15.84
2 °	5.08	14.28	19.36
4 °	4.29	18.84	23.13
5 °	3.88	22.50	26.38
6 °	3.42	23.39	26.81
6.5 °	3.29	24.53	27.82
7 °	3.21	25.59	28.80

3.5.4 The effects of HTF operating parameters

3.5.4.1 Effect of HTF inlet temperature

Figure 3.8 presents variations of melting and solidification times under different HTF inlet temperature differences (i.e., the difference between the HTF inlet temperature and the PCM average melting temperature). The HTF inlet velocity is 0.01 m/s. The HTF inlet temperature difference ranges from 12 to 22 °C during the melting process and from 22 to 42 °C for the solidification process. It is found that both total melting and solidification times decrease as the HTF inlet temperature difference increases. Taking the 4° tilting angle unit as an example, as the HTF inlet temperature difference increases from 12 to 17 °C and from 17 to 22 °C during the melting process, the total melting times drop by 31% and 24%, respectively. Similarly, as the HTF inlet temperature difference increases from 22 to 42 °C, the total solidification time reduces by 43.2%. This is because an increase in HTF inlet temperature difference improves the heat transfer driving force and hence enhances the heat transfer rate. Furthermore, Figs. 8a and b also show that there is no significant difference in the total melting time or solidification time when the tilting angle is beyond 5°. This indicates again that the effect of titling angle on the LHTES system performance is only effective for small titling angles.

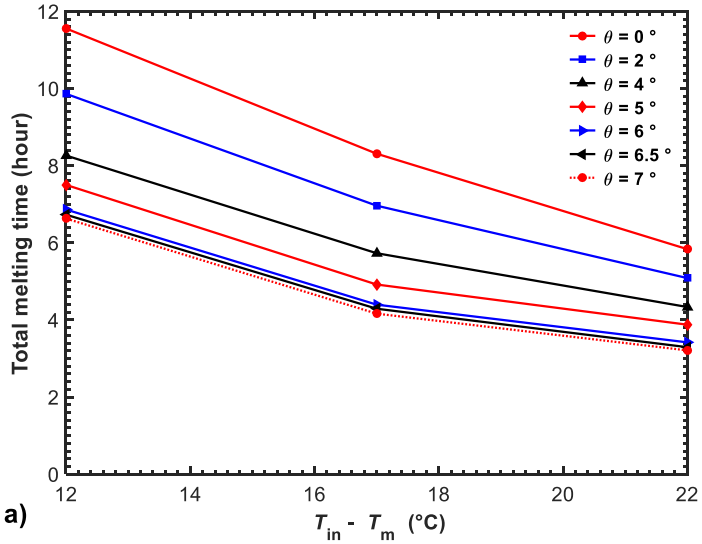

a)

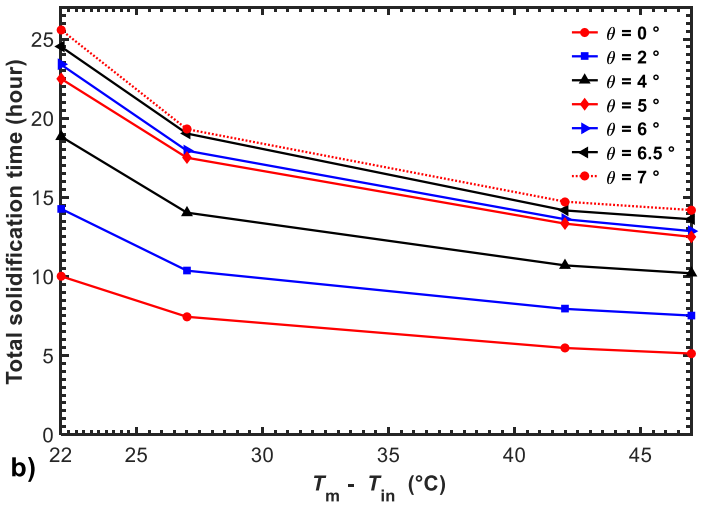

Fig. 3.8. Effect of HTF inlet temperature difference on the melting and solidification processes, (a) total melting time; (b) total solidification time.

3.5.4.2 Effect of HTF inlet velocity and Reynolds number

The effect of HTF inlet velocity and Reynolds number is examined for the LHTES unit with a tilting angle of 4°. Figure 3.9 presents variation of the PCM liquid fraction during the melting and solidification processes under four HTF inlet velocities. The HTF inlet temperature is 80 °C for the melting process and 36 °C for the solidification process. For the melting process, it is shown that the total melting time is reduced by 38.5% as the HTF inlet velocity increases from 0.01 to 0.4 m/s. This is because an increase in the HTF inlet velocity increases the Reynolds number as shown in Table 3.5 and hence increases the convective heat transfer coefficient. Therefore, the heat transfer rate from the HTF to the PCM increases, which enhances energy transfer during the melting process.

In the solidification process, the high HTF velocity also exhibits a positive effect. However, the effect of flow velocity on the total solidification time is not as significant as on the total melting time. This is caused by the different heat transfer mechanisms. In the melting process, the main heat transfer mechanism is convection and hence an increase in the heat transfer rate between the HTF and the HTF tube surface enhances the energy transfer. During the solidification process, the heat transfer between the PCM and the HTF is dominated by thermal conduction. Due to the higher thermal resistance of the solid PCM layer between the liquid PCM and the tube, increasing the heat transfer coefficient between the HTF and the tube surface does not significantly enhance the overall heat transfer.

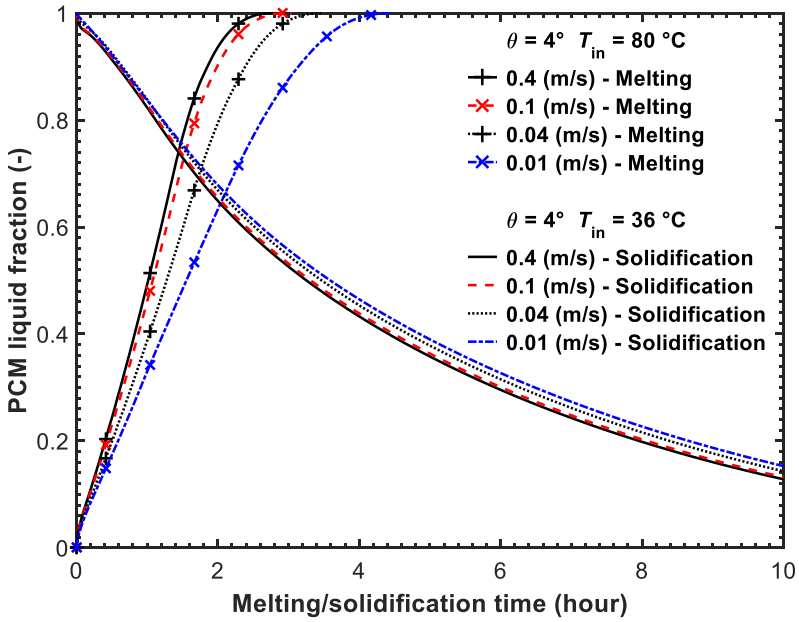

Fig. 3.9. Effect of HTF average inlet velocity on PCM liquid fraction.

TABLE 3.5 HTF properties, Reynolds numbers and velocities.

Heat transfer fluid	Temperature (°C)	Density (kg/m^3)	Dynamic viscosity (kg/(m·s))
Water	80	971.8	0.354e-3
	36	992.2	0.653e-3
Re	HTF inlet velocity		
	Melting (m/s)	Solidification (m/s)	
630	0.01	0.018	
1950	0.031	0.056	
2500	0.04	0.072	
6300	0.1	0.181	
14000	0.221	0.4	

Figure 3.9 also shows that the total melting time does not change significantly for the velocities above 0.1 m/s. This can be explained by the HTF flow in the tube. Table 3.5 lists the working conditions with different Reynolds numbers and corresponding HTF inlet velocities.

Figure 3.10 shows the variation in the total melting and solidification times under different Reynolds numbers for the units with tilting angles of 0° and 4°. In the laminar (Re < 2300) and transition flow (2300 < Re < 4000) regions, the total melting and solidification times drop very quickly as the Re number increases. This is because the heat transfer coefficient between the HTF and tube surface during these flow regions is relatively small and comparable with that between the HTF tube outer surface and PCM. An increase in the HTF heat transfer coefficient reduces the total thermal resistance between the HTF and PCM, and hence reduces the total melting and solidification times. As the Re number increases in the turbulent flow region (Re > 4000), the HTF heat transfer coefficient increases tremendously and is relatively much larger than that between the HTF tube outer surface and PCM. Its effect on the total thermal resistance between the HTF and PCM is insignificant. The heat transfer rate is mainly dominated by the heat transfer coefficient between the HTF tube outer surface and PCM. The reduction in the total melting or solidification time is negligible for large Re numbers. This explains the finding reported in the literature [13, 14] in which the flow rate did not show significant effect on the melting and solidification processes.

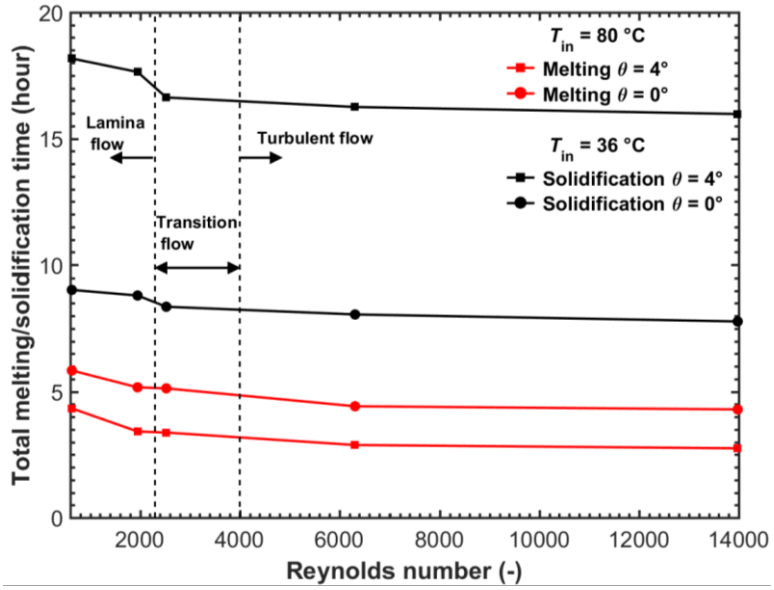

Fig. 3.10. Total melting and solidification times versus Reynolds numbers.

3.5.4.3 Comparisons of HTF outlet temperatures

Figure 3.11 shows variations of HTF outlet temperatures for LHTES systems under different tilting angles . The HTF inlet temperature is 80 °C for the melting and 36 °C for the

solidification while the HTF inlet velocity 0.01 m/s is selected for both processes. As shown in Figure 3.11a, initially (melting time less than 0.2 hrs), the HTF outlet temperatures are almost the same for all the studied units. The heat transfer is dominated by thermal conduction. As the PCM melts, the melting process enters the stage in which natural convection dominates the heat transfer. During this stage, the HTF outlet temperatures of LHTES systems with large tilting angles are lower than those of systems with small tilting angles. This indicates that the heat transfer between the HTF and PCM in the larger tilting angle unit is higher and more energy is stored. This pattern is consistent with the energy storage fraction evolution trend during the melting process shown in Figure 3.6b. In the later stage when most PCM is melted, the heat transfer rate from the HTF to PCM in LHTES systems with large tilting angles decreases. Therefore, the HTF outlet temperature starts to rise and gradually exceeds that of the smaller tilting angle units. In the later stage, since there is still much solid PCM in the systems with small tilting angles and energy transfer in these systems is much higher than that in the large tilting angle units, the HTF outlet temperature of the system with small tilting angles is lower than that in the large tilting angle system. Furthermore, all the HTF outlet temperatures are approaching the inlet temperature of 80 °C at the end, indicating that the melting processes are approaching the thermal equilibrium.

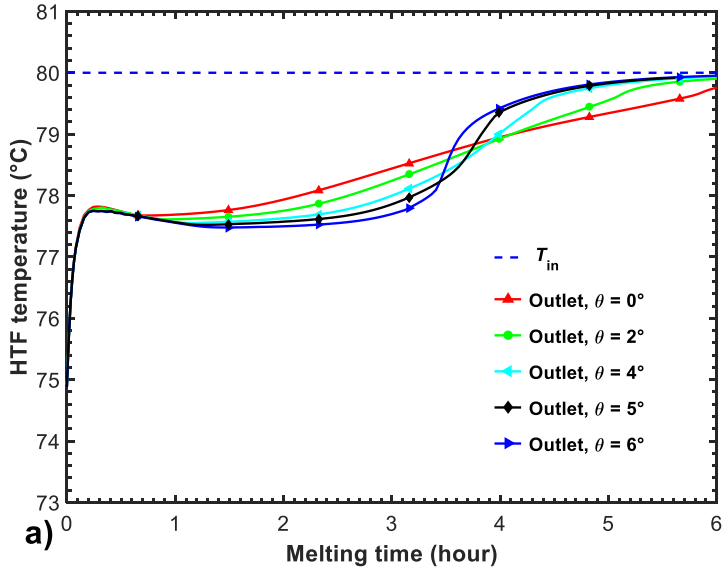

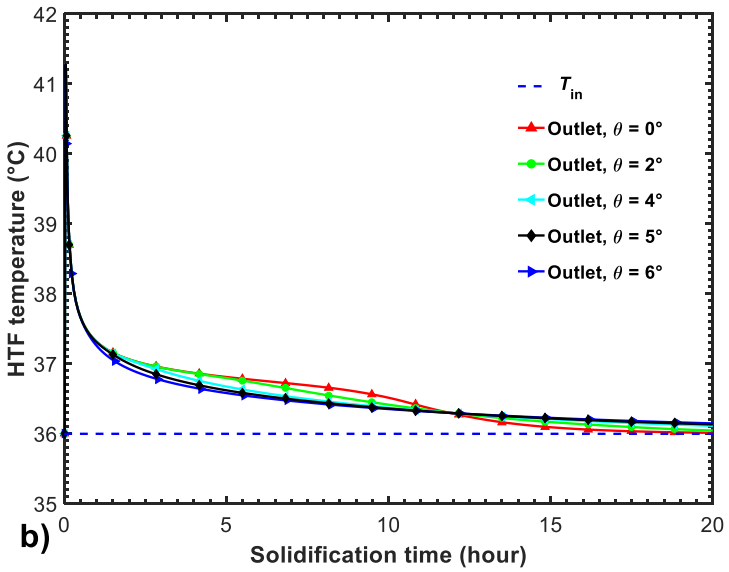

Fig. 3.11. HTF outlet temperatures during (a) the melting and (b) solidification processes.

The HTF outlet temperature profiles in the solidification process in Figure 3.11b do not show a significant difference between the studied LHTES systems. At the beginning stage, the HTF outlet temperature drops sharply. This is due to the natural convection which dominates the heat transfer between the HTF and PCM. Very quickly, the drop in HTF outlet temperature becomes very small. This indicates that the heat transfer mechanism in the LHTES system changes from natural convection to thermal conduction. The results also show that the HTF outlet temperature in the larger tilting angle system drops slightly faster than that in the smaller tilting angle system. This indicates that the energy discharging rate in the larger tilting angle system is lower than that in the smaller tilting angle unit. This is consistent with that reported in Figure 3.7. This is because the solid-liquid front length is shorter in the large tilting angle unit and the thermal heat transfer surface area is small.

Figure 3.11 also shows that the HTF temperature difference between the inlet and outlet is not large. This indicates that the assumption of constant surface temperature boundary condition used in our previous simulation model (Seddegh et al., 2015, 2016) is appropriate for investigating the heat transfer mechanism in the PCM at large HTF flow rates. This can simplify the theoretical analysis for the future research in this field.

3.6 Conclusions

A mathematical model combining the HTF, HTF tube and PCM storage zones was developed to investigate the thermal performance of a vertical shell-and-tube LHTES system with different tilting lateral surface angles. This model was first validated using experimental data available in the literature. The comparison results showed that the proposed model could accurately predict thermal characteristics of vertical shell-and-tube LHTES systems. This model was then used to investigate the thermal performance of the LHTES systems during melting and solidification processes. It was found that the tilting lateral surface could substantially enhance the melting process by shortening the total melting time by 43% with the tilting angle increasing from 0° to 7°; however, it has a negative effect on the solidification process. The optimal tilting angle needs to consider the trade-off between the melting and solidification processes. The tilting lateral surface configuration is recommended to be used in areas having lower sunshine duration to assist the exploitation of solar energy.

The effect of HTF operating parameters on the energy storage and release performance was further evaluated. For the LHTES system with a tilting angle of 4°, the total melting and solidification times decreased by up to 47.5% and 45.9%, respectively as the HTF inlet temperature differences increased from 12 to 22 ℃ for the melting process and from 22 to 47 °C for the solidification process. The analysis also showed that increasing the HTF Reynolds number substantially reduced the melting and solidification times if the HTF flow is in the laminar and transition flow regions, and had negligible effect on the melting and solidification processes if the HTF flow is in the turbulent flow region. The evaluation of the HTF outlet temperature showed that the HTF temperature drop along the HTF tube was insignificant. This demonstrated that the assumption of constant HTF surface temperature boundary for investigating heat transfer mechanism in PCM in the literature is reasonable. Thisstudy provides useful information for design and optimization of vertical LHTES systems.

This chapter demonstrates tilting the shell design and HTF operating conditions are critical in improving the thermal performance of a shell-and-tube LHTES system. This prompts a necessity to study another important design parameter, the shell-to-tube radius ratio in a cylindrical LHTES system, which will be addressed in the following chapters 4 and 5.

3.7 References

1. Akgün, M., Aydın, O., Kaygusuz, K., 2008. Thermal energy storage performance of paraffin in a novel tube-in-shell system. Appl Therm Eng. 28(5–6), 405-413.
2. Al-Abidi, A.A., Mat, S., Sopian, K., Sulaiman, M.Y., Mohammad, A.T., 2013. Numerical study of PCM solidification in a triplex tube heat exchanger with internal and external fins. Int J Heat Mass Transf. 61, 684-695.
3. Aydın, O., Akgün, M., Kaygusuz, K., 2007. An experimental optimization study on a tube-in-shell latent heat storage. Int J Energy Res. 31(3), 274-287.
4. Bellecci, C., Conti, M., 1993. Phase change thermal storage: transient behaviour analysis of a solar receiver/storage module using the enthalpy method. Int J Heat Mass Transf. 36(8), 2157-2163.
5. Bellecci, C., Conti, M., 1993. Latent heat thermal storage for solar dynamic power generation. Solar Energy. 51(3), 169-173.
6. Esen, M., Durmuş, A., Durmuş, A., 1998. Geometric design of solar-aided latent heat store depending on various parameters and phase change materials. Sol Energy. 62(1), 19-28.
7. Fornarelli, F., Camporeale, S.M., Fortunato, B., 2016. CFD analysis of melting process in a shell-and-tube latent heat storage for concentrated solar power plants. Appl Energy. 164, 711-722.
8. Hasan, A., 1994a. Phase change material energy storage system employing palmitic acid. Sol. Energy. 52, 143-154.
9. Hasan, A., 1994b. Thermal energy storage system with stearic acid as phase change material. Energy Conv. Manag. 35, 843-856.
10. Ismail, K., Melo, C., 1998. Convection‐based model for a PCM vertical storage unit. Int J Energy Res. 22(14), 1249-1265.
11. Ismail, K., Goncalves, M., 1999. Thermal performance of a PCM storage unit. Energy Conv Manag. 40(2), 115-138.

12. Iten, M., Liu, S., Shukla, A., Silva, P.D., 2017. Investigating the impact of Cp-T values determined by DSC on the PCM-CFD model. Appl Therm Eng. 117, 65-75.
13. Khan, Z., Khan, Z., Ghafoor, A., 2016. A review of performance enhancement of PCM based latent heat storage system within the context of materials, thermal stability and compatibility. Energy Conv Manag.115, 132-158.
14. Longeon, M., Soupart, A., Fourmigué, J.F., Bruch, A., Marty, P., 2013. Experimental and numerical study of annular PCM storage in the presence of natural convection. Appl Energy. 112, 175-184.
15. Rathod, M., Banerjee, J., 2014. Experimental investigations on latent heat storage unit using paraffin wax as phase change material. Exp Heat Transf. 27(1), 40-55.
16. Rathod, M.K., Banerjee, J., 2015. Thermal performance enhancement of shell and tube Latent Heat Storage Unit using longitudinal fins. Appl Therm Eng. 75, 1084-1092.
17. RT60 Data Sheet. Rubitherm Technologies GmbH. https://www.rubitherm.eu/en/index.php/productcategory/organische-pcm-rt. Accessed May 22, 2019
18. Sciacovelli, A., Colella, F., Verda, V., 2013. Melting of PCM in a thermal energy storage unit: Numerical investigation and effect of nanoparticle enhancement. Int J Energy Res. 37 (13), 1610-1623.
19. Seddegh, S., Wang, X., Henderson, A.D., Xing, Z., 2015a. Solar domestic hot water systems using latent heat energy storage medium: A review. Renew Sust Energ Rev. 49, 517-533.
20. Seddegh, S., Wang, X., Henderson, A.D., 2015b. Numerical investigation of heat transfer mechanism in a vertical shell and tube latent heat energy storage system. Appl Therm Eng. 87, 698-706.
21. Seddegh, S., Wang, X., Henderson, A.D., 2016. A comparative study of thermal behaviour of a horizontal and vertical shell-and-tube energy storage using phase change materials. Appl Therm Eng. 93, 348-358.
22. Seddegh, S., Wang, X., Joybari, M.M., Haghighat, F., 2017. Investigation of the effect of geometric and operating parameters on thermal behavior of vertical shell-and-tube latent heat energy storage systems. Energy. 137, 69-82.
23. Seddegh, S., Tehrani, S.S.M., Wang, X., Cao, F., Taylor, R.A., 2018. Comparison of heat transfer between cylindrical and conical vertical shell-and-tube latent heat thermal energy storage systems. Appl Therm Eng. 130, 1349-1362.

24. Shukla, A., Buddhi, D. ,Sawhney, R. L., 2009. Solar water heaters with phase change material thermal energy storage medium: A review. Renew. Sust. Energ. Rev. 13, 2119-2125.
25. Trp, A., Lenic, K., Frankovic, B., 2006. Analysis of the influence of operating conditions and geometric parameters on heat transfer in water-paraffin shell-and-tube latent thermal energy storage unit. Appl Therm Eng. 26(16), 1830-1839.
26. Xiao, X., Zhang, P., 2015. Numerical and experimental study of heat transfer characteristics of a shell-tube latent heat storage system: Part I – Charging process. Energy. 79, 337-350.
27. Zheng, Z.J., Li, M.J., He, Y.L., 2017. Thermal analysis of solar central receiver tube with porous inserts and non-uniform heat flux. Appl Energy. 185, 1152-1161.

Chapter 4: Numerical investigation on optimal shell-to-tube radius ratio in vertical cylindrical latent heat storage systems under a fixed tube radius

4.1. Chapter summary

The last chapter highlights the role of improving the geometrical design in enhancing the melting and solidification performances for an LHTES system. This chapter investigates another notable design parameter, the shell-to-tube radius ratio, to optimize thermal response in a vertical cylindrical PCM storage system. A series of geometrical designs is formulated by changing the PCM shell radius (R) based on a constant HTF-tube radius (r_f), comprising the shell-to-tube radius ratios (R/r_f) of 2 to 8. A variation in the unit height is also considered along with the different radius ratios. A conjugate analytic model integrating the HTF, HTF tube and PCM zones was developed and then validated with experimental results. The numerical investigation compares and evaluates the energy storage/release ratio, total stored/released energy, average energy storage/release rate, and energy storage/release density under the different R/r_f and unit heights. The results indicate the R/r_f of 5 can achieve the optimal charging and discharging performance simultaneously. A R/r_f smaller than 5 substantially decreases the energy storage capacity while A R/r_f greater than 5 leads to a significant decline in the energy release efficiency during discharging. The unit height is found to show a gentle

influence on the optimal radius ratio in the charging process and a negligible influence in the discharging process.

4.2. Introduction

Chapters 2 and 3 confirm the significance of optimizing the system configuration and geometrical design as such improvements would not use extra highly conductive material and reduce the heat storage capacity and density. Except for the shell lateral surface tilting angle investigated in chapter 3, another notable design parameter, the shell-to-tube radius ratio, has also received intense research interests. These studies were accomplished in relation to both horizontal and vertical LHTES systems.

In a pioneering study by Cao and Faghri [7], the geometrical parameters including radius ratio (r_o/D) and length ratio (L/D) in a horizontal shell-and-tube LHTES system were numerically investigated. The results showed an augmentation in r_o/D considerably reduced the energy storage density, while a rise in L/D more effectively boosted the total latent energy. A numerical study by Cao et al. [8] compared two horizontal LHTES systems, one configured with an annular HTF flow and another with both central and annular HTF flows. Better energy storage performance was observed in the latter configuration, in which a larger length-to-diameter ratio augmented the total energy stored but dramatically lowered the energy storage density. Following developing an enthalpy-based numerical model, Lacroix [9] assessed the effects of shell radii and HTF operating parameters in a horizontal cylindrical LHTES module. It was concluded that the shell size and working conditions must be considered carefully for acquiring a better thermal performance.

Conti et al. [10] conducted a numerical study to analyse the effects of geometrical designs on the Second-Law efficiency in a horizontal PCM storage module and concluded that a higher length-to-diameter ratio ($\geqslant$ 45) with a radius ratio of 2.6 gave rise to the minimal entropy

generation number. Tao et al. [11] held the PCM amount constant to numerically investigate the effect of HTF-tube size in a horizontal storage unit and found that a larger HTF-tube radius resulted in a longer melting time due to a corresponding slower HTF flow velocity. Wang et al. [12] found that in a horizontal shell-and-tube LHTES system, an increase in the radius ratio decreased the energy efficiency ratio and the heat storage rate simultaneously, but the decreasing effect weakened once the radius ratio exceeded a specific value. Further, as reported by the same authors [13], increasing the shell length in a horizontal finned-tube LHTES system obtained a higher heat storage rate but a lower energy efficiency ratio, whereas the effect of a variation in the shell radius on the thermal responses was more pronounced in comparison with that in the shell length. Erek and Dincer [14] developed a two-dimensional conjugate model to predict the thermal characteristics in a horizontal cylindrical component with water as PCM and Ethyl alcohol as HTF. The results of the dimensionless heat transfer rate, the energy efficiency and exergy efficiency were presented in relation to the design parameters (R_{inf} and X_L). It was claimed that the efficiency analysis played a crucial role in assessing the thermal performance. Ezan et al. [15] 's experimental study of horizontal shell-and-tube units revealed that an increase in shell diameter augmented the total stored energy and HTF inlet temperature more effectively enhanced the discharging performance compared with its flow rate. Tan [16] reported that in a horizontal cylindrical unit, an increase in the PCM radial thickness decreased the capacity effectiveness (η_Q) but the weaken effect turned to be negligible with a lower HTF mass flow rate operated.

Apart from the horizontal configuration, the vertical PCM storage unit also received many research efforts regarding geometrical designs. Ismail and Melo [17] established a two-dimensional axisymmetric numerical model to examine the impact of geometrical parameters in vertical cylindrical LHTES units. The total melting time was found to rise with an augmentation in H/r_0 or R_0/r_0 and a formula was deduced to correlate the mean heat transfer

rate with R_0/r_0. Ismail and Abugderah [18] reported that the sensible and latent heats augmented nearly linearly with the height increase in a vertical thermal storage system and the complete melting times were substantially sensitive to a variation in the PCM layer thickness regardless of HTF operating conditions. Trp et al. [19] experimentally and numerically studied the phase change and heat transfer phenomena in vertical shell-and-tube components. Through analysing the effects of geometrical definitions (L/D and r_o/D) on charging and discharging they concluded the selection of geometrical parameters highly depended on a designated heat transfer rate and the required energy storage and delivery times.

Seddegh et al. [3] experimentally investigated the thermal performance in vertical cylindrical LHTES units with shell-to-tube radius ratio from 2.1 to 8. PCM liquid fraction, average PCM temperature and the total stored/released energy during charging and discharging were determined and compared. The study revealed the radius ratio of 5.4 can best balance the total stored energy and the total charging and discharging times.

The numerical analysis of a vertical tube-in-tank or multiple-tube LHTES unit was commonly simplified to a single-pass shell-and-tube model. Esen et al. [20] investigated the effects of PCM-HTF packing modes and geometrical parameters in a vertical tube-in-tank LHTES system with the assistance of a single-pass shell-and-tube numerical model. The results demonstrated the model with PCM packed in annulus could store more energy than that with HTF packed in annulus over a given time. Pirasaci and Goswami [21] stated that the system length and HTF-tube size exhibited more significant influences on the storage effectiveness compared with the tube pitch in a high-temperature tube-in-tank LHTES system. Tehrani et al. [22] examined the energy storage/delivery characteristics in a tube-in-tank LHTES system for aiding a solar thermal power plant. With a simplified two-dimensional asymmetrical model assisted the numerical study found the optimal shell length and radius ratios fell in around 40-60 and 1.3-1.8 respectively, depending on PCM type.

A pure heat conduction model neglecting PCM natural convection was employed by several numerical studies to determine the thermal response without considering the effect of unit orientation. Ismail and Goncalves [23] built an enthalpy and pure heat conduction model to study the solidification cycle in a cylindrical LHTES heat exchanger. The outer-to-inner radius ratio of 4 was recommended based upon the evaluation of the number of thermal unit. Guo and Zhang [24] found that in a high-temperature LHTES system, once the HTF-tube dimension exceeded a certain value its influence on the total discharging time turned to be less pronounced. Fang et al. [25] presented a series of parametric studies neglecting PCM natural convection and claimed that a specific volume ratio of PCM to the whole LHTES unit was capable of achieving the maximum effective energy storage ratio.

The thermal performance of an LHTES unit and its configuration and design has been widely studied and many studies revealed the effects of geometrical parameters including the shell-to-tube radius ratio on the thermal response. However, most studies still have one or more of the following limitations, i) the assessment of an LHTES performance was made based on investigation of only one heat transfer process, either storage or release; ii) PCM natural convection was neglected by some studies; and iii) most literature reported general trends in geometrical effect and only limited studies obtained optimal design parameters.

In this chapter, a series of geometries in a vertical shell-and-tube type LHTES system is investigated based on both heat storage and release performance. The series of geometries is defined by varying the shell radius (R) with the HTF-tube radius (r_f) fixed. A rise in the unit height is also investigated along with the radius change in PCM shell. The investigation on the elaborate geometrical definition not only help design an effective single pass shell-and-tube LHTES unit but also could contribute to a multiple-tube or tube-in-tank LHTES design. For a multiple-tube storage design, findings from investigating this series of definitions may enable an appropriate setting of the tube pitch. A PCM-HTF conjugate model is developed to deal

with the transient energy transfer, phase change and natural/forced convection flow in the PCM storage unit. The energy storage/release ratio, the total stored/released energy, the average energy storage/release rate, and energy storage/release density are chosen as performance indicators to assess the charging and discharging processes in the context of solar thermal energy storage.

4.3. Numerical study

4.3.1. Physical model

Fig. 4.1 shows the schematic of the physical model and the series of geometrical definitions in a vertical LHTES unit which consists of concentric cylindrical passes with HTF flowing in the inner tube and PCM packed in the outer shell. This series definition is to vary the shell radius (R) with a fixed HTF-tube radius (r_f) of 12.7 mm (Fig. 4.1b), consisting of five radius ratios from 2 to 8. A variation in the unit height from 0.6 m to 1.2 m is also investigated along with the different radius ratios. The HTF-tube is made of copper with a constant thickness of 1.2 mm across all geometries. The inner tube size (DN25) was chosen to comply with AS1432, the Copper tube used for both domestic and industrial applications. The preliminary simulation indicates that when $R/r > 9$, the discharging-to-charging time ratio increases substantially due to a much lower discharging efficiency. Therefore, the maximum R/r is limited to 9. Water is used as the HTF circulating into the LHTES unit from the bottom end with a volume flow rate of 5 L/min and inlet temperature of 88 °C for charging or 28 °C for discharging. Table 4.1 summarizes the geometrical and HTF working parameters.

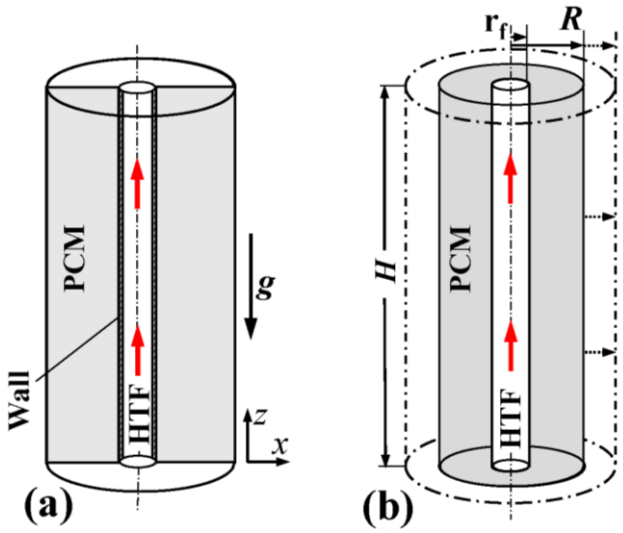

Fig. 4.1. Schematic of the physical model (a) and geometrical definitions: (b) varying the shell radius with HTF-tube radius fixed.

Table 4.1 Summary of geometrical parameters and HTF working conditions.

Varying shell radius with a fixed tube radius r_f (12.7 mm)				
Unit height H (m)	Radius ratio R/r_f (-)	Shell inner radius R (mm)	Total PCM mass for H = 0.6 m (kg)	HTF inlet velocity (m/s)/ Re (-)
0.6, 1.2	2	25.4	0.70	0.201/7010
	4	50.8	3.51	
	5	63.5	5.62	
	6	76.2	8.19	
	8	101.6	14.74	

4.3.2. PCM properties

The study uses a commercial product paraffin wax RT 60 from Rubitherm Technologies Gmbh [28] as the heat storage medium. To accurately predict PCM heating and cooling characteristics, a variable specific heat method is implemented by integrating the latent heat with the specific heat [24, 25]. Fig. 4.2 plots RT 60 variable specific heat during the phase

transition measured by the manufacturer and Table 4.2 presents the other PCM thermophysical properties.

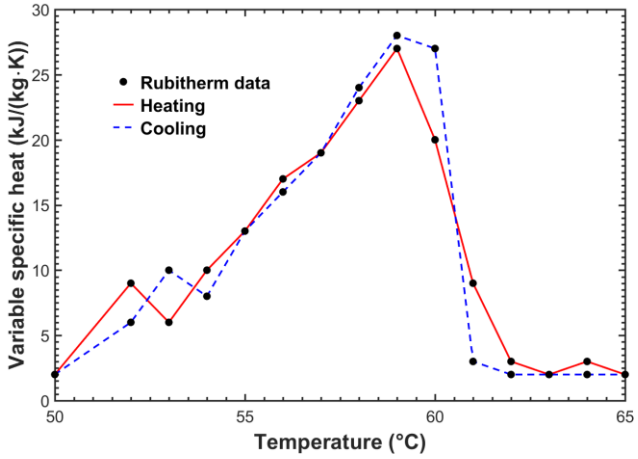

Fig. 4.2. PCM variable specific heat during heating and cooling cycles.

Table 4.2 Thermophysical properties of RT 60 [28].

Properties	Value
Phase transition temperature range	55-61 °C ($T_{p,\ Solidus}$ -$T_{p,\ Liquidus}$)
Average phase transition temperature	58 °C
Density (80 °C)	770 kg/m^3
Thermal conductivity, liquid/solid	0.2 W/(m·K)
Thermal expansion coefficient of liquid phase	0.76E-3 /K
Dynamic viscosity	3.08E-3 kg/(m·s)
Specific heat ($T \leqslant$ 50 °C and $T \geqslant$ 65 °)	2000 J/(kg·K)
Variable specific heat (50 °C < T < 65 °C)	illustrated in Fig. 4.2

4.3.3. Governing equations

A quasi-three-dimensional model is developed to carry out a conjugate analysis of the transient heat transfer, fluid flow and melting/solidification phenomena in the cylindrical storage unit. To simplify the numerical study the following assumptions are made: i) PCM volume change during melting/solidification is neglected and PCM is homogeneous and isotropic; ii) The liquid PCM is incompressible and its flow is laminar; iii) Viscous dissipations in HTF and PCM flows are negligible.

4.3.3.1. Governing equations in HTF zone

The mass conservation equation has the form,

$$\nabla \cdot \left(\rho_{\mathrm{f}} \vec{v}_{\mathrm{f}} \right) = 0 \tag{4.1}$$

The standard *k*-ε model is employed to solve the HTF turbulent flow. The momentum and energy equations describing HTF turbulent flow are given by Eqs. (2) and (3),

$$\rho_{\mathrm{f}} \frac{\partial}{\partial t}\left(\vec{v}_{\mathrm{f}} \right) + \rho_{\mathrm{f}} \nabla \cdot \left(\vec{v}_{\mathrm{f}} \vec{v}_{\mathrm{f}} \right) = \nabla \cdot \left(\left(\mu_{\mathrm{f}} + \mu_{\mathrm{t,f}} \right) \nabla \vec{v}_{\mathrm{f}} \right) + \rho_{\mathrm{f}} g - \nabla p_{\mathrm{f}} \tag{4.2}$$

$$\frac{\partial \left(\rho_{\mathrm{f}} C_{p,\mathrm{f}} T_{\mathrm{f}} \right)}{\partial t} + \nabla \cdot \left(\vec{v}_{\mathrm{f}} \left(p_{\mathrm{f}} + \rho_{\mathrm{f}} C_{p,\mathrm{f}} T_{\mathrm{f}} \right) \right) = \nabla \cdot \left(\left(k_{\mathrm{f}} + \frac{\mu_{\mathrm{t,f}} C_{p,\mathrm{f}}}{0.85} \right) \nabla T_{\mathrm{f}} \right) \tag{4.3}$$

where $C_{p,\mathrm{f}}$ and μ_{f} are HTF specific heat and dynamic viscosity respectively, and the HTF turbulent viscosity $\mu_{\mathrm{t,f}}$ is determined by,

$$\mu_{\mathrm{t,f}} = 0.09 \rho_{\mathrm{f}} \frac{k^2}{\varepsilon} \tag{4.4}$$

where *k* and ε are turbulence kinetic energy and the dissipation rate of turbulence kinetic energy respectively. The standard *k*-ε model equations [29] are combined with Eqs. (1)-(4) to solve the HTF turbulent flow.

4.3.3.2. Governing equations in HTF-tube wall zone

The energy equation can be written as,

$$\rho_{\mathrm{w}} \frac{\partial}{\partial t}\left(h_{\mathrm{w}}\right)=k_{\mathrm{w}} \nabla \cdot\left(\nabla T_{\mathrm{w}}\right) \tag{4.5}$$

where the enthalpy h_{w} is calculated by,

$$h_{\mathrm{w}}=\int_{T_{\mathrm{ref}}}^{T_{\mathrm{w}}} C_{p, \mathrm{w}} dT \tag{4.6}$$

In Eqs. (5) and (6) k_{w} and $C_{p,\,\mathrm{w}}$ are the tube wall thermal conductivity and specific heat respectively. T_{ref} is the reference temperature assigned as 25 °C in this study.

4.3.3.3. Governing equations in PCM zone

The mass conservation, momentum and energy equations solved in PCM zone are given by Eqs (7)-(9):

$$\nabla \cdot\left(\rho_{\mathrm{P}} \vec{v}_{\mathrm{P}}\right)=0 \tag{4.7}$$

$$\rho_{\mathrm{P}}\left(\frac{\partial}{\partial t}\left(\vec{v}_{\mathrm{P}}\right)+\nabla \cdot\left(\vec{v}_{\mathrm{P}} \vec{v}_{\mathrm{P}}\right)\right)=\nabla \cdot\left(\mu_{\mathrm{P}} \nabla\left(\vec{v}_{\mathrm{P}}\right)\right)+\rho_{\mathrm{P}}(1-\beta(T-T_{\mathrm{o}}))g-\nabla p_{\mathrm{P}}+\vec{S} \tag{4.8}$$

$$\frac{\partial\left(\rho_{\mathrm{P}} h_{\mathrm{p}}\right)}{\partial t}+\nabla \cdot\left(\rho_{\mathrm{P}} \vec{v}_{\mathrm{P}} h_{\mathrm{p}}\right)=\nabla \cdot\left(k_{\mathrm{P}} \nabla\left(T_{\mathrm{P}}\right)\right) \tag{4.9}$$

In Eqs. (7)-(9), μ_{P} is PCM dynamic viscosity, $\vec{v}$ is the liquid PCM velocity, and p_{P} is the static pressure. The body force term $\rho_{\mathrm{P}}(1-\beta(T-T_{\mathrm{o}}))g$ in Eq. (8) follows the Boussinesq approximation law to take account of the effect of PCM natural convection, where β is the PCM volumetric thermal expansion coefficient at liquid phase, and ρ_{P} is PCM density at the operating temperature T_{o}, set at 80 °C in this study. The PCM total volumetric enthalpy h_{P} and the momentum sink term $\vec{S}$ are expressed by Eqs. (10) and (12),

$$h_{\mathrm{P}}=h_{\mathrm{ref}}+\int_{T_{\mathrm{ref}}}^{T} C_{p,\mathrm{var}} dT+\phi L \tag{4.10}$$

where h_{ref} is the PCM reference enthalpy evaluated at T_{ref}. As the PCM variable specific heat $C_{p,\mathrm{var}}$ already incorporates PCM latent heat of fusion, the PCM latent heat L in Eq. (10) is set as being close to zero (1×10^{-5}). The PCM liquid volume fraction ϕ is defined as,

$$\phi = \begin{cases} 0, & T \le T_{\text{P,solidus}} \\ \dfrac{T - T_{\text{PCM,solidus}}}{T_{\text{PCM,liquidus}} - T_{\text{PCM,solidus}}}, & T_{\text{PCM,solidus}} < T < T_{\text{PCM,liquidus}} \\ 1, & T \ge T_{\text{PCM,liquidus}} \end{cases} \tag{4.11}$$

A liquid fraction ϕ between zero and one indicates the existing of a mushy zone, which is treated as a porous medium with porosity being equal to ϕ. Following the Carman-Kozeny law to account for a pressure drop due to the decreasing porosity in a solidifying cell, the momentum sink term $\vec{S}$ in Eq. (8) takes the form [30, 31],

$$\vec{S} = A_{\text{cons}} \frac{(1-\phi)^2}{\phi^3 + \gamma} \vec{v}_{\text{PCM}} \tag{4.12}$$

where A_{cons} is the mushy zone constant denoting the rate of velocity decrease as a cell is solidifying and chosen as 1×10^5 kg/(m^3·s) [32, 33] in this study. γ is a small constant (0.001) [34] to avoid division by zero when ϕ decreases to zero along with a cell totally solidifying.

The simulation is performed using the commercial CFD solver ANSYS Fluent 17.2. The geometry and mesh are created in ANSYS DesignModeler and Meshing modules. The SIMPLE algorithm is chosen as an approach to couple the pressure correction and velocity in a cell for solving the mass conservation equation and determining the pressure field. The Second Order Upwind approach is used to achieve a higher-order accuracy at cell face values, while the Least Squares Cell-Based scheme is employed to calculate the gradients between cell values. The PRESTO! procedure is selected to take account of pressure gradients on cell faces in the presence of body forces. The predetermined convergence levels for continuity, momentum, turbulence and energy equations are 1×10^{-5}, 1×10^{-6}, 1×10^{-9} and 1×10^{-9}, respectively.

4.3.4. Initial and boundary conditions

The initial conditions are set as follows for PCM, HTF and tube wall zones:

$t = 0$, $T_f = T_w = T_{inlet}$, $T_P = T_{ini}$ = 28 °C / 88 °C (charging/discharging), $u = v = 0$.

The boundary conditions ($t > 0$) are,

PCM and tube outer boundaries, i) $x = R$, $0 < z < H$, ii) $r_{in} < x < R$, $z = 0$, and iii) $r_{in} < x < R$, $z = H$:

$$\frac{\partial T}{\partial x} = 0\,,\ \frac{\partial T}{\partial z} = 0$$

The PCM boundary adjacent to the tube wall, $x = r$, $0 < z < H$:

$$u = v = 0,\ k_w(\frac{\partial T_W}{\partial x}) = k_P(\frac{\partial T_P}{\partial x})$$

The HTF boundary adjacent to the tube wall, $x = r_{in}$, $0 < z < H$:

$$u = v = 0,\ k_w(\frac{\partial T_W}{\partial x}) = k_f(\frac{\partial T_f}{\partial x})$$

The symmetric axis boundary, $x = 0$, $0 < z < H$: $u = 0$, $\frac{\partial v}{\partial x} = 0\,,\ \frac{\partial T_f}{\partial x} = 0$

The HTF inlet surface, $0 < x < r_{in}$, $z = 0$: $u = 0$, $v = V_{inlet}$, $T = T_{inlet}$

The HTF outlet surface, $0 < x < r_{in}$, $z = H$: $\frac{\partial u}{\partial x} = 0\,,\ \frac{\partial v}{\partial x} = 0\,,\ \frac{\partial T}{\partial x} = 0$

4.3.5. Performance indicators

The heat storage capacity Q_c is calculated by

$$Q_c = \rho_p V \int_{T_{ini}}^{T_{inlet}} C_{p,var}\,dT \tag{4.13}$$

where V is the PCM total volume.

The accumulated energy stored/retrieved at a time instant t, $Q(t)$ is

$$Q(t) = H_{int} - H_{ini} \tag{4.14}$$

where H_{int} is the PCM integral enthalpy during charging and discharging processes calculated by

$$H_{\text{int}} = \int_0^V h_{\text{p}} \rho_{\text{p}} dV \tag{4.15}$$

Energy storage/ retrieved ratio E is defined by

$$E = \frac{Q(t)}{Q_{\text{c}}} \tag{4.16}$$

The average energy storage rate is defined by

$$\bar{q} = \frac{Q_{\text{c}}^{\text{tot}}}{t^{\text{tot}}} \tag{4.17}$$

The energy storage/retrieved density is calculated by

$$Q_m = \frac{Q(t)}{m_{\text{P}}} \tag{4.18}$$

where m_{p} is the PCM total mass.

4.4. Model Verification and validation

4.4.1. Verifications of grid size and time step

The verifications of grid size and time step are conducted for charging and discharging on the geometry of $R/r_{\text{f}} = 4$ with $H = 0.6$ m. The default HTF operating parameters are applied throughout the verification tests. Three grid numbers of 15 × 150, 30 × 300, and 60 × 600 (radial × axial) in PCM domain are evaluated with a time step size 0.1 s for charging and 0.15 s for discharging. Fig. 4.3 indicates the increase in grid number from 30 × 300 to 60 × 600 shows marginal changes in PCM average temperature during both charging and discharging. Therefore, the grid arrangement of 30 × 300, corresponding to a quadrilateral-grid size of 1.3 × 2 mm in PCM domain, is employed for the geometry of $R/r_{\text{f}} = 4$ with $H = 0.6$ m. Further, the same quadrilateral-grid size is applied to PCM domains in all the other geometries.

Similarly, the tube wall or HTF zone also adopts an identical size of quadrilateral grid across all geometries investigated.

Further, the verification of time step is conducted with the verified grid arrangement of 30 × 300 in PCM domain. Time steps of 0.05, 0.1 and 0.15 s for charging and 0.1, 0.15 and 0.25 s for discharging are examined. The time step size shows a negligible impact on the PCM average temperatures of both charging and discharging. Moderate time steps of 0.1 and 0.15 s are respectively selected for charging and discharging calculations, in which all converge levels are closely monitored.

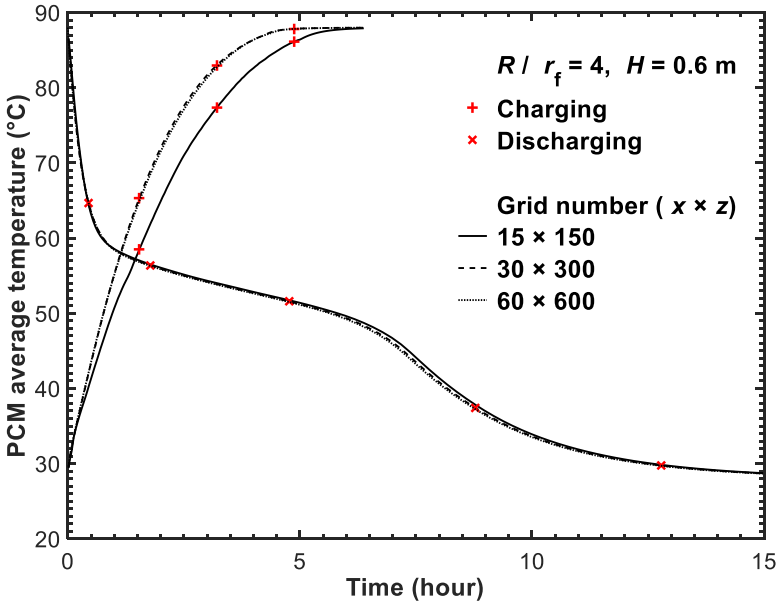

Fig. 4.3. The verification of grid size for charging and discharging processes.

4.4.2. Model validation

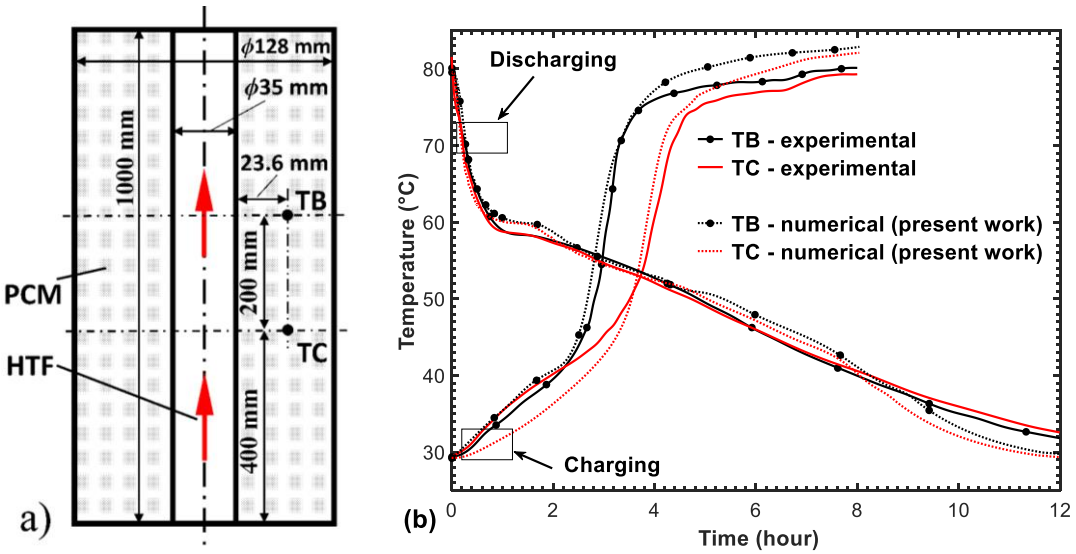

Fig. 4.4. (a) The schematic of the experimental setup and thermocouple positions [37], and (b) the numerical and experimental results for charging and discharging processes.

The numerical model is validated by experimental results in the literature [37], which used paraffin wax as PCM and water as HTF in the same type heat exchanger with the present work. The numerical prediction adopts the same physical configuration, material properties and operating conditions as the experimental study, more details on which are available in [37]. Fig. 4.4a gives the schematic of the experimental setup along with positions of thermocouples TB and TC, and Fig. 4.4b presents the comparison between experimental and numerical results. The same method RRMSD as used in Chapter 3 was employed to evaluate the deviation between the numerical and experimental results. The maximum RRMSD for charging or discharging is less than 3%. The deviations in charging can be interpreted by the heat loss to the environment during the experiments. The ambient conditions were not specified in the literature and cannot be accurately taken account of by the numerical model. Nevertheless, the comparisons demonstrate that the conjugate numerical model developed is capable of effectively reflecting the transient behaviour in heat transfer, PCM melting/solidification and liquid flows in the LHTES unit.

4.5. Results and discussion

Following the verifications of grid size and time step and validation of the numerical model, simulations are conducted to examine effects of geometries on the thermal storage/release behaviour. All defined cases are configured with the same initial and operating conditions related to a charging or discharging. Across all tests a constant HTF volume flow rate 5 L/min is operated and the corresponding Reynolds number for each unit is given by Table 4.2. For a charging (melting) process PCM is initially in the solid phase with a uniform temperature of 28 °C and the HTF inlet temperature is fixed at 88 °C. While over a discharging (solidification) PCM is initially in the liquid phase with a uniform temperature of 88 °C and the HTF inlet temperature is 28 °C. The thermal behaviour is first compared between geometries in terms of PCM average temperature, energy storage/release density, average heat transfer rate and the total stored/released energy in charging and discharging. Then, the overall charging and discharging performance is evaluated, which may deduce an optimal design. The Conclusion section finally summarizes the effects of all the geometrical factors investigated.

4.5.1. Charging process

Fig. 4.5a records PCM mass-averaged temperatures during charging for different radius ratios with H = 0.6 m. It is observed that radius ratios R/r_f = 2, 4, 5 and 6 take 0.6, 3.6, 5.7, 8.0 h respectively for the energy storage ratio E_{ch} to reach 0.95. Comparatively, even over a charging time as long as 10 h, PCM average temperature of R/r_f = 8 only rises to 75.5 °C,

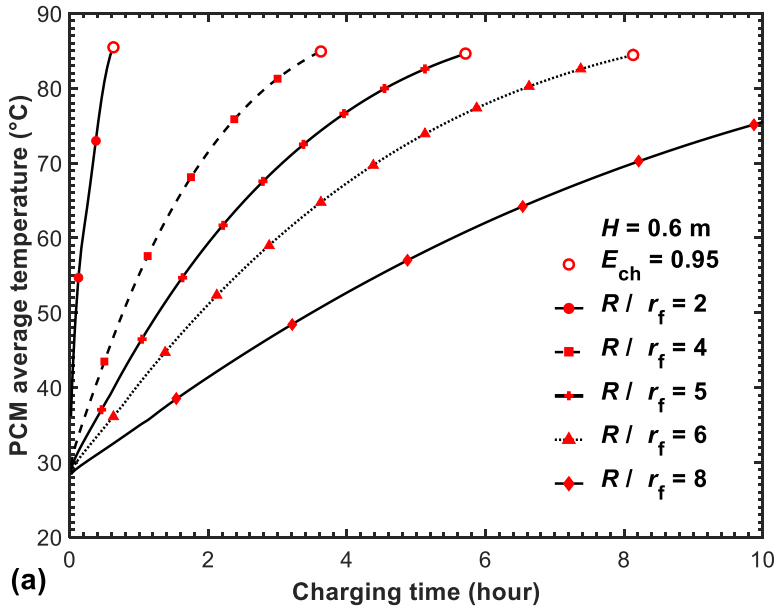
PCM average temperature (°C)
Charging time (hour)
(a)
H = 0.6 m
E_ch = 0.95
R / r_f = 2
R / r_f = 4
R / r_f = 5
R / r_f = 6
R / r_f = 8

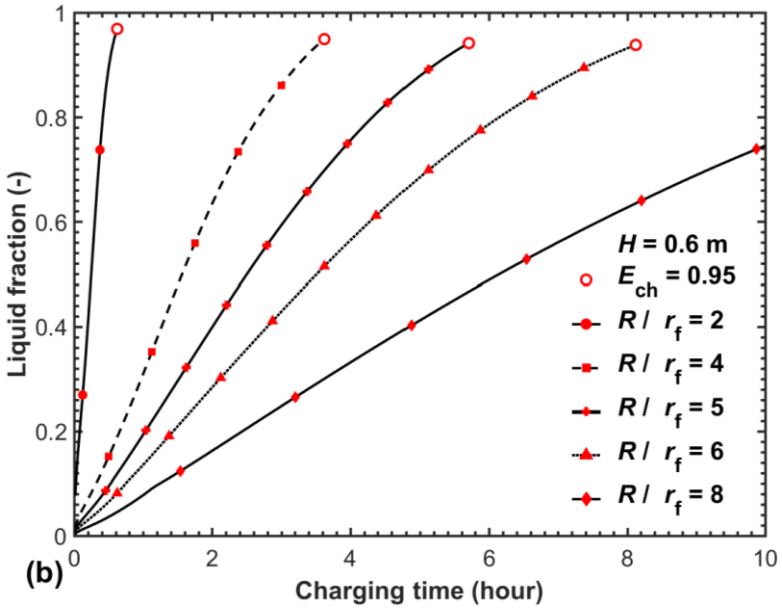
Liquid fraction (-)
Charging time (hour)
(b)
H = 0.6 m
E_ch = 0.95
R / r_f = 2
R / r_f = 4
R / r_f = 5
R / r_f = 6
R / r_f = 8

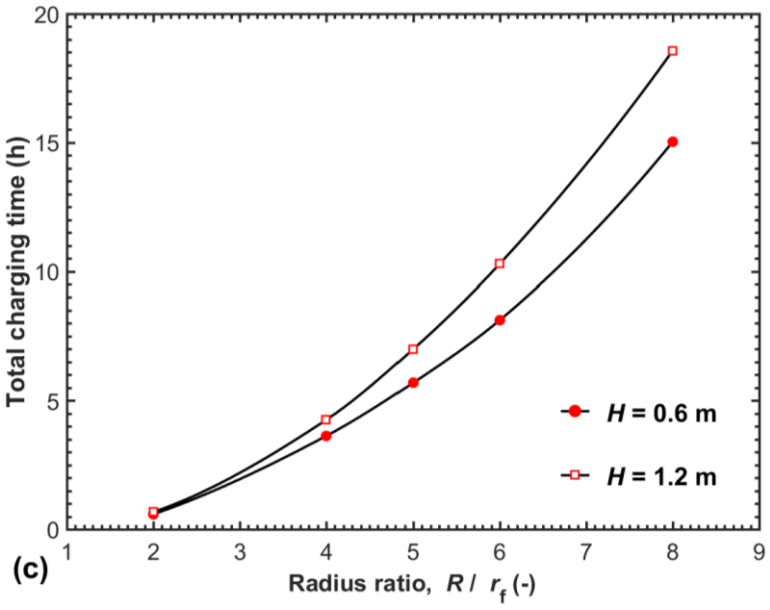

Fig. 4.5. Comparisons of (a) PCM average temperature, (b) PCM liquid fraction and (c) the total charging time.

Corresponding to a 76% of E_{ch}.

Fig. 4.5a reveals radius ratio R/r_f exerts a substantial influence on the PCM temperature evolution, with $R/r_f < 5$ seeing a quite rapidly charging ($t_{ch}^{tot} \leqslant 3.6$ h). As shown in Fig. 4.5b, the radius ratios of 4, 5, and 6 achieve almost the equal liquid fraction (~0.95) at the end of charging. By contrast, the liquid fraction in the radius ratio of 8 only rises to less than 0.75 at the charging time 10 h. Fig. 4.5c shows a rise in unit height H from 0.6 to 1.2 m leads to 14-26% longer total charging times, depending on R/r_f. Because the total stored energy increases proportionally with the unit height, a longer charging time for a higher unit indicates a relatively lower increase in the average energy storage rate.

Fig. 4.6a compares the average heat storage density in PCM at three instants, t = 4, 6, and 8 h for two sets of units H = 0.6 and 1.2 m. Over a charging duration of 6 h, radius ratio R/r_f = 5 with H = 0.6 m attains the optimal heat storage density Q_m^{opt} (corresponding to E_{ch} = 0.95), while radius ratios R/r_f = 6 and 8 with the same unit height only reach 85 and 55% of Q_m^{opt}. As the charging proceeds to 8 h, radius ratio R/r_f = 6 achieves Q_m^{opt} while R/r_f = 8 only rises to

69% of Q_m^{opt}. Fig. 4.6a also shows that a higher unit obtains a lower energy storage density, with 9-14% lower for R/r_f = 6 and 13-15% lower for R/r_f = 8 depending on the charging duration (4, 6, or 8 h). Fig. 4.6b presents the results of the average energy storage rate $\bar{q}_{ch}$ and the total stored energy Q_{ch}^{tot} in relation to R/r_f. It is shown that a rise in R/r_f increases Q_{ch}^{tot} but exhibits different effects on $\bar{q}_{ch}$. A variation in R/r_f from 2 to 4 drops $\bar{q}_{ch}$ by 19.4% for H = 0.6 m, and by 22.3% for H = 1.2 m. However, $\bar{q}_{ch}$ is minorly affected by R/r_f in the range of 4-8 for both unit heights, mainly due to the different enhancement effects from PCM natural convection in different R/r_f. On the other hand, a height rise from 0.6 to 1.2 m raises $\bar{q}_{ch}$ by 60-76% for different R/r_f, relatively lower compared with a 100% increase in the heat transfer surface area resulted from the height variation.

Fig. 4.6a reveals that an increase in R/r_f means a longer time needed to achieve the optimal heat storage density. Fig. 4.6b indicates that a longer charging time in the R/r_f range of 4, 5, 6 and 8 leads to a nearly linear augmentation in the total stored heat because of an almost equal $\bar{q}_{ch}$ among these radius ratios. From the heat storage aspect, the preferable radius ratio mainly depends on the charging duration which enables an LHTES unit to utilize its maximum possible energy storage capacity. In the context of solar thermal energy storage, the present study assumes the charging time available from a solar harvesting application to range from 6 to 8 h, a more moderate assumption compared with 10 h adopted by [21]. It can be seen from Fig. 4.6a that over a charging of 6-8 h, radius ratios R/r_f = 5 with both unit heights and R/r_f = 6 with H = 0.6 m attain the optimal energy storage density, while R/r_f = 6 with H = 1.2 m achieves 92% of Q_m^{opt}. Therefore, the optimal R/r_f range is found to be around 5-6 based on the heat storage performance.

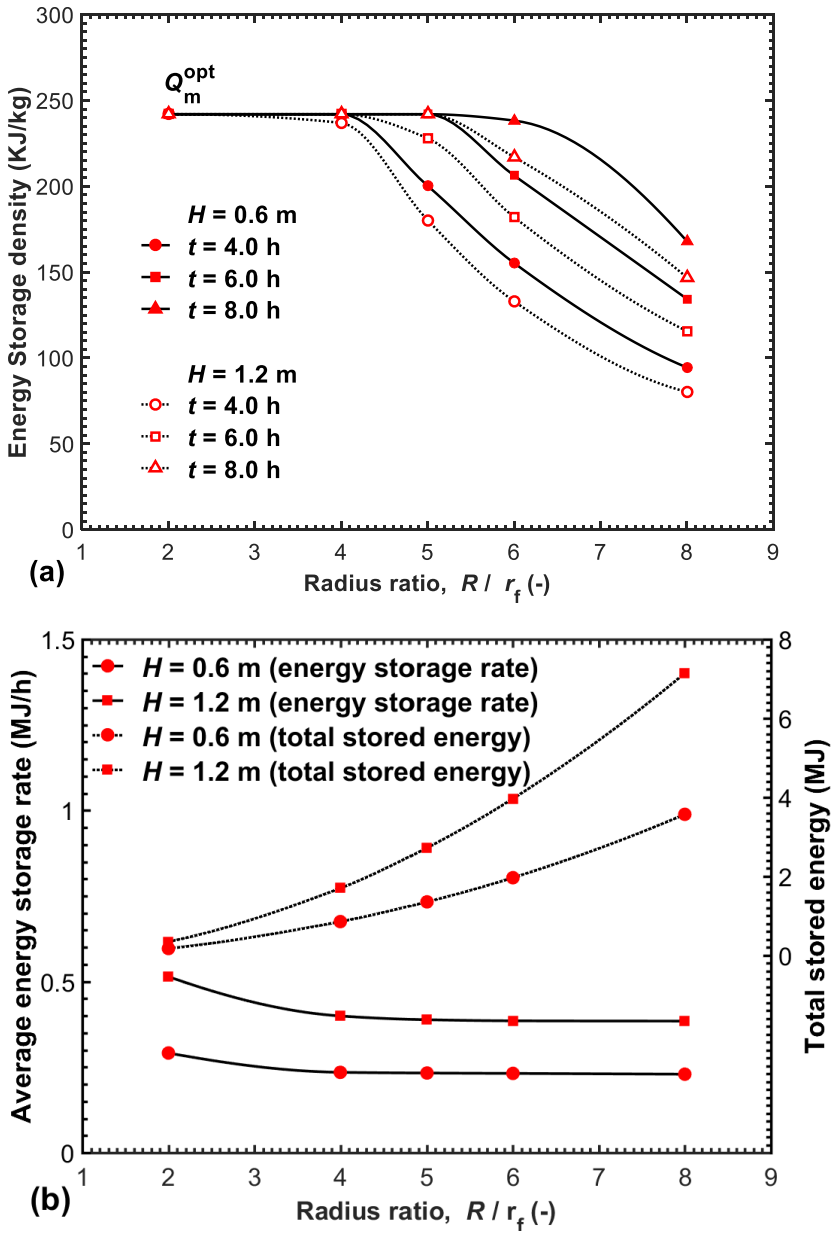

Fig. 4.6. Comparisons of (a) average energy storage density and (b) average energy storage rate and the total stored energy in relation to R/r_f during charging.

4.5.2. Discharging process

Fig. 4.7a records PCM mass-averaged temperatures during discharging for different R/r_f with H = 0.6 m. The fastest decline in PCM temperature is seen in radius ratio R/r_f = 2, E_{dis} of which rises to 0.95 within only 0.7 h. Comparatively, radius ratios R/r_f = 4 and 5 take approximate 8.0 and 15.4 h to complete the discharging. PCM temperatures in radius ratios

R/r_f = 6 and 8 turn to fall slowly at t = 2.5 h and persist with this trend beyond t = 20 h, implying the heat release rates in both radius ratios decline abruptly since t = 2.5 h. Fig. 4.7b shows the radius ratio R/r_f = 5 nearly totally solidify over around 15 h of discharging, while the liquid fraction in radius ratio R/r_f = 6 is still above 0.2 at the discharging time of 20 h. As a result, radius ratio R/r_f = 6 has a 68% longer total discharging time compared with R/r_f = 5, as shown in Fig. 4.7c. It is also evident from Fig. 4.7c that a rise in H performs minor influence on the total discharging time, which can be interpreted as follows, i) PCM solid-liquid interface

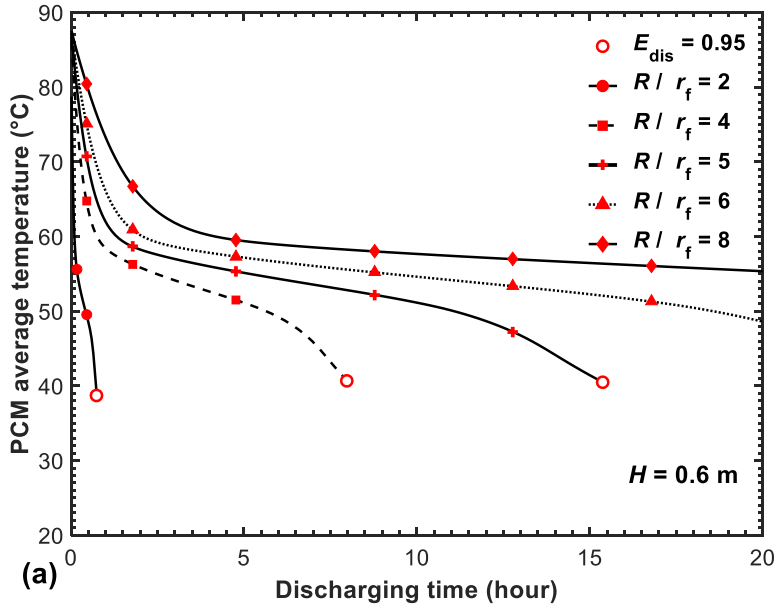

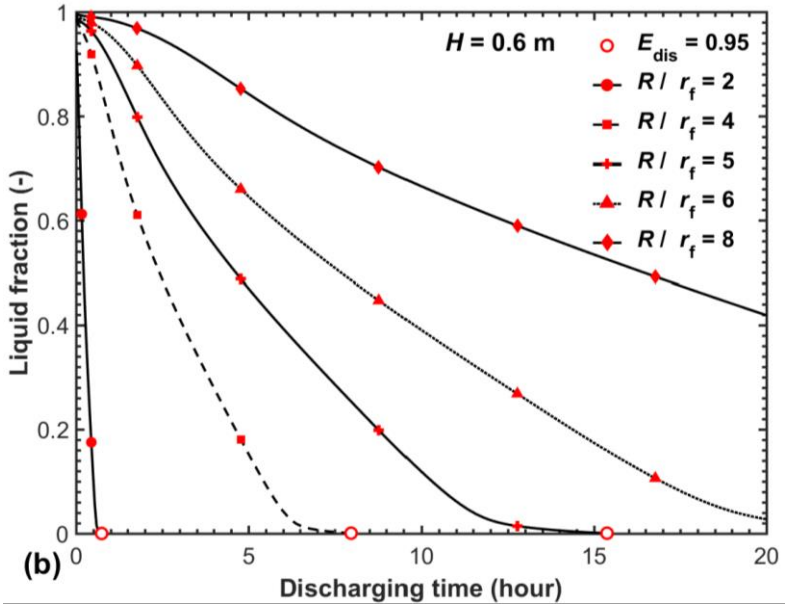

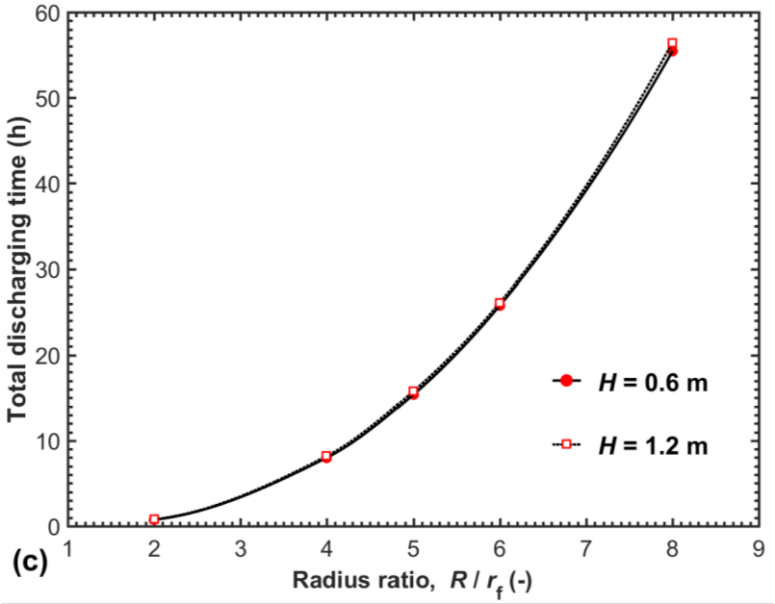

Fig. 4.7. Comparisons of (a) PCM average temperature, (b) PCM liquid fraction and (c) the total discharging time.

evolves outwards nearly in parallel with HTF-tube due to a conduction-dominated heat transfer in PCM solidification, ii) the difference in HTF-tube surface temperature along the axial direction is small thanks to a fast HTF flowing speed. Consequently, a rise in H leads to an almost proportional augmentation in heat release rate hence a nearly equal total discharging time between different heights.

Fig. 4.8a compares the average energy release density at three time instants t = 7.5, 15, and 20 h for different R/r_f with H = 0.6 and 1.2 m. Regardless of H, at t = 15 h radius ratio R/r_f = 5 is close to achieving the optimal heat release density Q_m^{opt} (corresponding to E_{dis} = 0.95), whereas radius ratios R/r_f = 6 and 8 reach only 69% and 47% of Q_m^{opt}. The heat release density evolutions in R/r_f = 6 and 8 from t = 7.5 to 20 h demonstrate that a R/r_f exceeding 5 results in a much lower heat release rate. In addition, Fig. 4.8a shows that the unit height has a slight influence on the energy release density over the same discharging duration, further evidencing the proportional relationship between variations in unit height and the heat release rate.

Fig. 4.8b presents the total released energy $Q_{\mathrm{dis}}^{\mathrm{tot}}$ and the average energy release rate $\bar{q}_{\mathrm{dis}}$ for different R/r_{f}. It is shown that in the set of units with H = 0.6 m, there are a 54.2% decrease in $\bar{q}_{\mathrm{dis}}$ with R/r_{f} increasing from 2 to 4 and decreases of 16.9%, 12.7% and 16.3% from 4 to 5, from 5 to 6 and from 6 to 8. On the other hand, variations in R/r_{f} from 2 to 4, 4 to 5, 5 to 6 and 6 to 8 respectively result in 404%, 60%, 46% and 80% higher $Q_{\mathrm{dis}}^{\mathrm{tot}}$. The combined effect on $Q_{\mathrm{dis}}^{\mathrm{tot}}$ and $\bar{q}_{\mathrm{dis}}$ from increases in R/r_{f} leads to the extremely long discharging times for R/r_{f} greater than 5 (Fig. 4.7b). More care needs to be taken with evaluating the effect of increasing R/r_{f} on discharging.

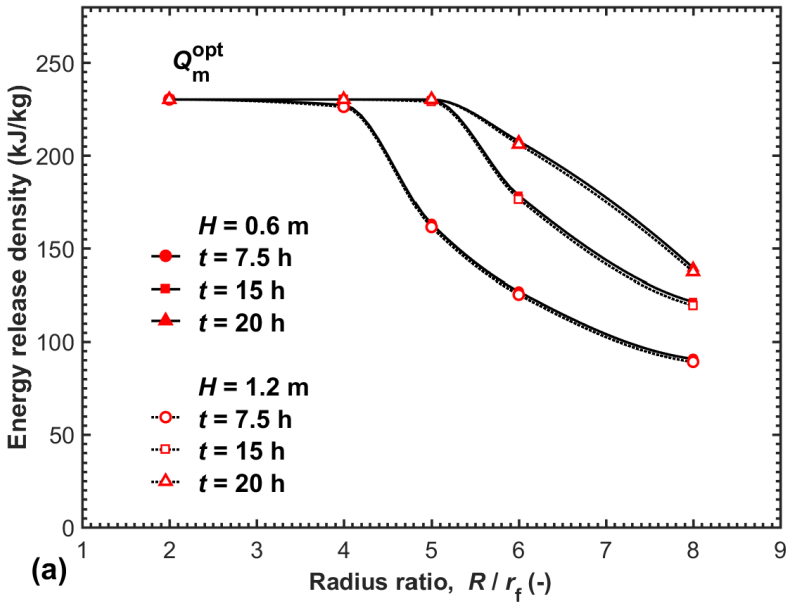

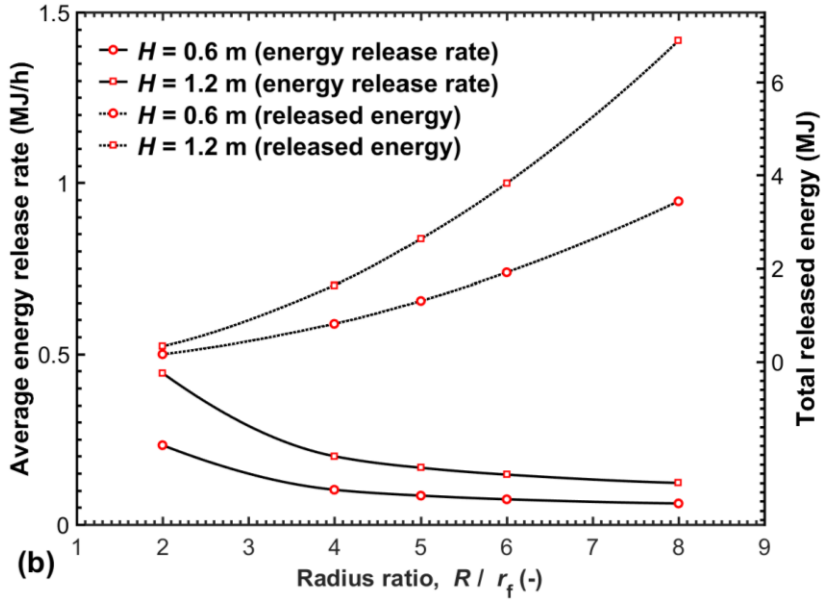

Fig. 4.8. Comparisons of (a) average energy release density and (b) average heat release rate and the total released energy.

4.5.3. Performance evaluation under both charging and discharging processes

Combining Sections 4.5.1.1 and 4.5.1.2, it is revealed that regardless of the unit height, an increase in radius ratio R/r_f greater than 2 shows a slight influence on the average energy storage rate but considerably decreases the average heat release rate, indicating the discharging is more sensitive to a variation in R/r_f. The total discharging time increases almost 6 times along with a rise in R/r_f from 4 to 8, compared with around 3 times increase in the total charging time. This pattern can be explained by that charging and discharging are dominated by different heat transfer mechanisms either natural convection or conduction [38], on which R/r_f exhibits different effects. A charging is believed to be faster than a discharging due to an enhancement effect by natural convection [36]. In the present study, the difference between durations of charging and discharging may characterize the difference in natural convection intensity between the two processes because PCM has the same properties in liquid and solid phases including thermal conductivity and specific heat, and because working temperatures are set

symmetrically relative to PCM average melting temperature. Table 4.3 summarizes the discharging-to-charging time ratios ($\Gamma = t_{dis}^{tot} / t_{ch}^{tot}$) for all radius ratios. Γ approximately equals to 1.1 for $R/r_f = 2$ with both heights, suggesting that natural convection effect on melting in such units is less pronounced. Along with further increases in R/r_f with H = 0.6 and 1.2 m, Γ rises to the range of 1.9-3.7, reflecting a noticeable role of natural convection on melting, accordingly a much slower discharging relative to charging.

Table 4.3 The discharging-to-charging time ratio (Γ) for different R/r_f.

R/r_f (-)	Γ (H = 0.6 m)	Γ (H = 1.2 m)
2	1.2	1.1
4	2.2	1.9
5	2.7	2.3
6	3.2	2.5
8	3.7	3.0

As the radius ratio R/r_f generates different effects on charging and discharging, it is necessary to further examine the overall charging and discharging performance in R/r_f = 5 and 6 which perform best during charging. Table 4.4 presents the released energy and the energy release ratio for R/r_f =5 and 6 over a total charging-and-discharging time of 24 h along with the total energy stored for charging. Though R/r_f = 6 stores 42% higher energy in charging compared with R/r_f = 5, its total discharged energy is only 10.4% higher for H = 0.6 m, and 2.5% higher for H = 1.2 m. R/r_f = 6 obtains a much smaller E_{dis} (0.76 for H = 0.6 m and 0.7 for H = 1.2 m), indicating a much lower energy release efficiency achieved. Moreover, it can be deduced from Tables 4.3 and 4.4 that regardless of the unit height, the radius ratio R/r_f greater than 6 will not increase the released energy meaningfully over a total charging-and-

discharging time of 24 h while its energy release efficiency will drop further because of a much slower discharging relative to charging. In conclusion, a radius ratio of 5 is found to have the best overall charging and discharging performance over a total charging-and-discharging duration of 24 h. A R/r_f greater than 5 will lead to a much lower energy release efficiency without a meaningful increase in the energy released.

Table 4.4 The total stored energy (Q_{ch}^{tot}) for R/r_f = 5 and 6 when E_{ch} = 0.95, and the released energy (Q_{dis}^{tot}) once E_{dis} rises to 0.95 or the total charging-and-discharging time reaches 24 h.

H (m)	R/r_f (-)	Q_{ch}^{tot} (kJ)	Q_{dis}^{tot} (kJ)	E_{dis} (-)
0.6	5	1365.3	1297.0	0.95
	6	1979.0	1512.5	0.76
1.2	5	2719.5	2583.5	0.95
	6	3965.8	2767.4	0.70

The numerical model developed ignores the effects of the PCM volume change which takes place due to the temperature variation and phase change. It is still unclear how the simplification influences the accuracy of the numerical result. Other limitations include the boundary condition settings and the variation in the mushy zone constant. The effects of these limitations need to be accounted for in future research.

4.6. Conclusions

In this chapter, the complex effects of geometrical design in a vertical shell-and-tube type LHTES system on charging and discharging are numerically investigated. The investigated cases are made up of various shell radii with an identical HTF-tube radius and two unit heights are considered simultaneously. Based on a validated PCM-HTF conjugate analytic model, PCM average temperature, the total charging/discharging time, heat storage/release density,

average heat storage/release rate, and the total stored/released energy are compared and analysed. The conclusions can be deduced as follows,

(1) As the HTF-tube radius is fixed, the optimal R/r_f range is found to be around 5-6 based on the evaluation of charging performance. However, with the discharging performance considered, the optimal R/r_f has to be limited to 5. A R/r_f smaller than 5 significantly decreases the energy storage capacity while greater than 5 leads to a sharp decline in the energy release efficiency.

(2) As the unit height increases, the optimal radius ratio slightly reduces in the charging process and shows no change in the discharging process. Hence, for the whole charging-discharging process, the unit height exhibits a negligible influence on the selection of the optimal radius ratio. However, a rise in unit height generates a nearly proportional increase in discharging rate but a relatively lower increase in charging rate.

Based on the physical model and numerical model developed above, next chapter will continue to investigate the radius ratio with a new series of parameters defined by varying the inner HTF-tube size while fixing the outer shell size. This is essential to a comprehensive understanding of this topic.

4.7. References

[1] Tao, Y. B., Liu, Y. K. ,He, Y.-L., Effects of PCM arrangement and natural convection on charging and discharging performance of shell-and-tube LHTES unit, Int. J. Heat Mass Transf. 115 (2017) 99-107.

[2] Han, G.-S., Ding, H.-S., Huang, Y., Tong, L.-G. ,Ding, Y.-L., A comparative study on the performances of different shell-and-tube type latent heat thermal energy storage units including the effects of natural convection, Int. Commun. Heat Mass. 88 (2017) 228-235.

[3] Seddegh, S., Wang, X., Joybari, M. M. ,Haghighat, F., Investigation of the effect of geometric and operating parameters on thermal behavior of vertical shell-and-tube latent heat energy storage systems, Energy. 137 (2017) 69-82.

[4] Shen, G., Wang, X., Chan, A., Cao, F. ,Yin, X., Study of the effect of tilting lateral surface angle and operating parameters on the performance of a vertical shell-and-tube latent heat energy storage system, Sol. Energy. 194 (2019) 103-113.

[5] Zheng, Z.-J., Xu, Y. ,Li, M.-J., Eccentricity optimization of a horizontal shell-and-tube latent-heat thermal energy storage unit based on melting and melting-solidifying performance, Appl. Energy. 220 (2018) 447-454.
[6] Akgün, M., Aydın, O. ,Kaygusuz, K., Thermal energy storage performance of paraffin in a novel tube-in-shell system, Appl. Therm. Eng. 28 (2008) 405-413.
[7] Cao, Y. ,Faghri, A., Performance characteristics of a thermal energy storage module: a transient PCM/forced convection conjugate analysis, Int. J. Heat Mass Transf. 34 (1991) 93-101.
[8] Cao, Y., Faghri, A. ,Juhasz, A., A PCM/forced convection conjugate transient analysis of energy storage systems with annular and countercurrent flows, J Heat Transf. 113 (1991) 37-42.
[9] Lacroix, M., Numerical simulation of a shell-and-tube latent heat thermal energy storage unit, Sol. Energy. 50 (1993) 357-367.
[10] Conti, M., Bellecci, C. ,Charach, C., Thermodynamic design of a phase change thermal storage module, Journal of solar energy engineering. 118 (1996) 89-96.
[11] Tao, Y.-B., Li, M.-J., He, Y.-L. ,Tao, W.-Q., Effects of parameters on performance of high temperature molten salt latent heat storage unit, Appl. Therm. Eng. 72 (2014) 48-55.
[12] Wang, W.-W., Wang, L.-B. ,He, Y.-L., The energy efficiency ratio of heat storage in one shell-and-one tube phase change thermal energy storage unit, Appl. Energy. 138 (2015) 169-182.
[13] Wang, W.-W., Wang, L.-B. ,He, Y.-L., Parameter effect of a phase change thermal energy storage unit with one shell and one finned tube on its energy efficiency ratio and heat storage rate, Appl. Therm. Eng. 93 (2016) 50-60.
[14] Erek, A. ,Dincer, I., An approach to entropy analysis of a latent heat storage module, Int. J. Therm. Sci. 47 (2008) 1077-1085.
[15] Ezan, M. A., Ozdogan, M. ,Erek, A., Experimental study on charging and discharging periods of water in a latent heat storage unit, Int. J. Therm. Sci. 50 (2011) 2205-2219.
[16] Tan, P. 2018. *On the Design Considerations for Thermal Energy Storage with Phase Change Materials: Material characterization and Modelling.* Licentiate thesis, Chalmers University of Technology.
[17] Ismail, K. ,Melo, C., Convection‐based model for a PCM vertical storage unit, Int. J. Energy Res. 22 (1998) 1249-1265.
[18] Ismail, K. a. R. ,Abugderah, M. M., Performance of a thermal storage system of the vertical tube type, Energy Conv. Manag. 41 (2000) 1165-1190.
[19] Trp, A., Lenic, K. ,Frankovic, B., Analysis of the influence of operating conditions and geometric parameters on heat transfer in water-paraffin shell-and-tube latent thermal energy storage unit, Appl. Therm. Eng. 26 (2006) 1830-1839.
[20] Esen, M., Durmuş, A. ,Durmuş, A., Geometric design of solar-aided latent heat store depending on various parameters and phase change materials, Sol. Energy. 62 (1998) 19-28.
[21] Pirasaci, T. ,Goswami, D. Y., Influence of design on performance of a latent heat storage system for a direct steam generation power plant, Appl. Energy. 162 (2016) 644-652.
[22] Tehrani, S. S. M., Taylor, R. A., Saberi, P. ,Diarce, G., Design and feasibility of high temperature shell and tube latent heat thermal energy storage system for solar thermal power plants, Renew. Energy. 96 (2016) 120-136.
[23] Ismail, K. ,Goncalves, M., Thermal performance of a PCM storage unit, Energy Conv. Manag. 40 (1999) 115-138.

[24] Guo, C. ,Zhang, W., Numerical simulation and parametric study on new type of high temperature latent heat thermal energy storage system, Energy Conv. Manag. 49 (2008) 919-927.
[25] Longeon, M., Soupart, A., Fourmigué, J.-F., Bruch, A. ,Marty, P., Experimental and numerical study of annular PCM storage in the presence of natural convection, Appl. Energy. 112 (2013) 175-184.
[26] Xiao, X. ,Zhang, P., Numerical and experimental study of heat transfer characteristics of a shell-tube latent heat storage system: Part I – Charging process, Energy. 79 (2015) 337-350.
[27] Fang, Y., Niu, J. ,Deng, S., Numerical analysis for maximizing effective energy storage capacity of thermal energy storage systems by enhancing heat transfer in PCM, Energy Build. 160 (2018) 10-18.
[28] RT60 Data Sheet. Rubitherm Technologies GmbH, (2019).
[29] Zheng, Z.-J., Li, M.-J. ,He, Y.-L., Thermal analysis of solar central receiver tube with porous inserts and non-uniform heat flux, Appl. Energy. 185 (2017) 1152-1161.
[30] Voller, V. R. ,Prakash, C., A fixed grid numerical modelling methodology for convection-diffusion mushy region phase-change problems, Int. J. Heat Mass Transf. 30 (1987) 1709-1719.
[31] Fornarelli, F., Camporeale, S. M., Fortunato, B., Torresi, M., Oresta, P., Magliocchetti, L., Miliozzi, A. ,Santo, G., CFD analysis of melting process in a shell-and-tube latent heat storage for concentrated solar power plants, Appl. Energy. 164 (2016) 711-722.
[32] Seddegh, S., Wang, X. ,Henderson, A. D., A comparative study of thermal behaviour of a horizontal and vertical shell-and-tube energy storage using phase change materials, Appl. Therm. Eng. 93 (2016) 348-358.
[33] Al-Abidi, A. A., Mat, S., Sopian, K., Sulaiman, M. Y. ,Mohammad, A. T., Numerical study of PCM solidification in a triplex tube heat exchanger with internal and external fins, Int. J. Heat Mass Transf. 61 (2013) 684-695.
[34] Hong, Y., Ye, W.-B., Huang, S.-M., Yang, M. ,Du, J., Thermal storage characteristics for rectangular cavity with partially active walls, Int. J. Heat Mass Transf. 126 (2018) 683-702.
[35] Adine, H. A. ,El Qarnia, H., Numerical analysis of the thermal behaviour of a shell-and-tube heat storage unit using phase change materials, Appl. Math. Model. 33 (2009) 2132-2144.
[36] Niyas, H., Prasad, S. ,Muthukumar, P., Performance investigation of a lab–scale latent heat storage prototype–Numerical results, Energy Conv. Manag. 135 (2017) 188-199.
[37] Rathod, M. ,Banerjee, J., Experimental investigations on latent heat storage unit using paraffin wax as phase change material, Exp. Heat Transf. 27 (2014) 40-55.
[38] Seddegh, S., Wang, X. ,Henderson, A. D., Numerical investigation of heat transfer mechanism in a vertical shell and tube latent heat energy storage system, Appl. Therm. Eng. 87 (2015) 698-706.

Chapter 5: Numerical investigation on optimal shell-to-tube radius ratio in vertical cylindrical latent heat storage systems under a fixed shell radius

5.1. Chapter summary

This chapter investigates the thermal performances of a series of geometrical designs in a vertical cylindrical latent heat storage system. This series of geometries is defined by varying the HTF-tube radius (r) with the PCM shell radius (R_f) fixed, featuring a range of 2.5 to 9 in the shell-to-tube radius ratio (R_f/r). A unit height variation from 0.6 m to 1.2 m is also considered along with the varied inner tube radius. This chapter follows and supplements the last chapter's investigation, which focuses on a series of geometries with the shell radius changed and the tube size fixed. For the comparison purpose, the PCM and HTF, the tube wall material, and the initial and boundary conditions used in this chapter are the same as those in the last chapter. The numerical model developed and validated in chapter 4 is also employed in this chapter to evaluate the performance of the new series of geometries. The examination reveals the R_f/r of 5 offers the optimal thermal performance by significantly boosting both heat storage and release rates while with minor influence on energy storage capacity. Besides, the unit height shows a negligible impact on the determined optimal radius ratio.

The research presented in this chapter and Chapter 4 has been combined to a draft manuscript, which has been submitted as: Gang Shen, Xiaolin Wang, Andrew Chan, Feng Cao, Xiang Yin, "Numerical investigation on optimal shell-to-tube radius ratio of a vertical cylindrical latent heat storage system", to Solar Energy.

5.2. Introduction

The last chapter shows that the appropriate geometrical design can maximise the boost to heat transfer in the LHTES system. Through a comprehensive numerical investigation, it was concluded that with a fixed HTF-tube radius, the shell size increasing to when R/r_f equals to 5 can best balance the energy storage capacity and the energy storage/release rate. Meanwhile, a further understanding of the effect of the HTF-tube size is essential to design an effective shell-and-tube PCM storage system. A variation in the HTF-tube size inevitably leads to changes in the HTF operating parameters and the heat transfer surface area between the PCM and HTF, which in turn affect the heat transfer coefficient in the LHTES system [1].

Seddegh et al. [2] hold the shell size constant and built four vertical cylindrical LHTES units with different inner tube radii. The experimental results and analysis indicate the R/r of 5.4 is superior in balancing the total amount of stored energy, the charging rate and discharging rate.

Tao et al. [3] developed and validated a simulation code to investigate the melting performance in a horizontal cylindrical PCM storage unit. With a constant HTF mass flow rate operating and the total PCM amount fixed, an increase in the HTF-tube radius was found to lead to a significant increase in the melting duration. Kibria et al. [4] experimentally and numerically studied melting and solidification characteristics of PCM in a shell-and-tube LHTES unit. The effects of HTF flow parameters and tube sizes including the tube radius and thickness were examined. The numerical results indicated the larger tube radius led the solidification cycle to be faster and observe the higher HTF outlet temperature.

Tan [5] modelled horizontal cylindrical PCM storage cases to perform the geometrical and operating parameter study. It was stated that the larger HTF-tube diameter enhanced the capacity effectiveness (η_Q) with the same HTF flow velocity operated, while the HTF-tube size showed a minor impact on the efficiency under the same HTF mass flow rate.

Liu et al. [6] held both PCM amount and outer shell diameter constant to numerically study a series of horizontal multitube LHTES systems. They altered the inner tube arrangement via two parameters, the tube number and tube radius, to investigate 16 cases in terms of melting time and exergy efficiency. It was stated that PCM melts faster with smaller outer-tube size.

Tehrani et al. [7] developed a two-dimensional numerical model and examined the energy storage/release performances in a multitube-in-tank PCM storage system. The study varied the geometrical parameters including L, L/d, and R/r_o while holding the total PCM volume constant. The results suggested that the optimal selection of the geometric parameters influenced each other and was also affected by the PCM type. The length ratio and radius ratio were recommended to be around 40-60 and 1.3-1.8 respectively for the PCMs chosen in the study.

Pirasaci and Goswami [8] formulated a two-dimensional model to study the discharging process operated at the high-temperature range in a multitube-in-tank LHTES system. They claimed that the HTF-tube radius affected the discharging effectiveness more significantly than the tube distance.

Esen et al. [9] numerically evaluated the effect of geometrical parameters in a vertical multitube-in-tank PCM storage. The results indicated that a larger HTF-tube size increased the total melting time for all the studied PCMs given that the PCM volume and HTF flow mass rate were kept constant.

The literature review above indicates there are limited reports on the optimal selection of the HTF-tube size. Seddegh et al. [2] proposed an optimal HTF-tube size (the shell-to-tube

radius ratio) for a vertical single-pass LHTES system, while Tehrani et al. [7] recommended the radius ratio range of 1.3-1.8 for a multitube-in-tank PCM storage module. Besides, several studies [3, 8, 9] assessed the effect of the HTF-tube size based on investigating only a single thermal cycle, either charging or discharging.

This chapter aims to investigate the effect of the tube size in the single pass shell-and-tube LHTES system during both charging and discharging cycles. Based on the physical model defined in the last chapter, this chapter further varies the inner HTF-tube radius (r) with the PCM shell radius (R_f) fixed, formulating a new series of geometrical definitions. The PCM-HTF conjugate model established in the last chapter is employed to deal with the transient heat transfer, HTF flow, phase transition, and natural convection flow in the PCM storage unit. The performance indices including E_{ch}/E_{dis}, $Q_{ch}^{tot}/Q_{dis}^{tot}$, $\overline{q}$ and Q_m are compared and evaluated for the charging and discharging processes in the context of solar thermal energy storage.

5.3. Numerical study under a fixed shell radius

5.3.1. Physical model

Fig. 5.1 shows the schematic of the physical model and the geometrical definition. With the shell radius (R_f) fixed to 63.5 mm, the HTF tube radius (r) varies from 7.06 to 25.4 mm, producing five radius ratios from 2.5 to 9. The two unit heights 0.6 m and 1.2 m are also considered with the different inner tube sizes. Table 5.1 lists the geometrical parameters and HTF average inlet velocities corresponding to each geometrical definition.

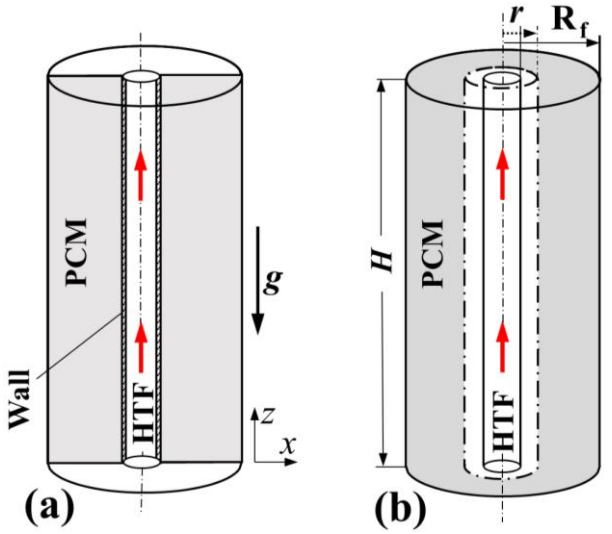

Fig. 5.1. Schematic of the physical model (a) and the geometrical definition of varying HTF-tube radius with shell radius fixed (b).

Table 5.1 Summary of geometrical parameters and HTF average inlet velocities.

Varying tube radius under a fixed shell radius R_f (63.5 mm)				
Unit height H (m)	Radius ratio R_f/r (-)	Tube outer radius r (mm)	Total PCM mass for H = 0.6 m (kg)	HTF inlet velocity (m/s)/ Re (-)
0.6, 1.2	2.5	25.4	4.91	0.045/3331
	4.0	15.9	5.48	0.123/5559
	6.7	9.50	5.72	0.382/9677
	9.0	7.06	5.78	0.774/13779

5.3.2. Numerical model

This chapter defines a new series of geometries, based on the same single pass shell-and-tube physical model investigated in the last chapter while varying the different geometry, the inner HTF-tube. As stated above, to provide better understanding of the optimal design in the vertical cylindrical LHTES system, the simulations in this chapter were performed using the same conjugate analytic model already developed and validated by the last chapter. Besides,

for the same purpose, the PCM type, performance indicators, as well as the initial and boundary conditions are also kept the same as those of the numerical examination in the last chapter.

5.4. Results and discussions

5.4.1. Charging process

Fig. 5.2a, b and c respectively plot PCM mass-averaged temperatures, liquid fraction and the total charging times for different R_f/r. It is noticeable from Fig. 5.2a that a smaller radius ratio R_f/r yields a quicker rise in PCM temperature and thus a faster charging. Fig. 5.2b highlights PCM liquid fraction evolves with a similar trend as the average temperature, smaller R_f/r melting faster. Fig. 5.2c shows that the total charging time more than doubles for the rise in R_f/r from 2.5 to 9 with H = 0.6 m. The variations in PCM temperature and the total charging time across different R_f/r can be attributed to two factors, a smaller heat transfer surface area (75% smaller) and more PCM amount (23% more) in the radius ratio R_f/r = 9 compared with R_f/r = 2.5. It is also worth noting that a larger radius ratio

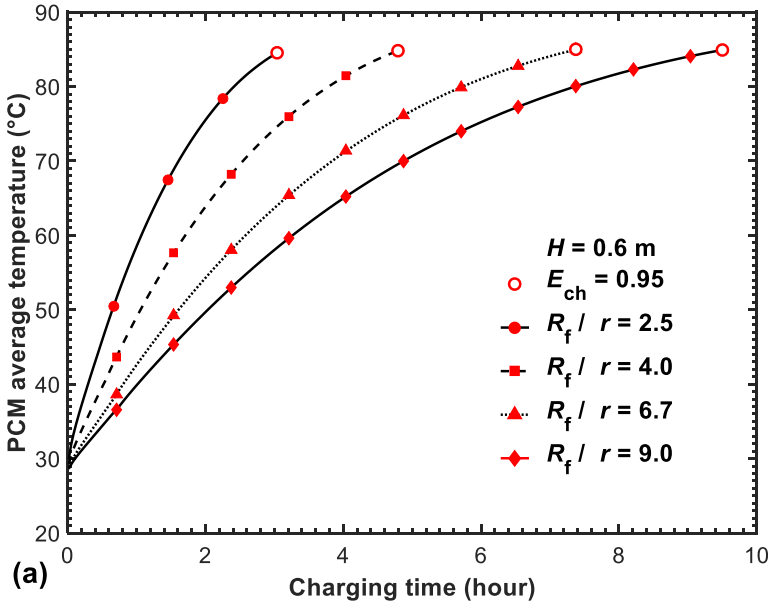

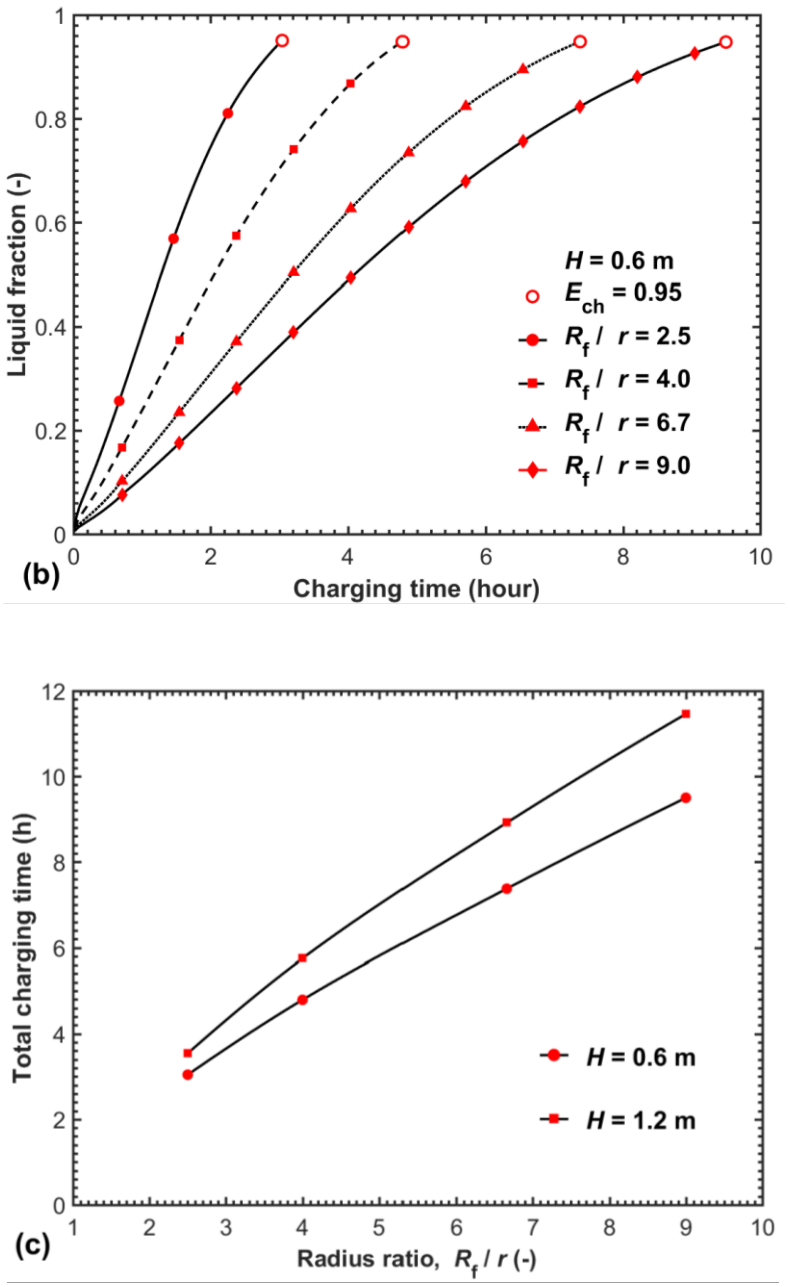

Fig. 5.2. (a) PCM average temperature, (b) PCM liquid fraction and (c) total charging time during charging.

R_f/r has a higher HTF Reynolds number (Table 5.1) which enhances heat transfer between HTF and PCM. However, its positive effect on the charging rate is marginal compared with the combined effect from a smaller heat transfer surface area and a more PCM amount.

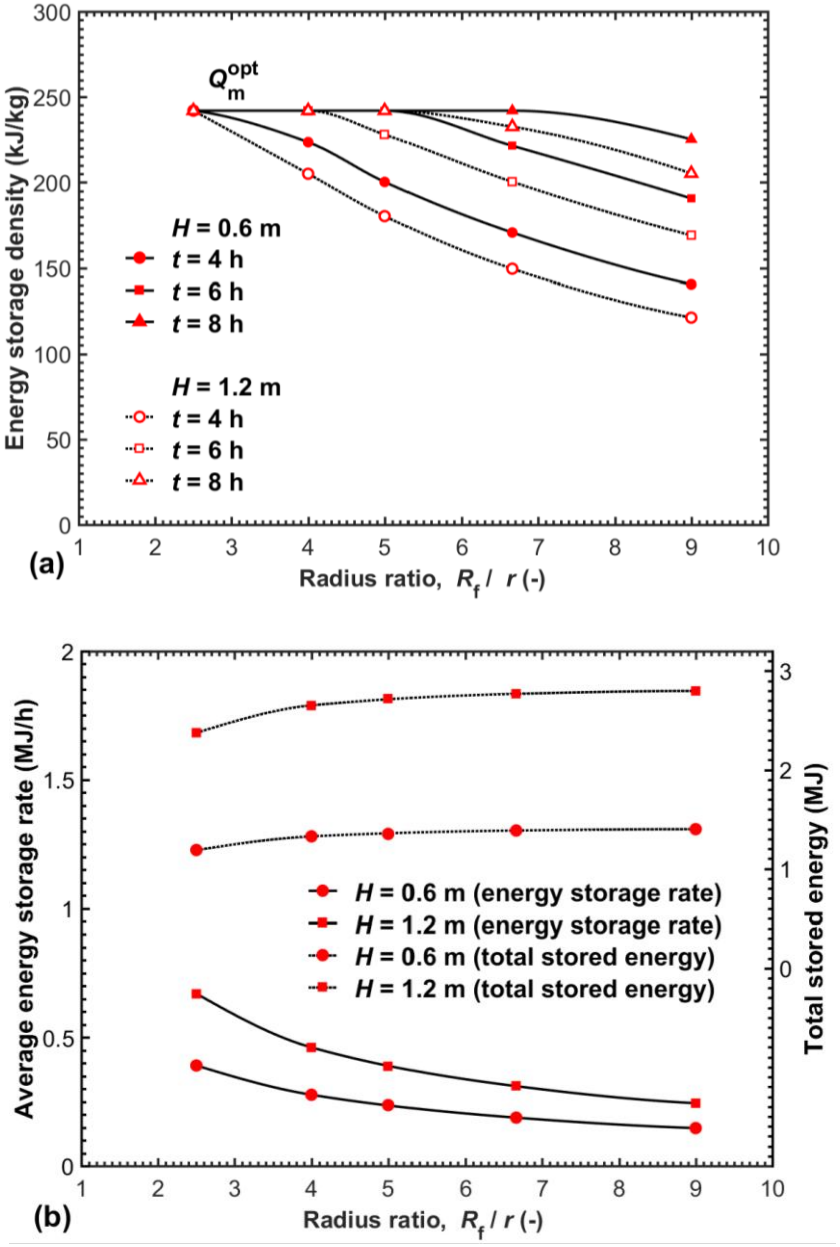

Fig. 5.3. Comparisons of (a) average energy storage density and (b) average energy storage rate and the total stored energy during charging.

Fig. 5.3a plots the average heat storage density for two sets of units with the different unit heights at three different time instants. It shows a radius ratio R_f/r equal and less than 5 with both heights H = 0.6 and 1.2 m can attain the optimal heat storage density Q_m^{opt} within a charging duration range of 6-8 h. Fig. 5.3b compares the average energy storage rate and total stored energy in relation to R_f/r. It is shown that in the set of units with H = 0.6 m the increases in R_f/r from 5 to 6.7 and from 6.7 to 9 lead to marginal augmentations in the total stored energy

Q_{ch}^{tot} but substantially lower the average energy storage rate $\bar{q}_{ch}$ by 20.6% and 21.6% respectively. On the other hand, for R_f/r to vary from 5 to 4, $\bar{q}_{ch}$ increases by 17% with a 3% loss in Q_{ch}^{tot}. But a further decrease in R_f/r from 4 to 2.5 will result in a as much as 10.4% loss in Q_{ch}^{tot}. A similar pattern is observed in the set of units with H = 1.2 m.

5.4.2. Discharging process

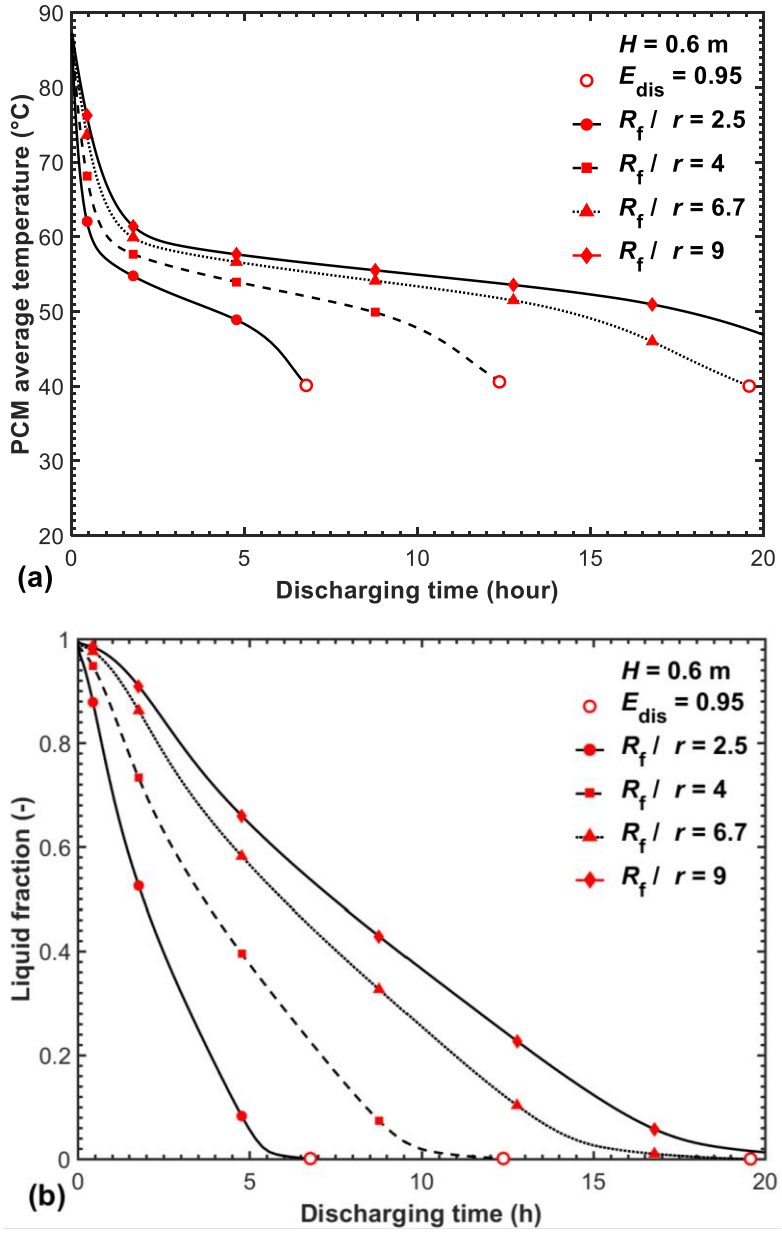

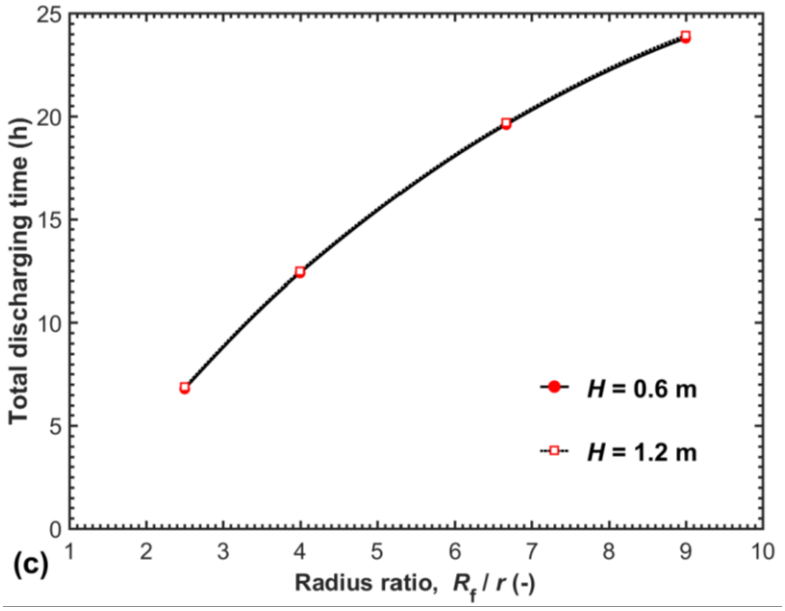

Fig. 5.4. (a) PCM temperature, (b) PCM liquid fraction and (c) total discharging time during discharging.

The comparisons of PCM mass-averaged temperatures, liquid fraction and the total discharging times are presented in relation to R_f/r by Fig. 5.4a, b and c. It is observed in Fig. 5.4a PCM temperatures in all radius ratios decline rapidly within the first hour and then turn to level off at different times, recording a consistently lower value in a smaller R_f/r. Fig. 5.4b shows the same pattern in PCM liquid fraction's evolving, the smaller R_f/r decreasing much faster. This is mainly due to the larger heat transfer area and the less PCM amount within a smaller R_f/r. Fig. 5.4c shows that a rise in R_f/r from 2.5 to 9 leads to more than 2.5 times increase in the total discharging time.

Fig. 5.5a compares the average energy release density at three different time instants in relation to R_f/r with H = 0.6 and 1.2 m. It is shown that a R_f/r between 4 to 5 can achieve the optimal heat release density Q_m^{opt} over a discharging duration of 15 to 20 h, while a selection of R_f/r exceeding 5 results in a much lower heat release density. Fig. 5.5b illustrates the effects of radius ratio R_f/r with H = 0.6 and 1.2 m on the average heat release rate ($\bar{q}_{dis}$) and total released energy (Q_{dis}^{tot}). Taking the set of units with H = 0.6 m for example, it is observed that

for R_f/r greater than 5, the positive effect on the total released energy Q_{dis}^{tot} becomes negligible, a 2.2% higher with R_f/r increasing from 5 to 6.7. Comparatively, the same increase in R_f/r leads to a pronounced 19.6% decrease in the average heat release rate $\bar{q}_{dis}$. On the other hand, for R_f/r to decrease from 5 to 4, $\bar{q}_{dis}$ increases by 21% with a 2.4% loss in Q_{dis}^{tot}. But a further decrease in R_f/r from 4 to 2.5 will lead to a more than 10% reduce in Q_{dis}^{tot}.

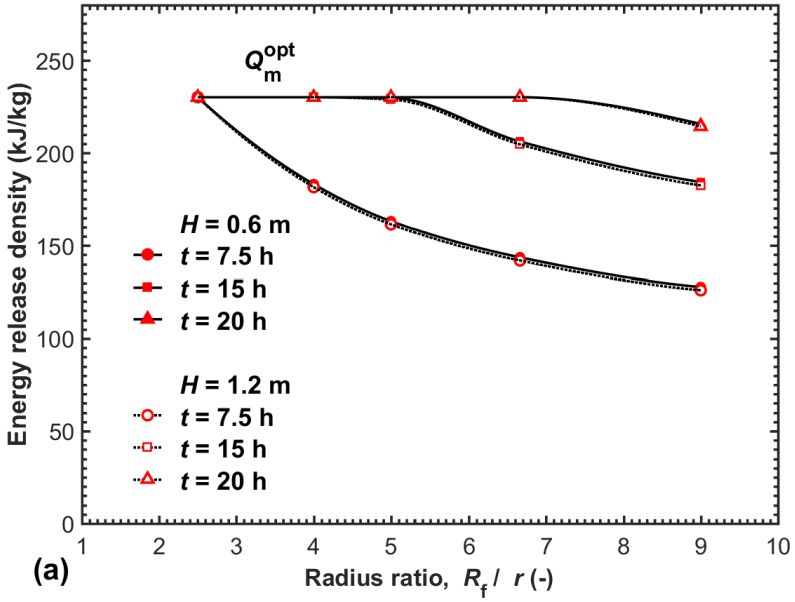

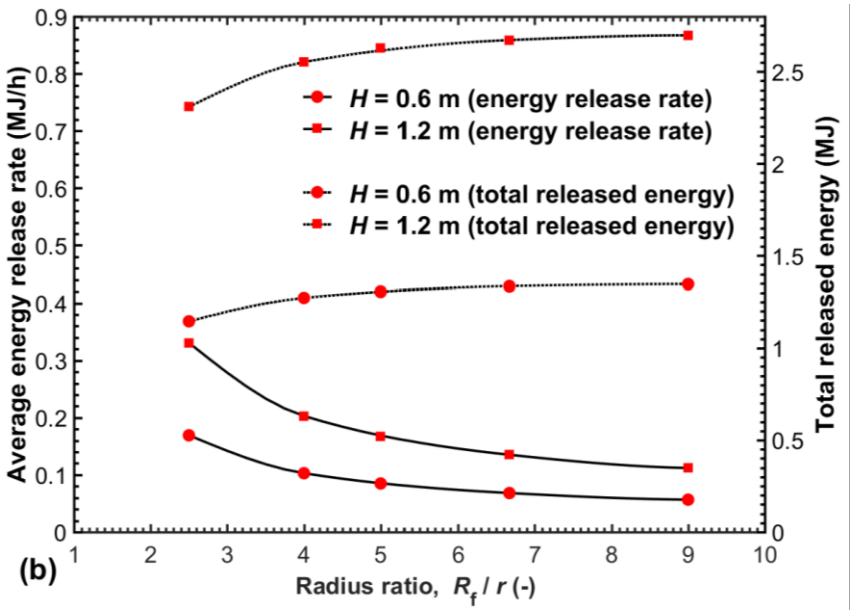

Fig. 5.5. Comparisons of (a) energy release density and (b) heat release rate and total released energy during discharging.

Sections 5.4.1 and 5.4.2 indicate an increase in HTF-tube size with shell radius fixed enhances charging and discharging simultaneously due to the larger heat transfer surface area and less PCM mass. the energy storage/retrieval capacity reaches the stable highest value for the studied charging/discharging time as the R_f/r reaches 5. Further increase in R_f/r does not increase the energy storage/discharging capacity. For the charging process, the energy storage density maintains its Q_m^{opt} until R_f/r is 5 for H=0.6 m and is 4 for H=1.2 m. However, during the discharging process, the optimal R_f/r is for both unit heights. Furthermore, the average heat storage/retrieval rate decreases substantially if the radius ratio R_f/r exceeds 5 and the total energy storage capacity considerably decreases as R_f/r is less than 4. In conclusion, in the case of varying HTF-tube radius with PCM shell radius fixed, a radius ratio R_f/r around 5 offers the optimal thermal performance by best balancing the heat storage/release rate, energy storage density and energy storage capacity. Moreover, the results show the unit height has a negligible influence on the optimal radius ratio selection when considering thermal behaviour during both charging and discharging processes.

5.5. Conclusions

This chapter defines a new series of geometries by varying the HTF-tube radius under a fixed shell radius, based on the same physical model of PCM packed in the annulus and HTF circulating in the central tube investigated in the last chapter. The effects of various HTF-tube radii with an identical shell radius on charging and discharging are numerically investigated. A variation in unit height is also considered along with the various HTF-tube radii. Through a PCM-HTF conjugate analytic model, PCM average temperature, the total charging/discharging time, heat storage/release density, average heat storage/release rate, and the total stored/released energy are determined and then compared. The conclusions are as follows.

(1) The investigation of varying HTF-tube size finds that the radius ratio R_f/r of 5 can best balance the charging and discharging performance in terms of the heat storage/release rate, energy storage density and energy storage capacity. Combining results from chapters 4 and 5, the optimal radius ratio R/r_f or R_f/r is found to be around 5 under the charging time of 6 to 8 h and the discharging of 15 to 20 h.

(2) Regarding the effect of the unit height, chapter 5 confirms the findings in chapter 4. When the whole charging-discharging process evaluated, the unit height shows a marginal influence on the optimal radius ratio. Chapter 5 also proves a variation in unit height results in a nearly proportional enhancement on the discharging rate but a relatively lower enhancement on the charging rate.

(3) As the charging time and discharging time increases, the optimal radius ratio increases slightly for both series of configurations.

The optimal radius ratio of 5 obtained from chapters 4 and 5 was applied to set the tube pitch in building a multitube LHTES rig. The experimental investigation of the multiple tube heat exchanger will be presented in the next chapter.

5.6. References

[1] Bergman, T. L., Incropera, F. P., Dewitt, D. P. ,Lavine, A. S., Fundamentals of heat and mass transfer, Seventh ed., John Wiley & Sons, (2011)

[2] Seddegh, S., Wang, X., Joybari, M. M. ,Haghighat, F., Investigation of the effect of geometric and operating parameters on thermal behavior of vertical shell-and-tube latent heat energy storage systems, Energy. 137 (2017) 69-82.

[3] Tao, Y.-B., Li, M.-J., He, Y.-L. ,Tao, W.-Q., Effects of parameters on performance of high temperature molten salt latent heat storage unit, Appl. Therm. Eng. 72 (2014) 48-55.

[4] Kibria, M. A., Anisur, M. R., Mahfuz, M. H., Saidur, R. ,Metselaar, I. H. S. C., Numerical and experimental investigation of heat transfer in a shell and tube thermal energy storage system, Int. Commun. Heat Mass. 53 (2014) 71-78.

[5] Tan, P. 2018. *On the Design Considerations for Thermal Energy Storage with Phase Change Materials: Material characterization and Modelling.* Licentiate thesis, Chalmers University of Technology.

[6] Liu, H., Li, S., Chen, Y. ,Sun, Z., The melting of phase change material in a cylinder shell with hierarchical heat sink array, Appl. Therm. Eng. 73 (2014) 975-983.

[7] Tehrani, S. S. M., Taylor, R. A., Saberi, P. ,Diarce, G., Design and feasibility of high temperature shell and tube latent heat thermal energy storage system for solar thermal power plants, Renew. Energy. 96 (2016) 120-136.
[8] Pirasaci, T. ,Goswami, D. Y., Influence of design on performance of a latent heat storage system for a direct steam generation power plant, Appl. Energy. 162 (2016) 644-652.
[9] Esen, M., Durmuş, A. ,Durmuş, A., Geometric design of solar-aided latent heat store depending on various parameters and phase change materials, Sol. Energy. 62 (1998) 19-28.

Chapter 6: Experimental investigation of the multitube LHTES system and operating parameters on complete charging and discharging cycles in vertical cylindrical latent heat storage systems

6.1 Chapter summary

In this chapter, a vertical multitube shell-and-tube LHTES rig was built and experimentally investigated. The inner tube pitch in the multitube heat exchanger was set based on the optimal radius ratio deduced from the comprehensive numerical investigations in chapters 4 and 5. As explained in these two chapters, the radius ratio of 5 can best balance the thermal performance in terms of heat storage/retrieval rate, energy storage capacity and energy storage density in an cylindrical LHTES system.

The multitube design in the shell-and-tube type LHTES system has received a considerable number of research attentions due to its promising benefits in enhancing heat storage efficiency. A well-known numerical solution in literature formulated a virtual cylindrical

domain along each tube to simplify the multitube problem to a single-tube model. First, the experimental study validates the numerical solution by comparing the thermal characteristics between a multiple-tube heat exchanger (MTHX) and a single-tube heat exchanger (STHX). The STHX's geometrical parameters coincided with a virtual cylindrical domain in the MTHX, being the same with those of the single-tube model formulated by the simplifying numerical solution to investigate the MTHX. The results showed there is a noticeable difference in the thermal characteristic between the STHX to the central or outer virtual cylindrical domain in the MTHX. Besides, the STHX differed substantially in the overall thermal performance with the MTHX. The comparison indicates an experimental study or three-dimensional numerical modelling is essential to reliably investigate the multitube problem. Second, the effects of tube number in the MTHXs was experimentally investigated. It was found that an increase in tube number boosted both charging and discharging rates without inhibiting the effect of natural convection. The five-tube configuration decreased the total charging and discharging duration by 50% compared to the two-tube one. Finally, the effect of HTF operating conditions was investigated on the five-tube MTHX. The results revealed that higher HTF temperature considerably improved the charging performance. The charging time decreased by up to 41% with the HTF temperature increasing from 70 °C to 80 °C. Meanwhile, a variation in the HTF flow rate from 5 to 20 L/min showed a more pronounced influence on charging than on discharging due to the different dominant heat transfer mechanisms.

6.2 Introduction

Over the last decades, significant research efforts have committed to improving the performance of LHTES systems in energy storage and retrieval. Al-Maghalseh and Mahkamov [1] summarized the heat transfer enhancement techniques coupled with the LHTES systems. Kalapala and Devanuri [2] reviewed research works on optimizing the designs and operating

parameters in the cylindrical LHTES systems. Mainly, the following aspects were examined by researchers to enhance the thermal performance of the cylindrical LHTES systems: (1) the system mounting orientation, such as vertical, horizontal or inclined with a specific angle [3, 4]; (2) the PCM and HTF arrangements like the pipe mode, cylinder mode [5], or the eccentrically-located HTF tube [6]; (3) the specific design parameter, e.g., the radius ratio [7] or the shell tilting angle [8]; and (4) the extension in heat transfer surface area, including finned-tube [10] or the multiple tubes [11-13]. As a promising configuration specifically for the cylindrical LHTES system, the multiple-tube design is efficient in increasing heat transfer area and enhancing PCM natural convection [14]. Moreover, the multiple-tube design offers flexibility for the LHTES to operate the HTF with distinct conditions in temperature, flow rate or HTF type [15-17].

Agyenim et al. [14] experimentally compared the melting performance of two inner-tube configurations in a horizontal cylindrical LHTES system, one with a single HTF tube and another with four HTF tubes. It was revealed that the separate flow cells formed around multiple tubes led to increased convection heat transfer hence a reduced melting time. Further, Agyenim [18] experimentally compared three enhancement techniques applied to a horizontal shell-and-tube LHTES unit, the multitube, the longitudinal-fin tube and the circular-fin tube. It was reported the multitube configuration showed superior performance in terms of the total melting time and overall utilization efficiency over the other ones.

Through numerically investigating a series of horizontal cylindrical LHTES systems, Esapour et al. [19, 20] found that the multitube design effectively increased heat flux, reducing the melting time up to 29%. Besides, given the same tube number, the lower locations of HTF tubes were advantageous to the melting performance compared to the other tube arrangements. Later Esapour et al. [21] numerically modelled a horizontal multiple-tube heat exchanger with metal foam embedded in PCM. The results showed the inner tube arrangement exhibited a

higher enhancement rate on charging than on discharging. Niyas et al. [22] numerically examined the effect of tube numbers in a set of horizontal multi-tube LHTES prototypes with a constant PCM amount packed. They found that an addition in tube number reduced the discharging time but the enhancement effect turned to be marginal with the tube number exceeding 25. Further, based on the optimal design obtained from the numerical study, Niyas et al. [23] built and tested a horizontal multi-tube LHTES experimental rig. It was reported that the charging process observed more significant variation in PCM temperature along the angular direction than the discharging, which demonstrated the different roles of natural convection between the charging and discharging processes.

With the lattice Boltzmann simulation model aided, Luo et al. [24] found that a multitube design in a horizontal LHTES unit could deliver a much higher melting rate compared to a single tube one. Besides, with the same inner tube number, the centrosymmetric allocation demonstrated better melting performance compared to inline and staggered arrangements. Kousha et al. [12] experimentally studied a set of horizontal multi-tube LHTES units with RT35 used as the storage medium. The team reported that a rise in tube number simultaneously boosted the melting and solidification rates while the enhancement magnitude depended on both the tube number and distribution.

Some studies presented the roles of fins and HTF operating conditions on the performance of a multitube LHTES system. An experimental investigation by Anish et al. [25] studied the effect of various HTF parameters in a horizontal multi-finned-tube LHTES system. It was noted that the HTF inlet temperature exhibited a more significant effect than its flow rate on the average temperature and storage effectiveness. Dandotiya and Banker [26] numerically analysed the role of fin placements on the thermal behaviour of a horizontal multitube heat exchanger. With the three-dimensional numerical model assisted, Bhagat et al. [27] optimized the fin designs in a vertical multi-tube LHTES unit to minimize the fluctuation in HTF outlet

temperature. They claimed that the number and thickness of fins were more important than the material of fins to enhance the heat transfer between PCM and HTF.

The literature review indicates a multitube design can effectively advance the heat transfer performance and the relationships between the thermal performance of a horizontal multitube LHTES system with its inner tube configuration have been widely investigated. Due to the presences of natural convection and multiple heat sources, the vertical MTHX (multiple-tube heat exchanger) and the horizontal one feature the distinctly different heat transfer mechanism. However, Limited experimental and numerical efforts have been undertaken on the vertical MTHX to reveal its thermal characteristics. Moreover, the numerical modelling of the vertical MTHX still commonly relies on a single tube model formulated from a virtual cylindrical domain concentric with each tube [28-31]. Although the validity of the simplifying solution has been questioned by a few studies [11, 14, 15], no experimental work has been carried out to verify it. Another limitation of the simplifying single tube model is unable to deal with the effects of inner tube number and allocation within a vertical MTHX. To address these research gaps, this work first experimentally compares the thermal characteristics of an STHX (single-tube heat exchanger) and a five-tube MTHX during a complete charging and discharging cycle. The STHX's geometrical parameters coincide with the virtual PCM cylindrical boundary formulated for the common numerical solution to simplify the multitube model. In this way, the comparative investigation of the STHX and MTHX explains to what extent the simplifying approach is valid. The work's second aim is to experimentally investigate the effect of the inner tube numbers in vertical MTHXs. This was done by building two and four inner-tube HXs (heat exchangers) with the same storage container and PCM amount as those of the five-tube MTHX, and comparing the thermal responses among the three HXs. Finally, the effect of HTF operating parameters was experimentally studied on the five-tube MTHX. The study aims to

present valuable insights into the multitube design to maximize a cylindrical LHTES system's thermal performance.

6.3 Experimental setup

6.3.1 Experimental rig and procedure

Fig. 6.1 shows the schematic drawing of the experimental system, which consists of vertical shell-and-tube HXs, hot and cold water tanks, as well as pumps. These components were connected using copper tubes and valves to form charging and discharging loops for water as the HTF to circulate through the HXs. A Sick ultrasonic flow meter (FFUS15-1G1IO) was installed at the outlet end of the HX to measure the HTF flow rate. Type T thermocouples with an accuracy of ±0.2 °C were used to measure PCM temperatures as well as HTF inlet and outlet temperatures. The desktop-computer-based data loggers (National Instruments) along with the software package were used to manage the recordings of the measured data.

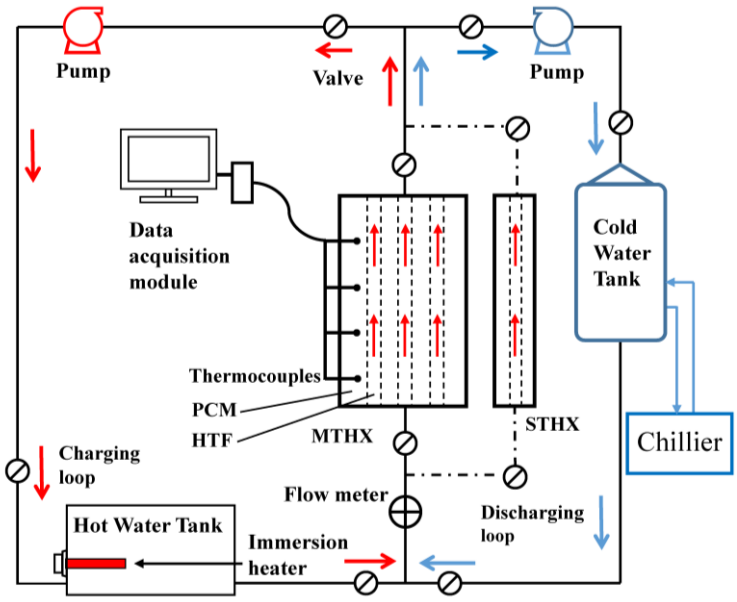

Fig. 6.1. Schematic of the experimental system

Two 2.4 kW electric immersion heaters with a precise temperature controller were installed at the hot water tank to maintain the water at a required temperature. A 20 kW chiller

produces the HTF at 15 °C in the cold water tank. During charging, the hot HTF was driven by a vertical centrifugal pump to flow upward through the vertical LHTES unit to melt the PCM then flow back to the hot water tank. Immediately following the completion of charging, a discharging process was launched to solidify the PCM by flowing the cold HTF upward through the LHTES unit with a horizontal centrifugal pump. Prior to each test, the cold HTF of 15 °C was circulated through the LHTES unit, having all thermocouple readings stabilized to close to the HTF inlet temperature.

Fig. 6.2 presents the sketches of the MTHX and STHX employed as the LHTES units in the study, which were manufactured with the same height of 500 mm. The inner tube spacing in the MTHX was set according to the optimal shell-to-tube radius ratio of 5 obtained in chapters 4 and 5. The STHX was built with a shell inner diameter of 100 mm and with the same inner tube as those in the MTHX, matching exactly with the virtual PCM cylindrical boundary in the MTHX (shown by dotted lines around each tube in Fig. 6.2a and c). Both heat exchanger containers were made of transparent polypropylene with a thickness of 6 mm and a thermal conductivity of 0.11 W/m·K, insulated with Armaflex foam sheets with a thickness of 20 mm and a thermal conductivity of 0.036 W/m·K. In both heat exchangers the PCM was stored in the annulus between the outer shell and inner tube(s) while the HTF was forced to flow through the tube(s). Table 6.1 lists the key geometrical parameters of the studied STHX and MTHXs.

To compare the PCM solid-liquid phase change process, all thermocouples within the STHX and MTHX were placed at the same four height levels as shown in Fig. 6.2b. A set of thermocouples with the same radial location and at the different height levels was grouped as

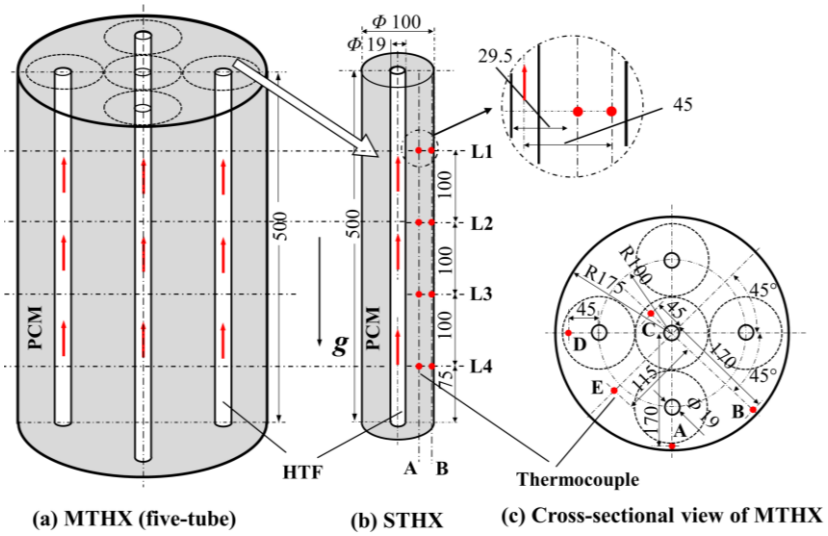

Fig. 6.2. The schematic of the five-tube MTHX (a), the thermocouple positions within the STHX (b), and the cross-sectional view of the MTHX (c) (Unit: mm).

Table 6.1
Key geometrical parameters of the STHX and the MTHXs.

LHTES unit	Tube number	Height	Tube outside diameter	Shell inner diameter	PCM mass
	(-)	H (mm)	r (mm)	R (mm)	m (kg)
STHX	1	500	19	100	2.9
MTHX	5 4 2	500	19	350	35.0

position A, B, C, D, or E. The STHX comprised positions A and B, which were fixed at respective radial distances of 29.5 and 45 mm from the tube central axis. The MTHX consisted of five positions A, B, C, D, and E as presented in a cross-sectional view (Fig. 6.2c). Positions A and B in the MTHX were mounted at the same radial distance of 5 mm from the shell inner surface while with different angular positions to monitor the PCM status. Positions C and D

were placed at 45 mm away from the central axes of central and outer tubes, reflecting the performance of central and outer tubes respectively. As positions C and D in the MTHX located the same radial distance from the tubes as position B in the STHX, they were comparable to reveal the deviation in thermal performance between the STHX and the central and outer virtual cylindrical boundaries in the MTHX. The comparison between these positions could be a way to verify the simplifying numerical approach in the modelling of the MTHX. Finally, position E was located 115 mm away from the container central axis, intending to monitor the combined effect from the adjacent tubes in the MTHX. Fig. 6.3 presents the photographs of the STHX and five-tube MTHX.

Fig. 6.3. The MTHX (left), the STHX (middle) and the MTHX with thermal insulation (right).

In the case of varying the inner tube number in the MTHXs, Fig. 6.4 shows the cross-sectional view of the two- and four-tube HXs. The thermocouple positions, tube dimensions and the tube radial distance from the container central axis in the two- and four-tube HXs remain the same as those in the five-tube HX. When varying the inner tube number, the total volume flow rate was fixed at 20L/min and evenly distributed among the inner tubes. Table 6.2 summarises the operating parameters for the studied STHX and MTHXs.

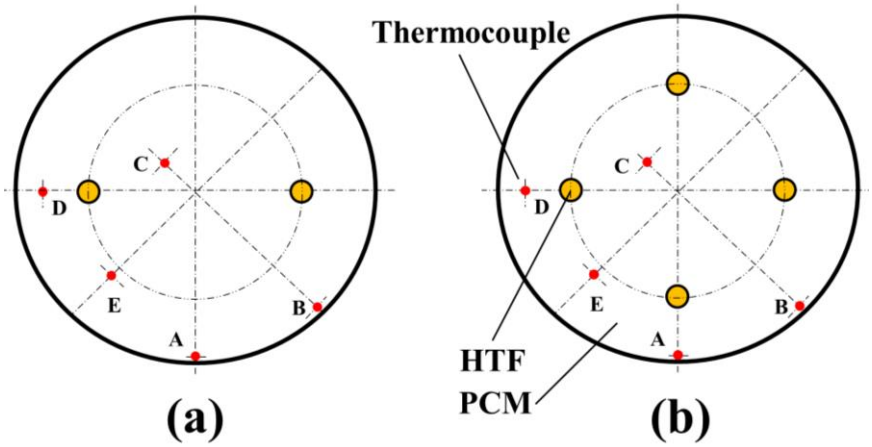

Fig. 6.4. Cross-sectional views of (a) two, and (b) four inner-tube in the MTHXs

Table 6.2
Studied operating parameters in the STHX and MTHXs.

LHTES unit	Tube number	HTF charging temperature	HTF discharging temperature	Total volume flow rate	Reynolds number per tube
	(-)	T_{ch} (°C)	T_{dis} (°C)	V (L/min)	Re (-)
STHX	1	80	15	4	14000
MTHX	5	85, 80, 75, 70	15	20/5	14000/3500
	4	80		20	17500
	2	80		20	35000

6.3.2 PCM properties

As explained in chapter 3, the commercial product, paraffin wax RT60 is a perfect storage medium for low-temperature heat storage applications with the solar collector assisted. The

same type PCM was used in the experimental study and its thermophysical properties can refer to Table 3.3 in Chapter 3.

6.4 Experimental data and heat loss analyses

6.4.1. Experimental data analysis

The charging and discharging times, the average temperature and total stored energy were utilized to evaluate the performance of the LHTES systems. The charging or discharging time was calculated given that all thermocouple readings in an HX did not change noticeably. Following an approach reported in the literature [7, 35], the present work applied the weighting method to calculate the average temperature and total stored energy for each HX with the thermocouples' recordings available.

The weighting factor ω_i assigned to the reading of a specific thermocouple is defined as the ratio of the volume of the PCM element surrounding the thermocouple to the total PCM volume in an HX. As described in Section 6.3.1, the total PCM amount and thermocouple positions differed greatly between the STHX and MTHX. As a result, each thermocouple had a different PCM volume surrounded depending on its location in the STHX or MTHX. Therefore, the weighting method was able to take account of the difference in the PCM element volume each thermocouple corresponds to. The average temperature in an HX is given by,

$$\overline{T} = \sum_{\mathrm{i}=1}^{\mathrm{n}} T_{\mathrm{i}} \omega_{\mathrm{i}} \tag{6.1}$$

Where T_{i} is the measured temperature assigned to the element surrounding the thermocouple and n is the total number of elements (thermocouples). The liquid fraction in each element is calculated as follows,

$$\phi_{\mathrm{i}} = \begin{cases} 0, & T_{\mathrm{i}} \le T_{\mathrm{solidus}} \\ \dfrac{T_{\mathrm{i}} - T_{\mathrm{solidus}}}{T_{\mathrm{liquidus}} - T_{\mathrm{solidus}}}, & T_{\mathrm{solidus}} < T_{\mathrm{i}} < T_{\mathrm{liquidus}} \\ 1, & T_{\mathrm{i}} \ge T_{\mathrm{liquidus}} \end{cases} \tag{6.2}$$

where T_{solidus} and T_{liquidus} are the PCM solidus and liquidus temperatures, respectively. With the local liquid fraction attained, the stored heat Q_{i} within each element and the total stored heat Q by the HX would be:

$$Q_{\mathrm{i}} = \begin{cases} m_{\mathrm{i}} C_p (T_{\mathrm{i}} - T_{\mathrm{ini}}), & T_{\mathrm{i}} \le T_{\mathrm{solidus}} \\ m_{\mathrm{i}} C_p (T_{\mathrm{i}} - T_{\mathrm{ini}}) + m_{\mathrm{i}} \phi_{\mathrm{i}} L, & T_{\mathrm{solidus}} < T_{\mathrm{i}} < T_{\mathrm{liquidus}} \\ m_{\mathrm{i}} C_p (T_{\mathrm{i}} - T_{\mathrm{ini}}) + m_{\mathrm{i}} \phi_{\mathrm{i}} L + m_{\mathrm{i}} C_p (T_{\mathrm{i}} - T_{\mathrm{liquidus}}), & T_{\mathrm{i}} \ge T_{\mathrm{liquidus}} \end{cases} \tag{6.3}$$

$$Q = \sum_{\mathrm{i}}^{\mathrm{n}} \omega_{\mathrm{i}} Q_{\mathrm{i}} \tag{6.4}$$

where T_{ini} is the initial temperature of PCM for both charging and discharging cycles and L is the latent heat of fusion. It can be deduced from Eqs. 3 and 4 that within a complete charging and discharging cycle, the total stored heat Q increased from zero at the test initial to a maximum value at the end of charging and then dropped back to zero once the discharging completed.

25 T-type thermocouples with the accuracy of ± 0.2 °C and an ultrasonic flow meter with the accuracy of 2 % were used in the testing. Following Moffat's method [36], the uncertainty of the stored energy was calculated. The maximum uncertainty was found to be around ± 6.5% for the charging with T_{ch} = 80 °C and V = 20 L/min.

6.4.2. Heat loss analysis

As noted in Section 6.3.1, the PCM storage enclosures used in the study were designed and built to minimize the heat loss caused by the temperature difference. The rate of heat loss to the environment is estimated as [37, 38],

$$\dot{Q}_{\text{loss}}(t) = UA(\bar{T}_{\text{inner}} - \bar{T}_{\text{outer}}) \tag{6.5}$$

Where U stands for the overall heat transfer coefficient, which is assumed to be equal between the STHX and the MTHX given that the same specifications in materials of the enclosure and the insulation. A is the outer surface area of an LHTES unit while $\bar{T}_{\text{outer}}$ is the average temperature of the environment recorded in the laboratory (~19 °C). $\bar{T}_{\text{inner}}$ is the temperature of the PCM layer adjacent to the container inner surface, evaluated with the average recordings of position B in the STHX or positions A and B in the MTHX. The maximum heat loss rate of the STHX with the charging temperature of 80 °C operated is approximately 10 W. According to Eq. 5, the maximum heat loss rate of the MTHX is estimated to be around four times that of the STHX under the same operating condition.

6.5 Experimental results and discussions

6.5.1 Comparative analysis of the STHX and MTHX

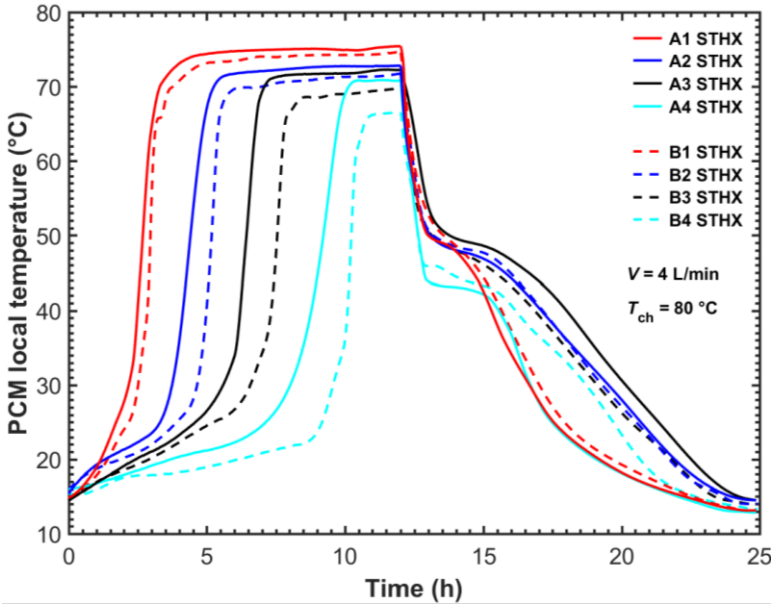

Fig. 6.5. PCM local temperature evolutions in the STHX.

Fig. 6.5 plots the evolution of PCM temperatures recorded at positions A and B (see Fig. 6.2a) during a complete charging and discharging process in the STHX. The charging was run

with the HTF inlet temperature of 80 °C and the flow rate of 4 L/min, immediately followed by the discharging with the inlet temperature of 15 °C and the same flow rate. For both positions A and B, it is noticeable that the PCM temperature at a higher level rose faster and began to stabilize sooner than that at a lower level, demonstrating the dominant role of natural convection on the melting process. At the same height level, position B recorded lower temperatures than position A as it located more distantly from the HTF tube and exposed more to heat loss to the environment. On the other hand, with heat conduction dominating heat transfer throughout the solidification, the height level did not show a significant influence on the pattern of PCM temperature evolution. The STHX was observed to experience around 25 h of a total charging and discharging duration with the charging temperature set at 80 °C.

Fig. 6.6 plots PCM temperatures recorded at positions A, B, C, D and E within the five-tube HX during a complete charging and discharging process with the charging temperature of 80 °C and discharging temperature of 15 °C. The total HTF flow rate was set at 20 L/min on the five-tube MTHX such that each tube within it was operated with the same

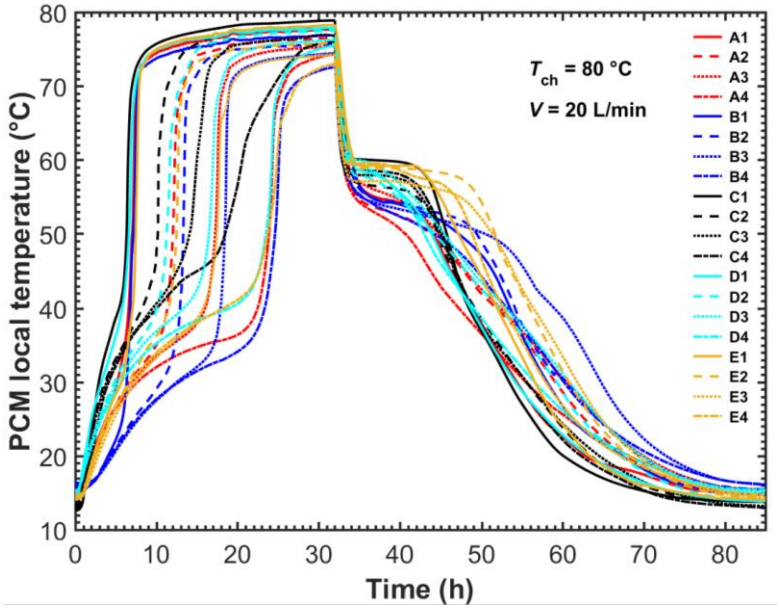

Fig. 6.6. PCM local temperature evolution in the five-tube HX.

HTF flow rate (4 L/min) as the tube within the STHX. It is observed from Fig. 6.6 that during the charging PCM melted faster and its temperature stabilized sooner at a higher level, which

was similar as compared to the STHX. Besides, as noted in Section 6.3.1, position B was the most faraway from HTF tubes and in turn, could signal when the level it resided was melted or solidified totally. The temperature recordings at position B indicated that a whole liquid PCM pool emerged at the PCM top region at the charging time t = 6 h, combined from the separate melted PCM layers along HTF tubes. The whole liquid volume gradually extended downwards and the lowest level sensor B4 surpassed 61 °C (PCM liquidus temperature) at around 26 h of charging. Overall, the evolution pattern in the whole liquid PCM volume inside the MTHX was similar to that in a single-tube cylindrical LHTES unit. However, with the multiple heat sources and complex PCM solid-liquid fronts presented, the natural convection was more effective in the MTHX. The complete charging and discharging process of the five-tube MTHX lasted around 85 h.

To verify the common numerical modelling to simplify the multitube model into a single-tube one, Fig. 6.7 compares the temperature evolutions between position B in the STHX and positions C and D in the five-tube MTHX. According to Fig. 6.2b and c, position B inside the

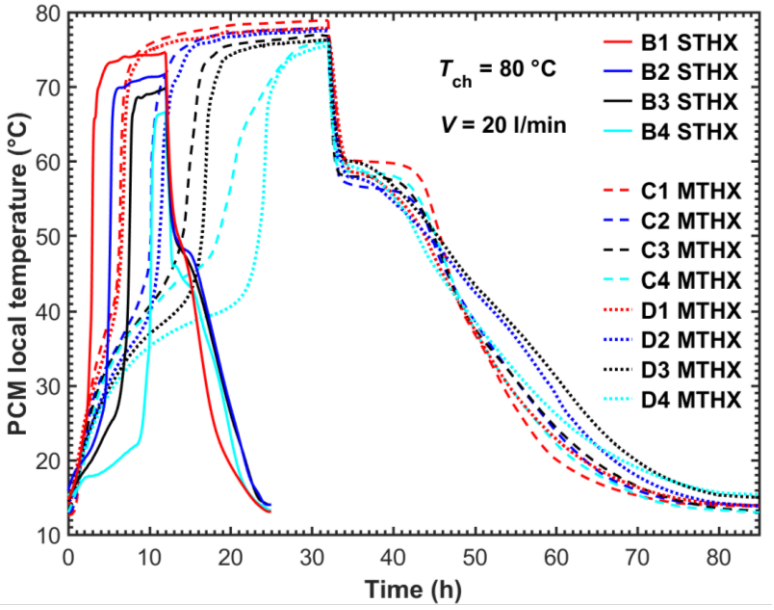

Fig. 6.7. Comparison of local temperatures between the STHX and five-tube MTHX.

STHX was mounted 45 mm away from the HTF tube central axis, while positions C and D inside the MTHX were placed at the same distance from the central- and outer-tube axes respectively. Positions C and D of the MTHX could be used to reflect the thermal characteristics of the central and outer virtual cylindrical boundaries. Therefore, position B of the STHX and positions C and D of the five-tube MTHX are comparable to reflect the deviation in thermal behaviour between the STHX and the virtual cylindrical boundaries in the MTHX. It is worth noting that the initial average temperature at position B in the STHX was around 1.5 °C higher than those at positions C and D in the MTHX. As described in Section 6.3.1, prior to each charging, the LHTES unit was circulated by the HTF of 15 °C until all thermocouple readings stabilized approximately to the HTF inlet temperature. However, it was not feasible to obtain a uniform temperature across all the thermocouples in a storage unit because of the low thermal conductivity of PCM. Moreover, it was more difficult for the comparable thermocouples in the two HXs to attain the similar initial temperature due to the significantly different PCM amounts between them as well as the impact from the difference in the tube number. Nevertheless, considering the noticeable deviations in the overall results between the two storages, and that the initial energy deviation due to the temperature difference accounted for ~1% of their respective total stored heats, the influence of the difference in initial temperature between the two HXs was negligible. It is observed from Fig. 6.7 that at each level position C or D in the MTHX melted much slower than position B in the STHX. This is mainly because the MTHX contained more than ten times the amount of PCM but had five times heat transfer area configured compared to the STHX. Moreover, positions C and D in the MTHX were observed to climb to higher temperatures by the end of charging despite the lower initial temperatures compared to position B in the STHX. This can be explained by the more effective natural convection resulted from the multiple heat sources.

Within the MTHX, the results at positions C and D reveal there was a noticeable difference in thermal performance between central and outer HTF tubes. It can be seen that at the same height level, position C melted faster and then recorded a higher maximum temperature at the end of charging. The difference can be attributed to two factors, (1) apart from the central tube, two adjacent outer tubes also affected position C and (2) position D suffered more heat loss to the surrounding.

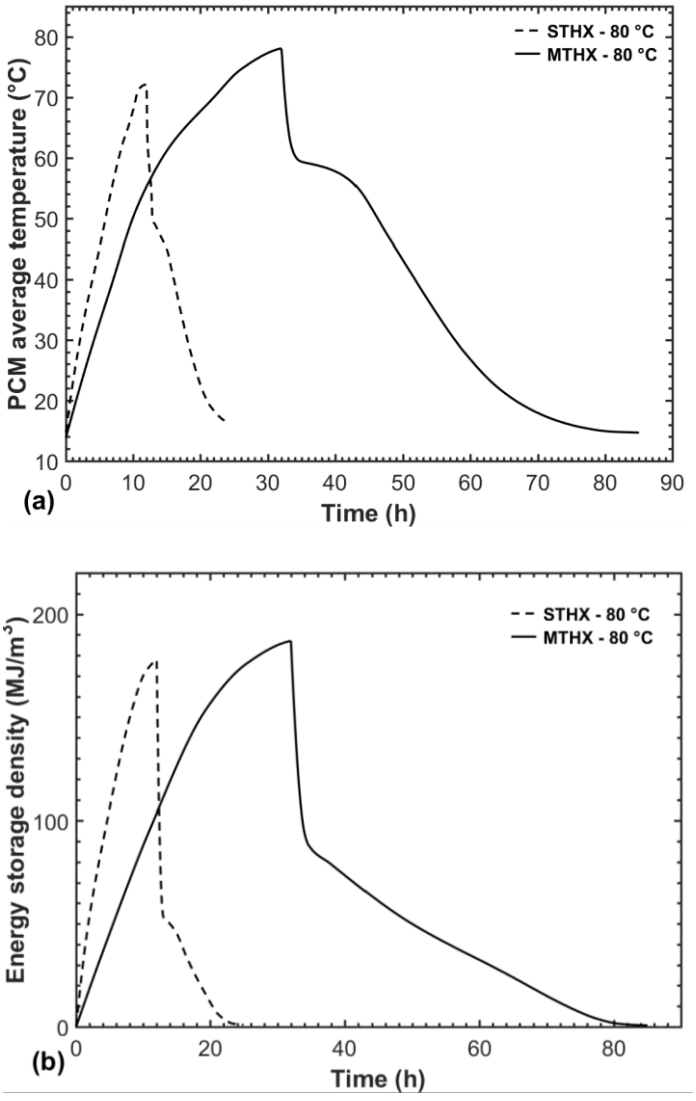

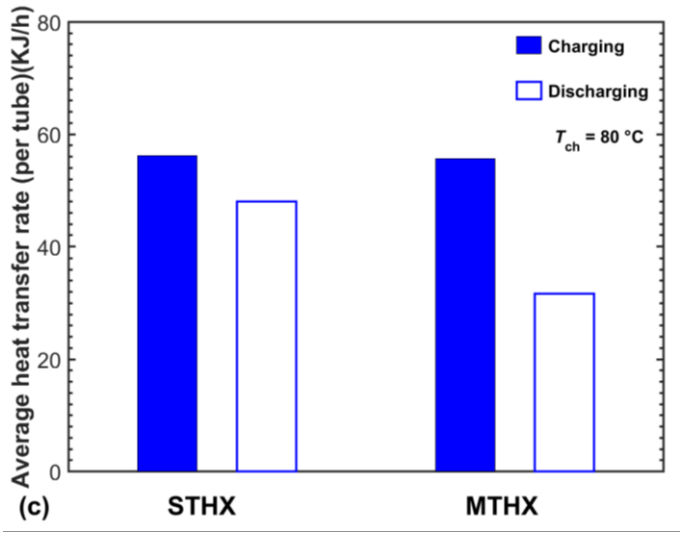

Fig. 6.8. Comparisons of thermal responses between the STHX and MTHX in terms of (a) PCM average temperature, (b) energy storage density and (c) average heat exchange rate of per tube.

Fig. 6.8 compares the overall performance between the STHX and the five-tube MTHX in terms of the average PCM temperatures, energy storage density and average heat exchange rate of per tube. It is shown that the MTHX attained a higher maximum average temperature of 77 °C compared to 72 °C by the STHX with the same HTF inlet temperature. During melting in the MTHX multiple liquid PCM cells initially developed along the tubes and then merged into a whole pool at the top PCM region due to natural convection flow. The extended solid-liquid fronts and multiple heat sources contributed to more effective natural convection in the MTHX. Moreover, the MTHX experienced a much longer charging time (32 h), leading the melted PCM to be continually heated and thus resulting in a higher maximum average temperature by the end of charging. Fig. 6.8a shows that the STHX was around 62.5% faster in charging (t_{ch}, 12 vs 32 h) and 75% faster in discharging (t_{dis}, 14 vs 53 h) than the MTHX. This can be explained by the much larger ratio of PCM mass (~12) compared to the ratio of heat transfer surface area (5) between the two heat exchangers.

Fig. 6.8b compares the energy storage density (Q/v) between the STHX and MTHX. The cumulative energy Q is calculated for each heat exchanger using Eq. 4. The maximum energy

storage density in the MTHX is higher than that in the STHX, due to the difference in sensible heat over a much longer charging time. Fig. 6.8c compares the average heat transfer rate of per tube within the STHX and MTHX. The average heat transfer rate is calculated as $Q/(t \times n)$, where t is the total charging/discharging time and n is the tube number.

During charging the average heat storage rate differs slightly between the two heat exchangers. However, it should be noted that the average heat storage rate of per tube in the MTHX is influenced by more complex factors, including tube distribution, tube number and the total PCM mass. On the other hand, the average discharging rate of per tube in the MTHX is significantly lower compared to the STHX. This can be explained by the much longer discharging time and the evolution of PCM solid-liquid interfaces in the MTHX. At the later stage of discharging in the MTHX, the PCM solidifies extremely slowly between the solid-liquid interfaces, which initiate from each tube surface and develop outward, continually increasing the thermal resistance between the HTF and liquid PCM.

In this study, a large portion of PCM was excluded from the virtual cylindrical boundaries formulated in the MTHX due to the specific tube number and the tube spacing intending to agree with the optimal shell-to-tube radius ratio. This factor largely leads to the significant differences in charging and discharging processes between the STHX and the MTHX. However, even with much more tubes appropriately arranged within the MTHX, part of PCM will be inevitably excluded from virtual cylindrical boundaries. There are still deviations existing between the STHX to the central or outer virtual cylindrical boundary in the MTHX, and between the two HXs in the overall thermal response.

Besides, the total heat loss from an STHX or MTHX was not only affected by its outside surface area but also coupled with the dynamic temperature differences between PCM and the environment. And the single-tube modelling cannot address the difference in thermal performance between the outer and inner tubes in the MTHX as revealed by Fig. 6.7. In

summary, the comparative study of the two HXs clearly demonstrates that the study of the vertical multitube LHTES system should rely on an experimental study or three-dimensional numerical modelling.

6.5.2 Effect of tube number in the MTHXs

To study the effect of varying the inner tube number within the MTHXs, two and four inner-tube were configured with the same storage enclosure size and tube specifications as the five-tube MTHX. As the inner tube number varied from five to four or two, the thermocouple positions were placed at the same positions and the total PCM amount was held constant. The centrosymmetric placement of inner tubes in the three cases of the MTHX, as shown in Fig. 6.2c and Fig. 6.4, enables uniformly melting and solidifying of PCM. The constant total flow rate of 20 L/min was distributed among the inner tubes during this series of tests along with the HTF charging temperature of 80 °C and a discharging temperature of 15 °C.

6.5.2.1 Local temperature comparisons at central and outer tubes

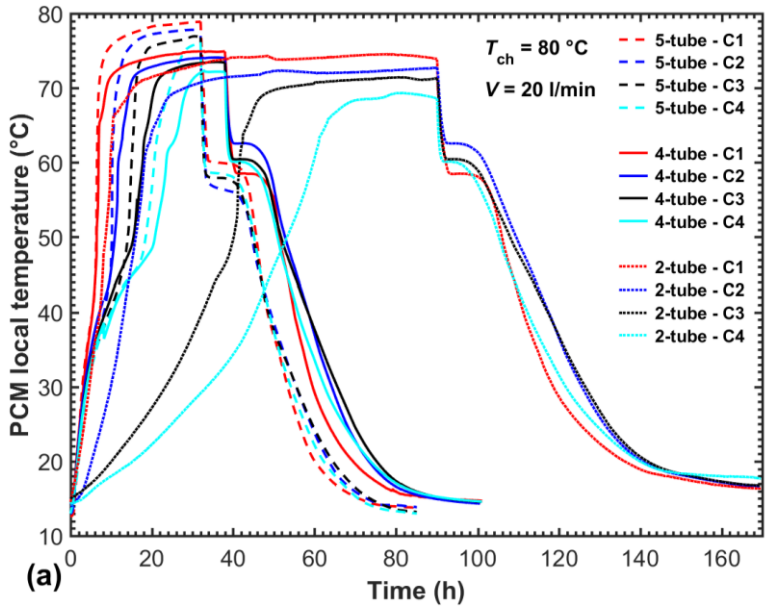

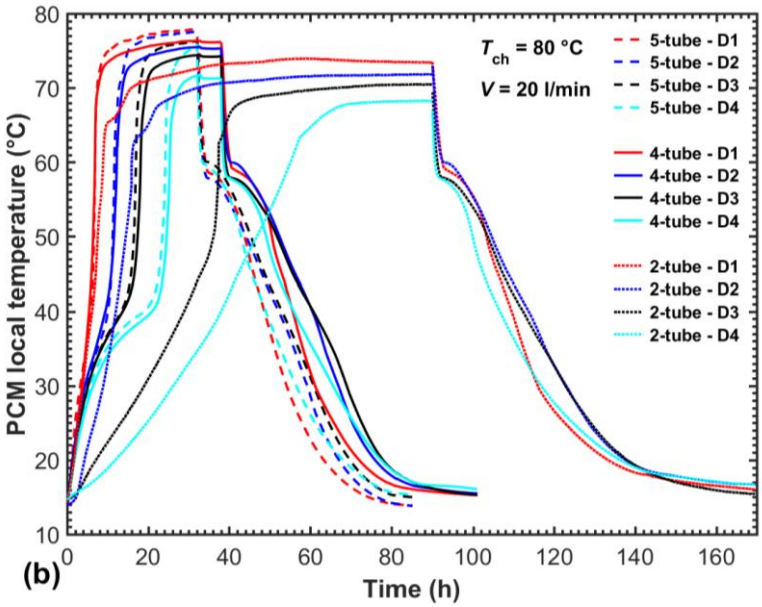

Fig. 6.9. Comparisons of the PCM local temperature at positions C (a) and D (b) under different tube numbers.

Fig. 6.9a and b compare the thermocouple readings at central (position C) and outer (position D) positions between the MTHXs with the different inner tube numbers. It can be seen that during the charging, position C within the five-tube case melted faster and attained the higher maximum temperature, compared to the same positions in the cases with less inner tubes. For instance, the highest level sensor C1 within the five-tube case attained the maximum temperature of 75 °C, compared to 72 °C at the same position within the four-tube case. This indicates the central tube within the five-tube case resulted in the higher heat transfer rate and more effective natural convection hence the higher maximum temperature at position C.

Fig. 6.9b shows the five-tube case also melted faster and recorded higher temperature at the outer region of PCM (position D) than the cases with less tube number. The result proves that an addition in tube number even helps enhance heat transfer to the remote region of PCM. For the discharging performance, it can be seen from Fig. 6.9a and b that despite the higher initial temperatures, positions C and D within the five-tube case both dropped faster in temperature, resulting in a shorter discharging duration.

6.5.2.2 Overall performance comparison

Fig. 6.10 presents the overall performance of the MTHXs with different tube numbers in terms of the average PCM temperature, total stored energy and the average heat transfer rate. Fig. 6.10a shows that the maximum average temperature was higher with an addition in the tube number, similar to the pattern revealed by the PCM local temperature. Fig. 6.10b indicates the maximum total stored heat by the five-tube case was 1.5% and 10% higher than those by the four- and two-tube cases respectively. Fig. 6.10c compares the average heat transfer rate within the MTHXs, which is calculated as Q/t where t is the total charging/discharging time. The tube number significantly affected the charging and discharging rates. The charging and discharging rates of the five-tube case were 202% and 115% respectively higher compared to the two-tube case.

In the vertical MTHX, PCM natural convection flow takes place between the HTF tubes. Figs. 9 and 10 demonstrate that more tubes added to a vertical MTHX promote both charging and discharging performance without inhibiting the natural convection. This is different from the findings regarding the horizontal MTHX in which tubes placed at the upper PCM region may interfere with natural convection thus reduce the charging rate [12]. However, adding more tubes is not always desirable because it would lead to the PCM amount loss and the cost increase in the LHTES unit. An optimal inner tube design needs to ensure the benefit in heat transfer from the tubes added is well worth the costs.

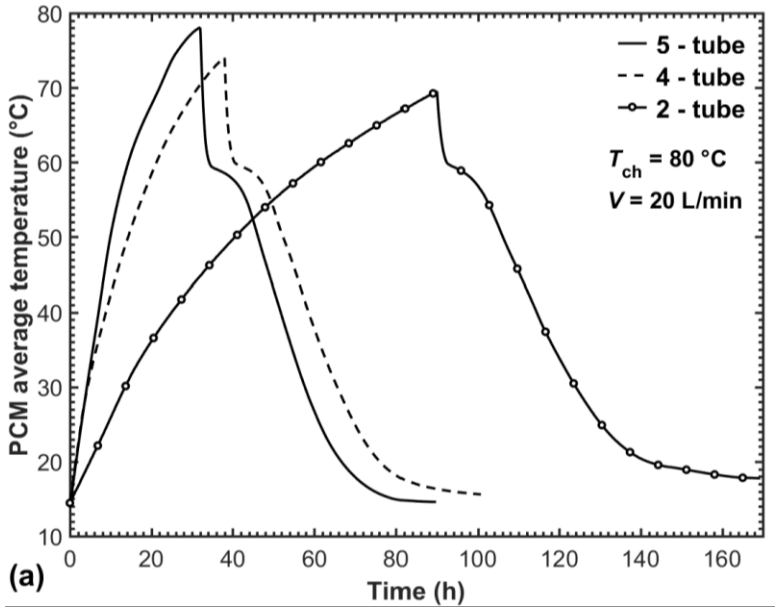
PCM average temperature (°C)
Time (h)
5 - tube
4 - tube
2 - tube
T_{ch} = 80 °C
V = 20 L/min
(a)

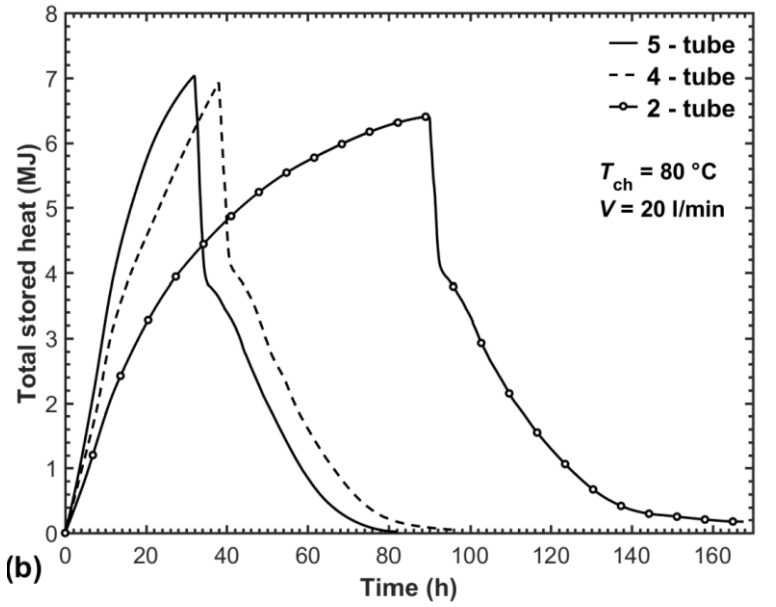
Total stored heat (MJ)
Time (h)
5 - tube
4 - tube
2 - tube
T_{ch} = 80 °C
V = 20 l/min
(b)

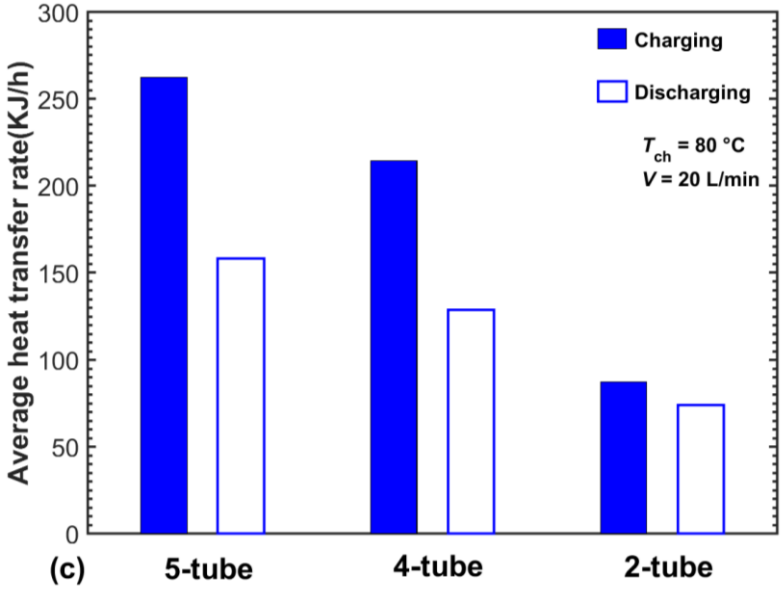
Average heat transfer rate(KJ/h)
Charging
Discharging
T_{ch} = 80 °C
V = 20 L/min
(c)
5-tube
4-tube
2-tube

Fig. 6.10. (a) The average temperature and (b) total stored energy and (c) average heat exchange rate in the MTHX with different tube numbers.

6.5.3 Effects of HTF operating parameters in the five-tube MTHX

6.5.3.1 HTF inlet temperature

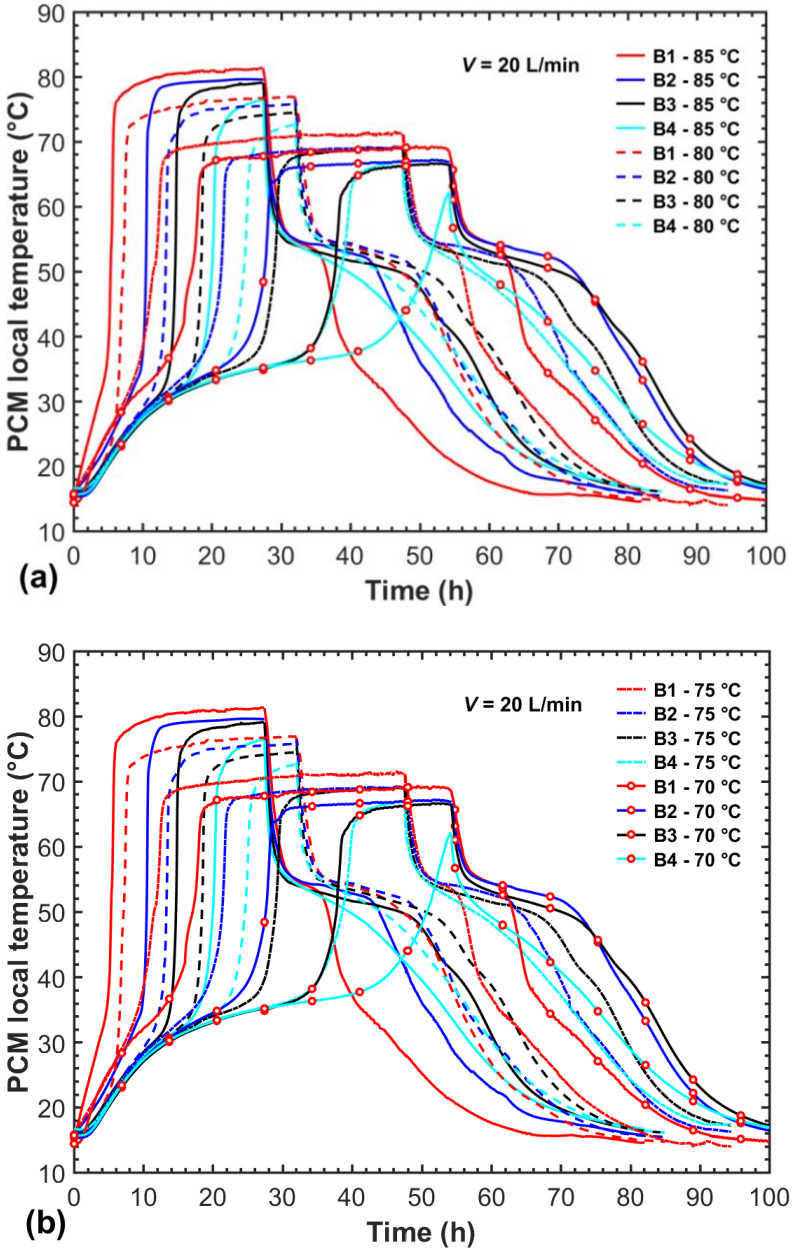

Fig. 6.11. Comparisons of temperatures at position B in the five-tube MTHX under different charging temperatures, (a) 85 vs. 80 °C and (b) 75 vs. 70 °C.

To analyse the effect of HTF inlet temperatures, the charging temperatures of 70 °C, 75 °C, 80 °C, and 85 °C combined with a constant discharging temperature of 15 °C were performed on the five-tube MTHX while the HTF flow rate was maintained at 20 L/min. Fig. 6.11a and b plot PCM temperature evolutions at position B during the complete charging and discharging process. As already stated, position B could signal the PCM status at the level it resided hence indicates the time when the charging or discharging was completed. It can be deduced from Fig. 6.11a and b that the HTF inlet temperature affected the charging time significantly but showed a relatively slight influence on the discharging time. The charging time reduced by 12%, 32% and 14% for the HTF inlet temperature to increase from 70 °C to 75 °C, from 75 °C to 80 °C, and from 80 °C to 85 °C respectively. At the same time, the corresponding increasing rates in the discharging time were 2%, 11% and 3%. This associates with the heat transfer mechanism in the PCM solidification process. The PCM temperature fell fast at the initial discharging stage (t_{dis} < 2 h) and then the thermal resistance between the HTF and liquid PCM increased considerably with the PCM layer continually solidifying on the tube surface. This led the difference in the PCM initial temperatures at discharging to play a less important role on the whole discharging duration. In other words, the total charging and discharging duration mainly depended on the charging section operated with different HTF charging temperatures.

Fig. 6.12a and b plot the average PCM temperature and the total stored heat to evaluate the overall performance with the four HTF inlet temperatures operated. It can be seen that the HTF temperature exhibited a noticeable influence on the average PCM temperature and the total amount of heat stored. As the HTF temperature increased from 75 °C to 80 °C, the maximum average temperature was around 7 °C higher and the maximum stored heat amounted by ~8% with the charging time reduced by 32%. The improvement in the total stored energy between the two charging temperatures could be attributed to the deviation in sensible heat as

the temperature profile shown in Fig. 6.11 indicates the PCM totally melted at the end of charging when the charging temperatures of 75 °C and 80 °C were operated.

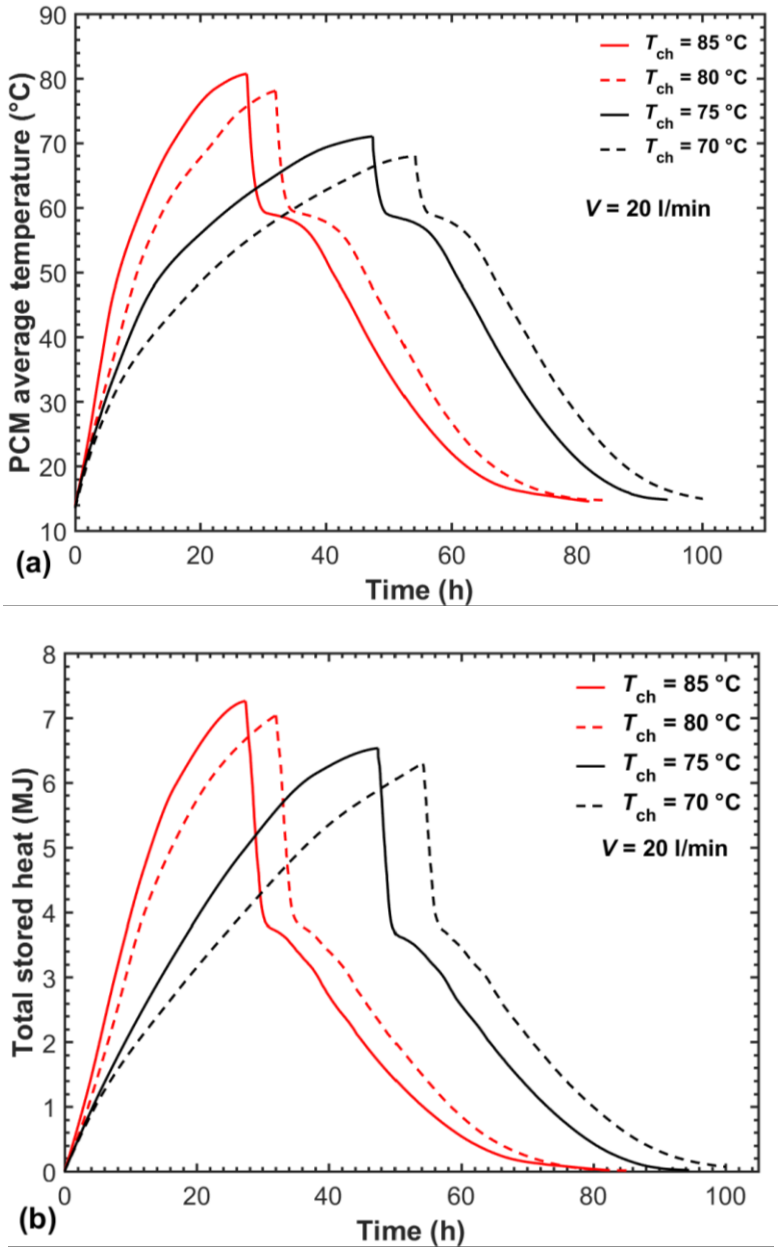

Fig. 6.12. Comparisons of PCM average temperature (a) and the total stored energy (b) in the five-tube MTHX under different charging temperatures.

6.5.3.2 Effect of the HTF flow rate

The HTF in the MTHXs was operated with a constant HTF flow rate of 20 L/min in results presented above. To investigate the effect of HTF flow rate, a lower flow rate of 5 L/min was

performed on the five-tube MTHX with the charging temperature set at 85 °C. Both flow rates of 5 and 20 L/min distributed equally among the five inner tubes, enforcing a turbulent flow with Reynolds numbers being 3500 and 14000 respectively within each tube. The comparisons between the flow rates are presented by the temperature evolutions at individual thermocouples (positions C and D) and the overall thermal performance in terms of the PCM average temperature and the total stored heat.

Fig. 6.13a and b plot the temperature evolutions under two HTF flow rates at positions C and D, which were located at the same radial distance from central and outer tubes respectively. It is shown the effect of HTF flow rate differed between the charging and discharging processes on the temperatures measured at positions C and D. A higher flow rate resulted in higher temperature during the charging process while showed a negligible effect on the discharging process. The PCM temperatures were independent on the HTF flow rate at the initial charging stage (t_{ch} < 1.5 h) and then increased faster with a higher flow rate operated. At the end of

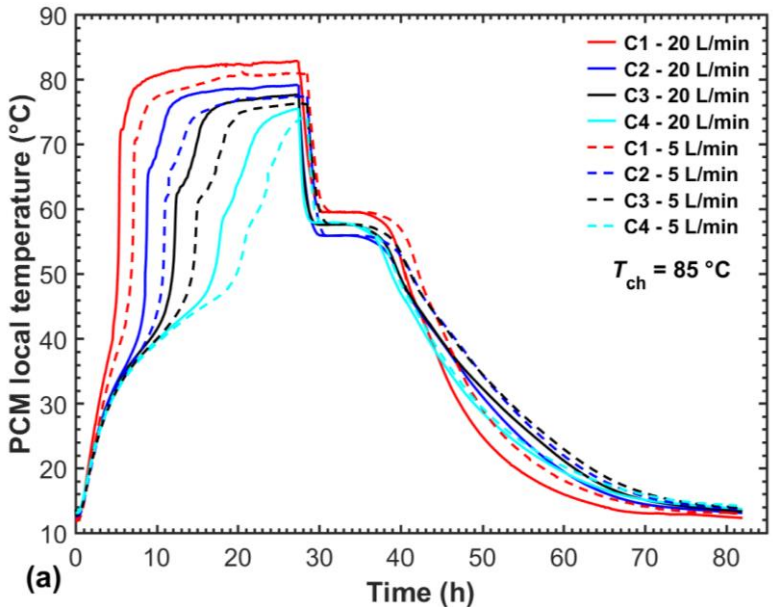

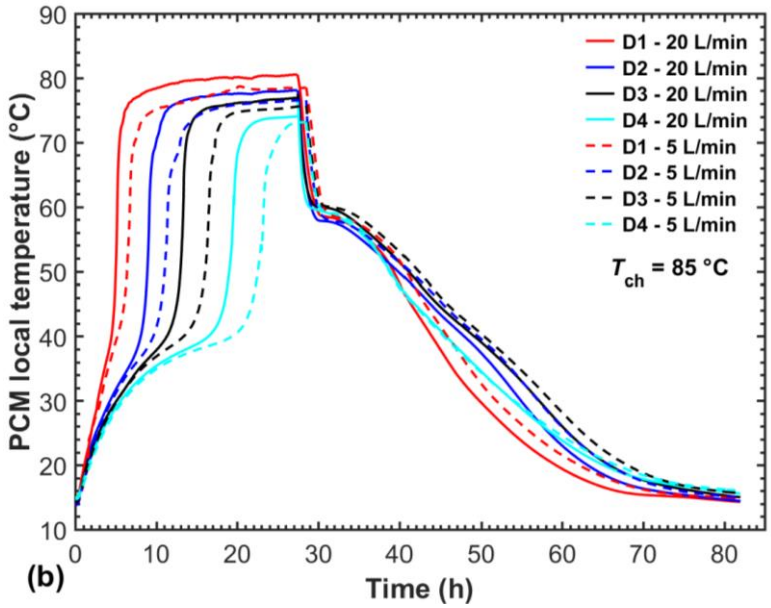

Fig. 6.13. Temperature evolutions at positions C (a) and D (b) under two HTF flow rates within the five-tube MTHX.

charging, the temperatures climbed to higher values with the flow rate of 20 L/min configured, indicating an improvement in the heat transfer. Comparatively, during the discharging, temperature plots at both positions C and D under the two HTF flow rates nearly overlapped following a short duration of discharging (~1 h). Such different effects on the charging and discharging can be explained by the different dominant heat transfer mechanisms over the two cycles. In the melting process, once liquid PCM layers were formed around the tubes, natural convection dominated heat transfer hence the enhancement effect by a higher HTF flow rate became pronounced. During the solidification process controlled by heat conduction, the higher thermal resistance of the solidified PCM layer on the tube inhibited heat transfer between the liquid PCM and the tube, resulting in a marginal impact by a higher HTF flow rate on the overall heat transfer rate. This finding is also in agreement with the results of the experimental studies [16, 39] and the numerical result presented in chapter 3.

The comparisons of PCM average temperature and the total stored energy under the two flow rates are presented in Fig. 6.14. Increasing the HTF flow rate from 5 to 20 L/min exhibited a more apparent effect on the average temperature evolution during the charging process. A

higher flow rate also enhanced the total stored heat during charging and led to approximately 1.5% higher maximum stored heat at the end of charging. However, the charging time decreased slightly while the total charging and discharging time was almost the same between the two HTF flow rates.

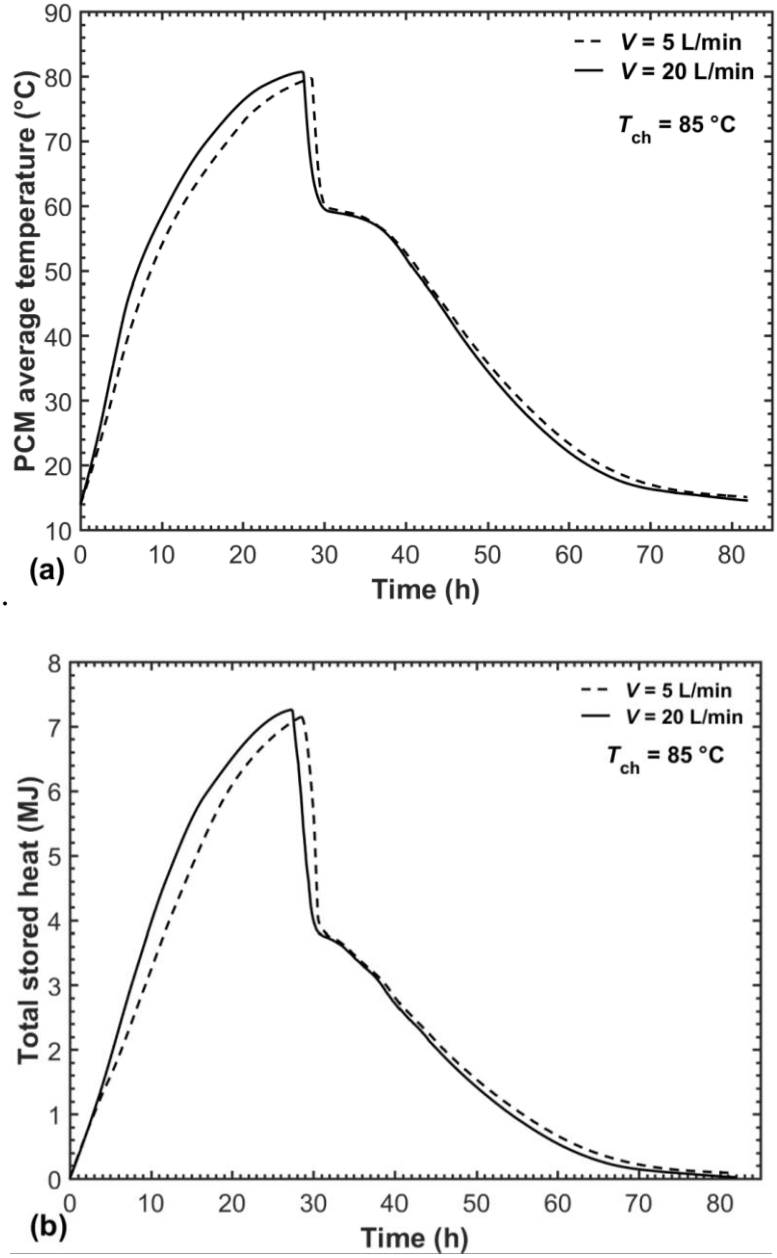

Fig. 6.14. Comparisons of (a) PCM average temperature, and (b) the total stored heat under different flow rates.

6.5 Problems and difficulties

The most challengeable issue encountered during the test was the PCM leakage, mostly taking place from the sealing of the structure (highlighted for the MTHX in Fig. 6.3) to the cylinder enclosure lateral surface. The structure was specifically designed to fix the sensor sealing assembly and the sealing of it to the cylinder enclosure is vulnerable to the high temperature variations (~15-80 °C) that the container experiences during the repeated consecutive charging and discharging cycles. Another difficulty is to identify and replace the faulty thermocouple in the experimental rig. A lot of handling and bending of the thermocouple may lead its wires inside the stainless steel sheath to eventually break. This type of failure cannot be repaired and the thermocouple must be replaced. Other problems include the water leakage and the failure for the chiller or the immersion heater to maintain the HTF at the required temperature.

Any problem above will halt the ongoing test. Once the problem is addressed, the whole test must be relaunched again. These difficulties inevitably delay the experiment proceeding. However, despite the limitations and difficulties, the author did monitor and maintain the operating parameters and conditions to the specific criteria, with seeking help from the supervisory team and the staff in the workshop, to make the results of each test as reliable as possible.

6.6 Conclusions

This chapter experimentally investigated the complete charging and discharging processes in the vertical STHX and MTHX. Water was forced to flow through the inner tube(s) of the heat exchangers as the HTF and paraffin wax RT60 was packed in the annulus as the storage medium. The geometrical configurations of the STHX and MTHX employed the optimal radius ratio obtained from chapters 4 and 5. The first aim of this chapter is to verify a common

numerical solution which formulates a virtual cylindrical PCM domain along each tube, simplifying a three-dimensional multitube problem to a two-dimensional single-tube model. The verification was done by comparing the thermal responses between the MTHX to the STHX which geometrical parameters precisely matched with the virtual cylindrical domain formulated by the simplifying numerical solution. Further, the impact of inner tube number in the MTHX on thermal performance was investigated in terms of PCM local temperatures, PCM average temperature and the total stored heat. Finally, the effects of HTF charging temperatures and flow rates were comprehensively examined on the five-tube MTHX. A summary of the key findings is as follows:

(1) Subject to the same operating conditions, the temperature results in the STHX were substantially different from those measured at the same position from the HTF tube in the central and outer virtual cylindrical domains in the five-tube MTHX. Moreover, the overall thermal behaviour also showed significant differences between the STHX and MTHX. The deviations can be credited to the following factors, (1) Regardless the tube number and placement, part of PCM was inevitably excluded from virtual cylindrical boundaries formulated in the MTHX and (2) The total heat loss from an LHTES unit not only associates with its outside surface area but also couples with the dynamic temperature differences between PCM and the environment. There is no linear or simple correlation in heat transfer between the STHX and the MTHX. Besides, due to the different magnitudes in heat loss exposed to the environment, the central and outer tubes in the MTHX showed different thermal characteristics, which the single-tube numerical model is unable to accurately address. The experimental approach or three-dimensional numerical modelling is a reliable way to study the vertical multitube problem.

(2) The centrosymmetric placement of inner tubes enabled more uniform melting and solidifying in a vertical MTHX. The larger tube number considerably improved both charging and discharging rates without inhibiting the natural convection.

(3) A higher HTF charging temperature significantly improved the charging rate in the MTHX, while the following discharging duration is less sensitive to the HTF charging temperature. Moreover, the HTF flow rate exhibited a more pronounced effect on the charging than on the discharging. This is mainly because that the growing PCM layer solidified on the tube surface continually increased the thermal resistance between liquid PCM and HTF, and thus minimized the effect of the HTF flow rate.

6.7 References

[1] Al-Maghalseh, M. ,Mahkamov, K., Methods of heat transfer intensification in PCM thermal storage systems: Review paper, Renew. Sust. Energ. Rev. 92 (2018) 62-94.

[2] Kalapala, L. ,Devanuri, J. K., Influence of operational and design parameters on the performance of a PCM based heat exchanger for thermal energy storage–A review, Journal of Energy Storage. 20 (2018) 497-519.

[3] Kousha, N., Hosseini, M. J., Aligoodarz, M. R., Pakrouh, R. ,Bahrampoury, R., Effect of inclination angle on the performance of a shell and tube heat storage unit – An experimental study, Appl. Therm. Eng. 112 (2017) 1497-1509.

[4] Seddegh, S., Wang, X. ,Henderson, A. D., A comparative study of thermal behaviour of a horizontal and vertical shell-and-tube energy storage using phase change materials, Appl. Therm. Eng. 93 (2016) 348-358.

[5] Han, G.-S., Ding, H.-S., Huang, Y., Tong, L.-G. ,Ding, Y.-L., A comparative study on the performances of different shell-and-tube type latent heat thermal energy storage units including the effects of natural convection, Int. Commun. Heat Mass. 88 (2017) 228-235.

[6] Zheng, Z.-J., Xu, Y. ,Li, M.-J., Eccentricity optimization of a horizontal shell-and-tube latent-heat thermal energy storage unit based on melting and melting-solidifying performance, Appl. Energy. 220 (2018) 447-454.

[7] Seddegh, S., Wang, X., Joybari, M. M. ,Haghighat, F., Investigation of the effect of geometric and operating parameters on thermal behavior of vertical shell-and-tube latent heat energy storage systems, Energy. 137 (2017) 69-82.

[8] Seddegh, S., Tehrani, S. S. M., Wang, X., Cao, F. ,Taylor, R. A., Comparison of heat transfer between cylindrical and conical vertical shell-and-tube latent heat thermal energy storage systems, Appl. Therm. Eng. 130 (2018) 1349-1362.

[9] Shen, G., Wang, X., Chan, A., Cao, F. ,Yin, X., Study of the effect of tilting lateral surface angle and operating parameters on the performance of a vertical shell-and-tube latent heat energy storage system, Sol. Energy. 194 (2019) 103-113.

[10] Rathod, M. K. ,Banerjee, J., Thermal performance enhancement of shell and tube Latent Heat Storage Unit using longitudinal fins, Appl. Therm. Eng. 75 (2015) 1084-1092.
[11] Joybari, M. M., Seddegh, S., Wang, X. ,Haghighat, F., Experimental investigation of multiple tube heat transfer enhancement in a vertical cylindrical latent heat thermal energy storage system, Renew. Energy. 140 (2019) 234-244.
[12] Kousha, N., Rahimi, M., Pakrouh, R. ,Bahrampoury, R., Experimental investigation of phase change in a multitube heat exchanger, Journal of Energy Storage. 23 (2019) 292-304.
[13] Shen, G., Wang, X. ,Chan, A., Experimental investigation of heat transfer characteristics in a vertical multi-tube latent heat thermal energy storage system, Energy Procedia. 160 (2019) 332-339.
[14] Agyenim, F., Eames, P. ,Smyth, M., Heat transfer enhancement in medium temperature thermal energy storage system using a multitube heat transfer array, Renew. Energy. 35 (2010) 198-207.
[15] Pizzolato, A., Sharma, A., Ge, R., Maute, K., Verda, V. ,Sciacovelli, A., Maximization of performance in multi-tube latent heat storage – Optimization of fins topology, effect of materials selection and flow arrangements, Energy. (2019).
[16] Murray, R. E. ,Groulx, D., Experimental study of the phase change and energy characteristics inside a cylindrical latent heat energy storage system: Part 1 consecutive charging and discharging, Renew. Energy. 62 (2014) 571-581.
[17] Murray, R. E. ,Groulx, D., Experimental study of the phase change and energy characteristics inside a cylindrical latent heat energy storage system: Part 2 simultaneous charging and discharging, Renew. Energy. 63 (2014) 724-734.
[18] Agyenim, F., The use of enhanced heat transfer phase change materials (PCM) to improve the coefficient of performance (COP) of solar powered LiBr/H2O absorption cooling systems, Renew. Energy. 87 (2016) 229-239.
[19] Esapour, M., Hosseini, M. J., Ranjbar, A. A. ,Bahrampoury, R., Numerical study on geometrical specifications and operational parameters of multi-tube heat storage systems, Appl. Therm. Eng. 109 (2016) 351-363.
[20] Esapour, M., Hosseini, M. J., Ranjbar, A. A., Pahamli, Y. ,Bahrampoury, R., Phase change in multi-tube heat exchangers, Renew. Energy. 85 (2016) 1017-1025.
[21] Esapour, M., Hamzehnezhad, A., Rabienataj Darzi, A. A. ,Jourabian, M., Melting and solidification of PCM embedded in porous metal foam in horizontal multi-tube heat storage system, Energy Conv. Manag. 171 (2018) 398-410.
[22] Niyas, H., Prasad, S. ,Muthukumar, P., Performance investigation of a lab–scale latent heat storage prototype–Numerical results, Energy Conv. Manag. 135 (2017) 188-199.
[23] Niyas, H., Rao, C. R. C. ,Muthukumar, P., Performance investigation of a lab-scale latent heat storage prototype – Experimental results, Sol. Energy. 155 (2017) 971-984.
[24] Luo, K., Yao, F.-J., Yi, H.-L. ,Tan, H.-P., Lattice Boltzmann simulation of convection melting in complex heat storage systems filled with phase change materials, Appl. Therm. Eng. 86 (2015) 238-250.
[25] Anish, R., Mariappan, V. ,Mastani Joybari, M., Experimental investigation on the melting and solidification behavior of erythritol in a horizontal shell and multi-finned tube latent heat storage unit, Appl. Therm. Eng. (2019) 114194.
[26] Dandotiya, D. ,Banker, N., Numerical investigation of heat transfer enhancement in a multitube thermal energy storage heat exchanger using fins, Numerical Heat Transfer, Part A: Applications. 72 (2017) 389-400.

[27] Bhagat, K., Prabhakar, M. ,Saha, S. K., Estimation of thermal performance and design optimization of finned multitube latent heat thermal energy storage, Journal of Energy Storage. 19 (2018) 135-144.
[28] Trp, A., Lenic, K. ,Frankovic, B., Analysis of the influence of operating conditions and geometric parameters on heat transfer in water-paraffin shell-and-tube latent thermal energy storage unit, Appl. Therm. Eng. 26 (2006) 1830-1839.
[29] Tehrani, S. S. M., Taylor, R. A., Saberi, P. ,Diarce, G., Design and feasibility of high temperature shell and tube latent heat thermal energy storage system for solar thermal power plants, Renew. Energy. 96 (2016) 120-136.
[30] Pirasaci, T. ,Goswami, D. Y., Influence of design on performance of a latent heat storage system for a direct steam generation power plant, Appl. Energy. 162 (2016) 644-652.
[31] Fang, Y., Niu, J. ,Deng, S., Numerical analysis for maximizing effective energy storage capacity of thermal energy storage systems by enhancing heat transfer in PCM, Energy Build. 160 (2018) 10-18.
[32] Shukla, A., Buddhi, D. ,Sawhney, R. L., Solar water heaters with phase change material thermal energy storage medium: A review, Renew. Sust. Energ. Rev. 13 (2009) 2119-2125.
[33] Seddegh, S., Wang, X., Henderson, A. D. ,Xing, Z., Solar domestic hot water systems using latent heat energy storage medium: A review, Renew. Sust. Energ. Rev. 49 (2015) 517-533.
[34] RT60 Data Sheet. Rubitherm Technologies GmbH, ⟨https://www.rubitherm.eu/en/index.php/productcategory/organische-pcm-rt⟩, (May 22, 2019).
[35] Caron-Soupart, A., Fourmigué, J.-F., Marty, P. ,Couturier, R., Performance analysis of thermal energy storage systems using phase change material, Appl. Therm. Eng. 98 (2016) 1286-1296.
[36] Moffat, R.J. 1988. Describing the uncertainties in experimental results. Exp. Therm. Fluid Sci. 1 (1), 3-17.
[37] Erek, A. ,Dincer, I., An approach to entropy analysis of a latent heat storage module, Int. J. Therm. Sci. 47 (2008) 1077-1085.
[38] Ezan, M. A., Ozdogan, M. ,Erek, A., Experimental study on charging and discharging periods of water in a latent heat storage unit, Int. J. Therm. Sci. 50 (2011) 2205-2219.
[39] Kabbara, M., Groulx, D. ,Joseph, A., Experimental investigations of a latent heat energy storage unit using finned tubes, Appl. Therm. Eng. 101 (2016) 601-611.

Chapter 7: Final conclusions and future research

7.1. Final conclusions

The main contributions of the thesis can be summarized as follows, (1) It was revealed that an optimal tilting shell design needs to trade off the charging and discharging performances depending on the sunshine conditions. The tilting shell design accelerates the charging rate and thus is advantageous to areas with less sunshine hours to store solar energy; (2) The numerical investigation on the effect of the R/r revealed that the R/r of 5 allows the charging and discharging performances to be best balanced with a negligible loss to the total heat storage capacity. The combined investigation on the R/r and H provides the meaningful implication for the practical design that once the optimal radius ratio is determined, a variation in the unit heat will effectively adapt to the demand of the system heat capacity with the minimal impact on the total charging and discharging rate; and (3) The study experimentally validated the common numerical solution which assumes that a single tube domain formulated within the multitube heat exchanger can reflect its overall thermal characteristic. It was concluded a three-dimensional numerical modelling or an experimental work is the reliable way to investigate the vertical multitube LHTES system.

The thesis started with an introduction stating the research's background, objectives and the thesis's structure. Chapter 2 focused on a literature review of the system configuration, design and operating parameters for designing an effective LHTES system. It was noted that the system configuration and design could effectively enhance heat transfer rate in an LHTES system. It was also suggested that heat storage and release performances should be

simultaneously evaluated for researchers to determine the optimal configuration and geometrical designs.

Chapter 3 numerically studied the effects of tilting the shell lateral surface in a vertical shell-and-tube LHTES system. A comprehensive numerical model addressing the conjugate analysis of the HTF, HTF tube and PCM zones was first developed and validated. Then the model was employed to investigate the melting and solidifying performance of the LHTES systems with different tilting shell lateral surface angles. The results showed that the tilting lateral surface design can substantially shorten the melting duration by up to 43% with the tilting angle varying from 0° to 7°. However, the tilting lateral surface design also exhibits a negative effect on the solidification process. The selection of the tilting angle for a vertical LHTES system needs to trade off the melting performance against the solidifying performance. It was concluded that the application of the tilting lateral surface design is advantageous to areas with less sunshine hours for assisting solar energy storage.

Chapters 4 and 5 continued to numerically study the effects of another important geometrical parameter, the shell-to-tube radius ratio on thermal storage performance of a vertical shell-and-tube PCM storage system. The two chapters respectively investigated two series of radius ratio variations, which were defined within a type of PCM storage configuration with PCM contained in the shell side and HTF flowing through the central tube. The first series definition varied the PCM shell radius while fixing the HTF-tube radius, comprising a range of from 2 to 8 in the shell-to-tube radius ratios (R/r_f). The second series definition varied the HTF-tube radius based on a fixed PCM shell radius, consisting of a range of 2.5 to 9 in the shell-to-tube radius ratio (R_f/r). A unit height increase from 0.6 m to 1.2 m was also considered along with both series of radius ratio variations. In the perspective of solar thermal energy storage, the numerical investigations compared and evaluated the defined thermal performance indexes across each series of definitions. It was revealed that the shell-to-tube radius ratio of

around 5 offers a significant boost on both energy storage and release rates while delivers a marginal loss in the total heat storage capacity. Besides, the variation in the height of the system does not show a significant influence on the optimal value of the radius ratio.

Chapter 6 presented an experimental study of a multitube LHTES rig, the tube pitch of which was set based on the optimal result obtained from the comprehensive numerical studies in chapters 4 and 5. The experimental study was committed to two aims. The first aim was to validate a common numerical solution which formulates a virtual single tube domain to reflect the thermal performance of the multitube heat exchanger. This was accomplished by experimentally comparing the thermal characteristics between the MTHX and an STHX which was built with the same geometrical dimensions with the virtual cylindrical domain simplified by the numerical solution. The second aim was to examine the effects of tube number and HTF operating parameters in the MTHXs.

The experimental data showed that the single tube heat exchanger recorded substantially different local temperatures from those measured in the central and outer cylindrical PCM zones in the five-tube heat exchanger. Besides, the overall thermal behaviour also deviated significantly between the single-tube and five-tube heat exchangers, prompting that the three-dimensional numerical model or the experiment is the reliable way to investigate the vertical multitube LHTES system. The comparations between the different inner tube numbers showed that in a vertical MTHX, more inner tubes considerably accelerate the charging and discharging rates without incurring the negative effect on the natural convection flow. Moreover, an increase in the HTF charging temperature in the MTHX significantly enhanced the charging rate while led to less apparent effect on the following discharging duration. It was also found that the HTF flow rate poses a more pronounced influence on the charging process than on the discharging process. This can be credited to the continually growing PCM layer on the tube

surface during the discharging, which leads to the increased thermal resistance between liquid PCM and HTF.

7.2. Future research topics

The research suggests the following perspectives and subjects to be considered for the future study on an LHTES system.

(1) The numerical modelling of the PCM storage system still relies on various assumptions on boundary conditions and working conditions. Except for Shmueli et al. [1]'s work, very limited numerical studies describe effects of the PCM volume change during phase transition and the corresponding moving interface between PCM and air. By contrast, the experimental results presented in chapter 6 of this study indicates the air cell at the cylinder's top may exert mighty impact on thermal behaviour in the LHTES system.

(2) The configuration and design of an LHTES system play crucial roles in its performance. The innovative designs, such as the tilting HTF-tube lateral surface as well as the elliptical-shape shell and tube are expected to receive more research efforts.

(3) The three-dimensional modelling is essential for accurately solving the vertical multitube LHTES problem. However, researchers will face the challenge of high computing cost of model validation and simulations.

(4) Finned-tube has been found to significantly enhances heat conduction in PCM but there is much less work focusing on its effect on convection heat transfer, especially in the horizontal PCM storage system.

(5) The micro-encapsulated PCM is appealing for low-temperature heat storage applications thanks to its significant improvement in thermal conductivity [2, 3]. However, the disadvantages including the low structural stability during the thermal cycles and reduced latent heat capacity need to be further addressed.

(6) A specific thermal enhancement solution like PCM macro-encapsulation or metal foam increases the total system volume thus reduces the PCM energy density. These negative effects need to be evaluated by future research.

(7) Apart from thermodynamic properties, other key properties of the PCM including the long-run stability, environmental impacts, cost, high-volume availability, and safety compliance are seldom covered in publications.

7.3. References

[1] Shmueli, H. , Ziskind, G. ,Letan, R., Melting in a vertical cylindrical tube: numerical investigation and comparison with experiments, Int. J. Heat Mass Transf. 53 (2010) 4082-4091.

[2] Yu, S. , Wang, X. ,Wu, D., Microencapsulation of n-octadecane phase change material with calcium carbonate shell for enhancement of thermal conductivity and serving durability: synthesis, microstructure, and performance evaluation, Appl. Energy. 114 (2014) 632-643.

[3] Giro-Paloma, J. , Martínez, M. , Cabeza, L. F. ,Fernández, A. I., Types, methods, techniques, and applications for microencapsulated phase change materials (MPCM): A review, Renew. Sust. Energ. Rev. 53 (2016) 1059-1075.